



### Core-Shell Nanostructures: Perspectives towards Drug Delivery Applications

Journal:	<i>Journal of Materials Chemistry B</i>
Manuscript ID	TB-REV-06-2020-001559.R1
Article Type:	Review Article
Date Submitted by the Author:	31-Jul-2020
Complete List of Authors:	<p>Kumar, Raj; University of Michigan, Pharmaceutical Sciences Mondal, kunal; Idaho National Laboratory, Materials Science &amp; Engineering; North Carolina State University, Chemical and Biomolecular Engineering Panda, Pritam; Uppsala Universitet, Department of Physics and Astronomy Kaushik, Ajeet; Florida Polytechnic University, Natural Sciences Abolhassani, Reza; Syddansk Universitet - Sønderborg, MCI/NanoSYD Ahuja, Rajeev; Uppsala Universitet, Physics and Astronomy Rubahn, Horst-Gunter; University of Southern Denmark, Mads Clausen Institute, NanoSYD Mishra, Yogendra; Syddansk Universitet - Campus Sønderborg, NanoSYD, Mads Clausen Institute</p>

# Core-Shell Nanostructures: Perspectives towards Drug Delivery Applications

**Raj Kumar,<sup>1a</sup> Kunal Mondal<sup>2</sup>, Pritam Kumar Panda<sup>3</sup>, Ajeet Kaushik<sup>4</sup>, Reza Abolhassani<sup>5</sup>,  
Rajeev Ahuja,<sup>3,6</sup> Horst-Günter Rubahn,<sup>5</sup> Yogendra Kumar Mishra<sup>5\*</sup>**

<sup>1</sup>Faculty of Engineering and Institute of Nanotechnology and Advanced Materials, Bar Ilan University, Ramat Gan-52900, Israel

<sup>2</sup>Materials Science and Engineering Department, Idaho National Laboratory, Idaho Falls, ID 83415, USA

<sup>3</sup>Condensed Matter Theory Group, Materials Theory Division, Department of Physics and Astronomy, Uppsala University, Box 516, SE-75120, Uppsala, Sweden

<sup>4</sup>NanoBioTech Laboratory, Department of Natural Sciences, Division of Sciences, Art, & Mathematics, Florida Polytechnic University, Lakeland, FL-33805, USA

<sup>5</sup>Mads Clausen Institute, NanoSYD, University of Southern Denmark, Alsion 2, DK-6400, Sønderborg, Denmark

<sup>6</sup>Applied Materials Physics, Department of Materials Science and Engineering, Royal Institute of Technology (KTH) SE-10044 Stockholm, Sweden

\*Corresponding Authors

[rk7410@gmail.com](mailto:rk7410@gmail.com) (R.K); [kunal.mondal@inl.gov](mailto:kunal.mondal@inl.gov) (K.M); [mishra@mci.sdu.dk](mailto:mishra@mci.sdu.dk), (YKM)

<sup>a</sup>Present address: Department of Pharmaceutical Sciences, University of Michigan, 2800 Plymouth Rd, Ann Arbor, Michigan 48105, United States

## ABSTRACT

Nano-systems have shown fostering outcomes and substantial progress in drug delivery and biomedical applications. However, control and targeted delivery of drugs or genes are limited due to their physicochemical and functional properties. In this regard, the core-shell type nanoparticles are promising nanocarrier systems for controlled and targeted drug delivery applications. These functional nanoparticles are being emerged as a particular class of nano-systems because of their unique advantages including high surface area, and easy surface modification and functionalization. Such unique advantages can facilitate core-shell nanoparticles towards selectively mingling of two or more different functional properties in a single nanosystem to achieve desired physicochemical properties essential for effective targeted drug delivery. Several types of core-shell nanoparticles such as metallic, magnetic, silica-based, upconversion, and carbon-based core-shell nanoparticles, etc. have been designed and developed for drug delivery applications. Keeping scope, demand, and challenges in view, the present review explores the state-of-the-art developments and advancements in core-shell nanoparticle systems, their desired structure-property relationships, newly generated properties, the effect of parameter controlling, surface modifications, functionalization, and last but not least, the promising applications in the field of drug delivery, biomedical, and tissue engineering. This review also supports significant future research to develop multi-cores and shells based functional nano-systems to investigate nano-therapies needed for advanced, precision and personalized healthcare systems

**Keywords:** nanoparticles; core-shell nanoparticles; magnetic nanoparticles; silica-coated core-shell nanoparticles; upconversion core-shell nanoparticles; drug delivery; biomedical imaging; MRI; tissue engineering

## 1. Introduction

Nanotechnology constantly advance in medical technologies, biomedical engineering, agricultural, environmental science, chemistry, materials sciences, physics, and electronics as a multidisciplinary branch compassing science<sup>1-5</sup>. The main objective of nanotechnology is to investigate novel materials at the nanoscale, and developing innovative devices in submicron scale with enhanced performance of existing devices<sup>6</sup>. The new avenues are opened by the advent of nanomaterials, including nanoparticles, synthesized using the fundamentals of nanoscience and nanotechnology. The properties of such advanced nano-systems, such as large surface-to-volume ratio which leads to high surface energy, optical, electronic, and magnetic properties, provide further advantages<sup>7</sup>. The high surface of nano-systems (nanoparticles/nanomaterials) allows the feasibility of surface modification, functionalization, high loading, induce stimuli-responsive entities, and hence excellent pharmacokinetics, improved bioavailability, time of circulation in the blood, and the feasibility to use them in other biomedical applications can be achieved<sup>8</sup>. The improved properties of nano-systems are the backbone of developing nano-enabled theranostics<sup>9,10</sup>, especially the drug delivery system. Such nano-enabled biomedical applications are helpful for developing effective treatment and therapy which involves minimum dosage and reduces side effects in comparison with respective bulk materials<sup>11</sup>. The introduction of the nano-system on therapy development is not only limited to the drug delivery, but also facilitates and monitors the drug release due to their novel optical properties at nanoscale<sup>12-14</sup>. Besides, control on nano-system properties upon applying appropriate stimulation makes these nano-systems suitable for developing the next generation drug delivery systems. For such advanced drug delivery applications, liposomes were introduced in 1965 by a group led by Bangham<sup>15</sup>. In 1995 the USA Food and Drug Administration (FDA) approved a liposomal formulation for doxorubicin (Doxil)

for the treatment of Kaposi sarcoma related to AIDS<sup>16</sup>. The FDA was allowed to provide clinical therapies for breast cancer, non-small cell lung cancer, and pancreatic cancer with an albumin-based nano-optic protein-based paclitaxel (Abraxane)<sup>17</sup> in 2005. In 2013, selective adotrastuzumab emtansine (DM1) (Kadcyla) was approved for use in patients suffering from positive breast cancer of a human epidermal growth factor receptor<sup>18</sup>.

Despite such advanced therapies and technologies, nanoparticles and biological systems are still communicating in many unclear aspects. For instance, bare nanoparticles such as gold (Au), silver (Ag), palladium (Pd), platinum (Pt), and iron (Fe) are limited to specific properties as most of the synthesis techniques relies on the surface of formed metal nanoparticles which are hydrophobic in nature. To use them in drug delivery, biomedical, and tissue engineering application, nanostructures must be transferred into water and exhibit improved colloidal stability and monodispersity<sup>19–21</sup>. Well known and simple process to obtain hydrophilic nanoparticles is the ligand exchange method. However, many parameters, such as the chemical composition of nanoparticles and surface binding affinity of hydrophilic ligand, affect the ligand exchange process, which should be stronger than hydrophobic ligand<sup>1,20,22</sup>. Moreover, there is no general and universal protocol so far for the ligand exchange method, which works for all types of metallic nanoparticles. Each type of nanoparticles has its own boundaries. For example, bare nanoparticles of gold are good carriers for molecules with thiol functional group (-SH), but magnetic nanoparticles are not<sup>23</sup>, whereas magnetic nanoparticles are easy to control in vivo using an external magnetic field to bring them at the desired site of action<sup>24–27</sup>. However, their poor efficacy towards the functional group concerning loading or conjugation with of drug/gene or even with biomolecule is a limiting factor. Similarly, silica nanostructures are simple and easy to prepare and control the size and

shape with the feasibility of very high drug loading capacity due to porous nature, but difficult to deliver at the site of demand <sup>28</sup>.

To overcome the aforementioned limitations, one of the approaches is to improve the connectivity between the drug and surface of bare inorganic/metallic nanoparticles through one or more types of suitable materials. As a result, this approach increases the size of the nanoparticle, and changes the overall formulation, results in less amount of drug loading and poor efficacy as new challenges. In this direction, core-shell nanoparticles have gained significant attention due to their unique and tunable features. Mostly, core-shell nanoparticles are composed of metals or metal oxides either as core or shell.

The protocols for the synthesis of core-shell nanoparticles have been well-established for approximately 15 years to achieve monodisperse nanoparticles with control over shapes and size using selective stabilizers <sup>29,30</sup>. Stabilizers show different types of interactions with different facets of nanoparticles. The combined properties of core-shell have made them interesting nanoparticles for several innovative and advanced applications <sup>31-33</sup>. Formulation of core-shell nanoparticles, such as magnetic nanoparticles coated with Au, allows loading of drugs due to thiol chemistry with gold, and magnetic nanoparticles are facilitated to deliver the drug at the site of action using external magnetic field even in the human body <sup>34,35</sup>. Another example is the loading percentage of payload on Au coated magnetic nanoparticles, which is less compared to porous silica-coated magnetic nanoparticles <sup>36-38</sup>. Hence, porous silica-coated core-shell nanoparticles further have several advantages. Therefore, it is more interesting to bring different types of nanomaterials and formulate them as core-shell type nanoparticles, which can be promising ineffective targeted and

control drug delivery. Core-shell nanoparticles can be further functionalized with different moieties/entities.

In this review, we carefully reviewed state-of-the-art core-shell nano-system, as schematically illustrated in Figure (I), to develop next generation drug delivery systems and nano-therapies. Furthermore, recent progress, the challenges, the gap, and future aspects of core-shell nanosystem enabled for nano-therapeutics for health wellness are also discussed in this report.

## **2. Core-Shell Nanomaterial**

Bare nanoparticles are toxic, which may cause damage/trouble to host tissues. Over bare nanoparticles, core-shell nanoparticles show improved properties such as less cytotoxicity, high dispersible nature biocompatibility, enhanced conjugation with biomolecules and drugs due to enhanced surface properties, and improved thermal and chemical stability <sup>39</sup>. The coating of biocompatible materials as the shell on top of core materials makes nanoparticles less toxic and biocompatible. The advantages of shell materials are not only limited to reduce toxicity, but they may also induce or change or enhance the properties of core material <sup>40</sup>. For example, the optical properties of semiconductor materials are improved by coating/doping with other materials <sup>41</sup>. The importance of hydrophilicity of nanoparticles in biological applications is also well-known <sup>42</sup>. Therefore, hydrophobic nanoparticles coated by hydrophilic materials can be suitable for biomedical applications, and hence, dispersibility can be enhanced. Core-shell nanoparticles can be further functionalized. Figure 1(II) presents the further functionalized core-shell nanoparticles with polymer, silane, dendrimers, and gold. This is because of the prominent nature of core material over shell composition. In biomedical and drug delivery applications, conjugation of biomolecules on the surface of nanoparticles is the key step for the successful formulation,

delivery, and effective therapeutic applications. Figure 1(III) presents the various strategies of inorganic nanoparticles surface engineering, but in many cases, conjugation of biomolecules on the surface of the materials of interest is difficult. This can be overcome through the coating of suitable materials as a shell over the choice of core material, which allows conjugation of biomolecules. This concept is the key step in targeted and control drug delivery and biomedical engineering. Some materials are sensitive to an external stimulus such as pH and thermal. Such materials can be used for coating on suitable core materials and can be served as stimuli-responsive nanocarrier.

A simple structure of the core-shell nanoparticles is presented in Figure 1. Core and shell nanomaterials are different types (Figure 1). The widely used core materials are such as drug/gene/protein/amino acid nanoparticles, metal nanoparticles, magnetic nanoparticles, silica nanoparticles, and shell materials are polymers, proteins, polysaccharides, silica, metals, and metal oxides.<sup>43</sup> Core-shell nanoparticles can be classified into different categories depending on physicochemical properties. The basic types are core-shell metallic nanoparticles, core-shell magnetic nanoparticles, core-shell polymer nanoparticles, core-shell silica nanoparticles, core-shell upconversion nanoparticles, and carbon nanomaterial-based core-shell nanoparticles<sup>29,44</sup>. Other classifications are based on core material such as core-shell nanoparticles of gold, silver, platinum, palladium, iron oxide, superparamagnetic, and silica nanoparticles. In the following sections, we schematically discuss the various types of core-shell nanoparticles.

### 3. Magnetic Core-Shell Nanostructures

Drug delivery was proposed by Paul Ehrlich for the first time, and he won Nobel Prize in medicine in 1908 for his contribution to drug delivery system development <sup>45</sup>. In 1960, Freeman *et al.*, proposed the magnetic nanoparticles-based drug delivery using an external magnetic field for localized delivery at the site of action needed <sup>46</sup>. In 1970, chemotherapeutics was delivered using magnetic nanoparticles <sup>47</sup>. Since the 1980s, several researchers have developed a magnetic nanoparticles-based delivery system for the delivery of different drug molecules and other entities <sup>48</sup>. Polymeric nanoparticles loaded by magnetic nanoparticles were reported by Hafeli *et al.*, for successful delivery to tumor <sup>49</sup>. Since then, numerous research groups around the globe started dedicatedly working on magnetic nanoparticles, fabricated magnetic nanoparticles through several methods, established the synthesis protocols, and employed for potential applications. Iron oxides (hematite, maghemite, magnetite) are widely used in magnetic nanoparticles. Iron oxides show different polymorphs such as  $\alpha$ -Fe<sub>2</sub>O<sub>3</sub> (hematite)  $\beta$ -Fe<sub>2</sub>O<sub>3</sub>,  $\gamma$ -Fe<sub>2</sub>O<sub>3</sub> (maghemite),  $\epsilon$ -Fe<sub>2</sub>O<sub>3</sub>, Fe<sub>3</sub>O<sub>4</sub> (magnetite), and other forms such as amorphous and high-pressure form. The coprecipitation reaction of ferrous and ferric chloride salts in the presence of stabilizers and basic solution generates the magnetic nanoparticles. The most widely used basic solution is ammonia, and the stabilizer is oleic acid. However, due to the limitation of bare magnetic nanoparticles, core-shell nanoparticles are developed as an alternative technique, which retains magnetic properties and facilitates the loading and release of drugs. Magnetic nanoparticles have been commercialized and widely used in MRI, hyperthermia, cell sorting, sensing, immunoassays, enzyme immobilization, and gene transfection <sup>50–57</sup>. Various biomedical applications demand core-shell magnetic nanoparticles as mentioned in the previous section. The oleic acid is the best stabilizer for magnetic nanoparticles to further coating with silica and functionalization <sup>25,27</sup>. Hafeli *et al.*, reported the

PEO (polyethylene oxide) coated functional magnetic nanoparticles <sup>49</sup>. Magnetic core-shell nanoparticles consist of metal or metal oxide core encapsulated in a shell material such as inorganic or polymer. The coating induces the properties such as biocompatibility and stability, and serves as support for biomolecules. The primary property of particles, the magnetic property, allows magnetic core-shell nanoparticles to be used as magnetic contrast agents, hyperthermia agents, and magnetic vectors. Figure 2(I) illustrates the various steps involved in the process of magnetic core-shell nanoparticles, from preparation to targeted drug delivery. Magnetic core-shell nanoparticles can be classified into five types depending on shell type, such as polymer-coated, protein-coated, silane coated, silica-coated, and other coating material based magnetic core-shell nanoparticles. However, widely used magnetic nanoparticles in drug delivery, biomedical, and tissue engineering applications are maghemite and magnetite <sup>58</sup>. In the following sections, we systematically discuss magnetic core-shell nanoparticles coated by different materials.

Polymers, which are mainly natural and synthetic are widely used as material for coating, stabilization, and encapsulation. A large number of polymers are widely available for researchers, which facilitate the choice of selection based on requirements. However, biopolymers are promising candidates for drug delivery applications due to their unique physicochemical and biological properties. Polymer coating on magnetic nanoparticles is one of the widely used techniques to improve the stability of nanoparticles. The polyethylene glycol (PEG) is also among one of the ideal candidates that exhibits desired biocompatibility. PEG coating induces required properties such as water solubility, lowered toxicity, enzymatic degradation, and enhances drug half-life *in-vivo* <sup>59</sup>. It has been demonstrated that PEG-coated magnetic nanoparticles on functionalization with APTES results in the amine (-NH<sub>2</sub>) functional group on the surface of the

particles<sup>60,61</sup>. The polymer cellulose acetate hydrogen phthalate coated magnetic core-shell nanoparticles are reported by Reshmi *et al.*, The polymer degradation facilitates the release of drug<sup>62</sup>. Hence, polymer biodegradation plays a key role in drug release kinetics. Polymers such as starch, dextran, and chitosan are used as coating materials on magnetic nanoparticles due to their hydrophilic nature and reduced dipole-dipole attractions between magnetic nanoparticles, and hence, results in well-dispersed aqueous suspension<sup>63,64</sup>. Chitosan coated magnetic ( $\text{Fe}_2\text{O}_3$ ) core-shell nanoparticles showed promising results in drug and gene delivery, investigated by Kumar *et al.*,<sup>65</sup>. A similar type of nanoparticles (chitosan-coated magnetic NPs) is also used in targeted photodynamic therapy<sup>66</sup>. By conjugation with protein, antibodies, or ligands with drugs, further advantages are offered.

Stimuli-responsive polymers coating results in the stimuli-responsive drug delivery systems such as pH-sensitive polymers, temperature-sensitive polymer, and light-sensitive polymers, which are suitable for drug release at the site of action<sup>67,68</sup>. Figure 2(II) presents the schematic view of stimuli (thermal responsive polymer) responsive magnetic core-shell nanoparticles and the effect of drug release at different conditions, for example, poly-(N-isopropylacrylamide) (PNIPAM), a thermosensitive polymer-coated magnetic nanoparticle ( $\text{Fe}_2\text{O}_3$ ) employed as a nanocarrier for chemotherapeutic drug release using magnetic targeting and hyperthermia by Purushotham *et al.*,<sup>69</sup>. Thermalsensitive polymer solution in water is stable, and above/below its critical temperature, they are separated as two different phases, i.e. the aqueous phase and polymer phase. Liu *et al.*, investigated the thermal responsive delivery using temperature-responsive polymer-coated magnetic nanoparticles; at below the critical temperature, they are stable, and above the critical temperature, the polymer releases the loaded drug<sup>70</sup>. Kurzhals *et al.*, reported the synthesis of

block copolymer modified superparamagnetic iron oxide nanoparticles<sup>71</sup>. Figure 2(III) presents the synthesis procedure. Zeng *et al.*, developed the multi stimuli-responsive magnetic core-shell nanoparticles using PMAA polymer as a shell. Polymer PNIPAM used as a gatekeeper on the surface through a two-stage distillation precipitation polymerization approach<sup>72</sup>. Figure 3(I) presents the preparation, biodegradation, and multi stimuli-responsive drug release mechanism. Magnetic core-shell nanoparticles composed of polymer shells are also reported by Lin *et al.*, for ibuprofen delivery<sup>73</sup>. Li *et al.*, reported the double core-shell (eccentric-(concentric- $\text{Fe}_3\text{O}_4@(\text{SiO}_2)@$ polyacrylic acid) multifunctional magnetic core-shell nanoparticles for pH depended on drug delivery<sup>74</sup>. Moreover, it needs to be taken care of the polymer toxicity, the thickness of the coating, and the concentration of polymer. Natural and biopolymers are the best choice of coating materials for biomedical applications. Lignin micro and nanoparticles have been formulated and employed as a nanocarrier for drug delivery<sup>75</sup>. Lignin is gaining significant attention in this aspect due to excellent biocompatibility, biodegradability, non-toxicity, easy availability, and renewable nature<sup>76</sup>. However, there are a large number of natural biopolymers that are needed to be explored for their potential use as coating materials, including core-shell nanoparticles.

The coating of magnetic nanoparticles (MNPs) is the best way to overcome the limits associated with bare magnetic nanoparticle *in vivo*, such as circulation time, pH, and aggregation. The coating on MNPs, most importantly, helps in stabilization. For example, silica-coated magnetic nanoparticles are negatively charged at blood pH, which creates electrostatic repulsion, inhibits the aggregation of nanoparticles, and therefore blood circulation time of nanoparticles is enhanced<sup>77</sup>. The coating of silica on magnetic nanoparticles provides hydrophilicity, and the available

hydroxyl functional group helps the covalent loading of targeted molecules. The coating of silica on magnetic nanoparticles has been widely used as a coating approach in the formulation of core-shell magnetic nanoparticles. Silica or mesoporous silica-coated magnetic core-shell nanoparticles are one of the widely studied/reported core-shell nanoparticles as per the best of our knowledge. This is due to the simple and easy coating methods and a good affinity of silica towards magnetic nanoparticles<sup>78</sup>. The coating thickness of the silica shell can be tunable simply by changing the concentration of silica precursor in the process. Huang *et al.*, reported the preparation of Fe<sub>3</sub>O<sub>4</sub>/SiO<sub>2</sub> nanoparticles method<sup>79</sup>. Recently, Deng *et al.*, formulated the core-shell nanoparticles of superparamagnetic nanoparticles coated with SiO<sub>2</sub><sup>80</sup>. The coated silica is capable to create various pore sizes to load the drug molecules for delivery. The major concern which is essential to be considered is the cytotoxicity of the silica, which is dependent on size, time, and concentration.

The surface of magnetic nanoparticles can be changed with silane, organosilane, and oleic acid. Oleic acid stabilized magnetic nanoparticles are the best choice for further coating, including silanes. Silanes are promising candidates for surface coating and further functionalization due to the availability of a large number of amine functional groups<sup>81</sup>. Cao *et al.*, employed core-shell nanoparticles of Fe<sub>3</sub>O<sub>4</sub>/SiO<sub>2</sub>-NH<sub>2</sub> functionalized with cyclodextrin in magnetic drug delivery<sup>82</sup>.

Proteins are more interesting materials for coating due to suitable biological properties, and they play a key role in human body functions. However, limited researchers attempted or investigated the coating of proteins on magnetic nanoparticles<sup>83,84</sup>. Due to the surface properties of MNP, direct protein coating is not generally possible for all types of proteins. Skaat *et al.*, coated amyloid-beta on magnetic nanoparticles for selective marking<sup>85</sup>. It is needed to study the interaction of magnetic

nanoparticles and proteins and to develop new approaches to facilitate it. Protein that are coated with magnetic gold nanoparticles are used for successful drug-delivery applications. Overall, protein usage in drug delivery is very limited as proteins are expensive to perform such studies. So, facile protein synthesis technology development is the way to boost protein usage in various applications, including core-shell nanoparticles.

There are several other compounds such as organic compounds and commercial products used for coating on magnetic nanoparticles to investigate their physicochemical properties and performance in drug delivery. However, very few attempts are reported, and most of them have not shown better performance than the aforementioned coating material-based magnetic core-shell nanoparticles. Liu *et al.*, used magnetic nanoparticles loaded in micelles and modified surfaces with Pluronic F127. Tetraheptylammonium also was applied as coating materials<sup>86,87</sup>. Interestingly, Lim *et al.*, investigated the metal coatings on magnetic nanoparticles and successfully formulated gold-coated magnetic core-shell nanoparticles<sup>88</sup>. More investigation is needed for further development of multimodal metallic core-shell nanoparticles such as iron oxides (IO)/Au/mSiO<sub>2</sub>, IO/Ag/mSiO<sub>2</sub>, IO/Ag/mSiO<sub>2</sub>/Au/mSiO<sub>2</sub> for further advancement in targeted controlled drug delivery for better healthcare in future.

#### **4. Silica-based Core-Shell Nanostructures**

In the above section, we discussed the impact of silica as a coating material in core-shell nanoparticles. Silica nanoparticles are one of the promising materials as bare nanoparticles and shell materials due to unique physicochemical properties and tunability. The range of different nanostructures of silica has been developed<sup>32,89</sup>. Most interesting silica nanoparticles are

mesoporous, hollow, and core-shell nanoparticles<sup>90</sup>. Moreover, the preparation of silica nanoparticles is very simple, easy, and cost-effective. Feasibility to tune the particle size, well established Stobers method for formulation of desired particle size, and tunable pore types and pore size make them excellent nanomaterials<sup>91</sup>. The available hydroxyl functional group on the surface of the particles further expands its horizon by providing simplicity in further functionalization with several types of compounds such as biomolecules, coating with various polymers, drugs, dyes, and porous surface which allows loading drug, gene, growth factors, biomolecules, and another promising nanocarrier for delivery system and tissue engineering<sup>92</sup>.

The porous structure further enhanced the high loading of drugs, genes, and other payload materials. The surface of silica can be used as the carrier for drug loading, functionalized with fluorescence entities to monitor the delivery inside the body, and conjugated with antibodies to allow the delivery of loaded drugs at the site of action<sup>91,93</sup>. Hence, silica nanostructures are one of the widely studied nanoparticles after metallic and magnetic nanoparticles. Multifunctional mesoporous silica nanoparticle is more interesting due to particles with a size less than 500 nm, high pore volume, large surface area, tunable pore sizes, good colloidal stability, and the feasibility of functionalization inner and outer pore systems<sup>90,94,95</sup>. These attractive properties make multifunctional silica nanoparticles a superior platform as shell in various core-shell nanoparticles for applications in drug delivery, biomedical, bioimaging, biosensing, biocatalysts, diagnostic, theragnostic, and tissue engineering<sup>90,93,94</sup>.

Various researchers employed silica or mesoporous silica-coated metallic nanoparticles in drug, gene, protein, amino acids, and growth factor delivery. Shefi *et al.*, used porous silica

nanostructures as a carrier for the delivery of nerve growth factor<sup>28</sup>. Results showed the enhanced neural differentiation and neural network outgrowth. Overall, core-shell silica nanoparticles are promising candidates for drug delivery. Cui *et al.*, synthesized multifunctional  $\text{Fe}_3\text{O}_4@m\text{SiO}_2@Au$  core-shell nanoparticles for pH-responsive drug delivery of Doxorubicin hydrochloride as a model drug<sup>96</sup>. Figure 3(II) presents the synthesis of the procedure of core-shell nanoparticles and their TEM images. Zhao *et al.*, fabricated core-shell nanoparticles ( $\text{Fe}_3\text{O}_4@n\text{SiO}_2@m\text{SiO}_2$ ) and functionalized with APTES. They investigated the interaction with etoposide on drug loading and release behavior. Figure 3(IV) presents the preparation process of core-shell microspheres, functionalization, drug loading, and release mechanism. Results suggested that the drug release is an endothermic reaction from 25 to 60 °C. Hence, it can be used to control drug delivery with external conditions and without any side effects to the human body<sup>97</sup>.

Although silica core-shell nanoparticles are more interesting, using the silica as the core is less interesting than the silica as shell materials. Moreover, it is challenging to coat the magnetic, metals, and metal oxides as shells on silica nanoparticles. This can facilitate the formulation of the multifunction and multidrug and multi stimuli-responsive targeted and controlled drug delivery by incorporation of different shells for different requirements. Hence, further studies are required to focus on the coating of inorganic materials on silica nanostructures to formulate core-shell nanoparticles.

## 5. Polymeric Core-Shell Nanostructures

Polymers are well known and widely used materials as the shell<sup>98</sup>. This is due to the availability of a large number of natural polymers and the feasibility to synthesize polymers of interest through chemical processes. A further advantage is the incorporation of a functional group of demand on polymer for drug loading/conjugation, delivery, further functionalization, targeting site of action, etc<sup>99,100</sup>. Considering the other core-shell nanoparticles, the preparation of core-shell nanoparticles using a polymer as the shell is easier due to the quick adhesion of polymers. The first choice of polymer for core-shell nanoparticles is PEG. PEG is an interesting polymeric substance for drug delivery, biomedical, and tissue engineering applications due to its excellent biocompatibility<sup>101</sup>. The self-organization ability of PEG creates micelles in an aqueous solution<sup>102</sup>. Micelles are considered as amphiphilic core-shell polymeric nanoparticles<sup>103</sup>. The typical size of micelles is in the range of 30-50 nm<sup>104</sup>. The core of the micelles is hydrophilic and can be loaded with targeted molecules/APIs. The outer surface of micelles is feasible for further functionalization to make them suitable for targeted delivery. Micelles deliver the drug slowly due to high stability, and hence results in slow dissociation of micelle structure<sup>22,105</sup>. Kataoka and co-workers formulated the core-shell type micelles using PEG-block-poly-(L-lysine) (PEG-b-PLL) and PEG-block-poly(alpha, beta-aspartic acid) (PEG-b-P(Asp))<sup>20,106</sup>. Meng *et al.*, synthesized the core-shell nanofibers of polymers composed of PEO core with TCS and PLA shell through a coaxial electrospinning process and investigated their use in the delivery of tenofovir *in vitro* and *in vivo*<sup>107</sup>. Yang *et al.*, utilized microfluidic technology to formulate novel type core-shell chitosan microcapsules for sequential drug release. Microcapsules contain cross-linked chitosan hydrogel shell and drug-free and drug-loaded PLGA nanoparticles in oily core<sup>108</sup>. The prepared microcapsules are employed for the treatment of acute gastritis. The drug releases under acidic conditions by decomposition of the chitosan shell. Drug release is slower in PLGA nanoparticles for several days based on the

degradation of PLGA. Figure 3(III) presenting the drug release mechanism from microcapsules<sup>108</sup>.

PEG is also used as stabilizer/coating or shell material for metal nanoparticles, including gold, iron, and iron oxides. Metal nanoparticles coated with the polymer can be prepared using Pearson's hard-soft template approach<sup>109</sup>. Metal ions are as soft acids, and acetates and perchlorates are as hard base. Chemical reduction results in the formation of nanosized metal nanoparticles. By the addition of metal salts to PEG-b-PEI aqueous solution and subsequent reduction, the formation of gold nanoparticles encapsulates polydisperse micelles core-shell nanoparticles will achieve<sup>110</sup>. Similarly, different metal salts such as PdCl<sub>2</sub> and H<sub>2</sub>PtCl<sub>6</sub> can be used to prepare respective core-shell nanoparticles<sup>111</sup>. Formation of PEG-coated metal nanoparticles are of two types: formation of metal nanoparticles and micellization simultaneously, or direct coating of PEG with the suitable functional group on metal nanoparticles. The coating of PEG can be achieved through the ligand exchange process or absorption of PEG during the nucleation and growth of the metal nanoparticles. PEG copolymers or derivatives with -SH functional group are suitable for in-situ coating of gold nanoparticles due to excellent chemistry between gold nanoparticle surface and thiol functional group<sup>112</sup>. Similarly, core-shell fluorescence nanoparticles are prepared by coating the polymer (PEG-b-PAMA) on fluorescence CdS nanoparticles at room temperature, used in biomedical applications<sup>113</sup>.

Kim *et al.*, developed the coating of the polymer through surface-initiated atom transfer radical polymerization process<sup>114</sup>. The successfully formulated poly-(N-isopropylacrylamide) (T<sub>i</sub> 33 °C)<sup>115</sup> and poly(methoxy oligo(ethyleneglycol) methacrylate) (transition temperature T<sub>i</sub> 55 °C)<sup>115</sup> are

the thermally responsive polymer. The pH-responsive polymers e.g. poly(4-vinylpyridine)<sup>116</sup> are coated on gold nanoparticles successfully. It is also reported that PS latex core (150 nm) is coated with PNIPAM shell (70 nm) nanoparticles<sup>117</sup>. At the temperature of 34 °C, the shell collapses and the drug releases. Ballauff *et al.*, reported the Ag nanoparticles coated with PNIPAM polymer core-shell nanoparticles<sup>118</sup>. The multi-shell nanoparticles, such as CdSe nanoparticles coated by ZnS, are more complex nanoparticles systems<sup>119,120</sup>. Such type of core-shell nanoparticles is more interesting due to further enhancement of optical properties such as fluorescence quantum yield. Despite significant progress in core-shell nanoparticle synthesis, coating with polymer and biomolecules remains a major challenge.

## 6. Upconversion Core-Shell Nanoparticles

Upconversion nanoparticles (UCNP) have been gaining significant attention from the researchers due to unique physicochemical and optical properties. The conversion of near-infrared to visible light has many advantages such as bio probe, deep light penetration, minimal photo-damage to the living organism, photostability, low toxicity, and stability<sup>1,121</sup>. The schematic view of the luminescence concept in conventional and upconversion nanoparticles is presented in Figure 4(I). Figure 4(II) presents the detailed mechanism of the upconversion of energy level diagrams<sup>1</sup>. Due to unique optical properties, along with carbon dots,<sup>122</sup> UCNPs are growing as a new class of materials for drug delivery, biomedical, and tissue engineering applications<sup>123–125</sup>. Several researchers employed UCNPs for various applications such as cell labeling, *in-vivo* imaging, FRET sensors, drug delivery, and photodynamic therapy<sup>1,124,126–129</sup>. The synthesis of UC is in the organic phase and stabilized with hydrophobic ligands. The most widely used ligand is oleic acid.

Hence, to use them in the biological application, surface modification into hydrophilic is essential. There are several approaches to the surface modification that have been developed specifically for UCNPs. Besides, several coating materials are widely used such as silica and PAA (poly(acrylic acid)), PEI (poly(ethyleneimine)), PEG, and mesoporous silica<sup>121,125,127,129</sup>.

Reddy *et al.*, successfully synthesized the UCNPs ( $\text{NaYF}_4$ ) and thoroughly investigated the different metal/metal oxide doped UCNPs and the effect of various parameters. They also developed a technique for the formulation of UCNPs through the microwave process. Formulated various types of UCNPs showed promising results in curcumin delivery, cellular uptake, biocompatibility against cancer cells, photocatalytic performance, and bioimaging<sup>123,124,126,127</sup>. Figure 4(III) presents the step by step synthesis process of silica-coated upconversion nanoparticle functionalization for drug delivery application. Wang *et al.*, developed a controlled dual responsive anticancer delivery using UCNPs polymer (UCNP-PNIPAM) core-shell nanoparticles<sup>130</sup>. Figure 5(I, II) shows the formulation, drug loading, release processes, and TEM images. UCNP-PMAA yolk-shell nanocapsules were synthesized by wang *et al.*,  $\text{NaYF}_4:\text{Yb}^{3+}/\text{Tm}^{3+}$  was used as core. PMAA is a pH and UV light-sensitive entity. Hence, formulated nanocapsules showed light- and pH-responsive delivery<sup>131</sup>. Figure 5(III, IV) shows the schematic preparation method and TEM images. Compared to the number of reports for UC core-shell nanoparticles, silica nanostructures are widely used as shell rather than polymers. Liu *et al.*, reported the synthesis of UCNP@mSiO<sub>2</sub> core-shell nanocomposites (Figure 6(I, II)). It showed promising results in infrared fluorescence and MRI imaging. Yang *et al.*, prepared  $\text{LaF}_3:\text{Yb},\text{Er}$  green upconversion monodispersed nanoparticles. Mesoporous silica was used as a shell for ibuprofen delivery applications. The synthesis process of  $\text{LaF}_3:\text{Yb}^{3+}$  and  $\text{Er}^{3+}@n\text{SiO}_2@m\text{SiO}_2$  core-shell nanoparticles is presented in

Figure 6(III) <sup>132</sup>. Recently, Reddy *et al.*, thoroughly reviewed the core-shell upconversion nanoparticle-based functional nanocarrier synthesis, properties, upconversion mechanism, factors affecting the physicochemical properties of UCNPs, and biomedical application <sup>1</sup>. Several researchers attempted silica coating on UCNPs for drug and gene delivery. However, low quantum yield and scale-up formulation still remain as major challenges in UCNPs.

The UCNPs have been used for fluorescence imaging of the drug delivery system. However, they also exhibit limitations regarding tissue penetration depth, photobleaching, and optical quenching. Hence, it is not possible to repeatedly monitor the drug delivery and distribution. Moreover, the background interface of tissue auto-fluorescence, light scattering, and poor signal to noise ratio are other disadvantages of the UCNPs. To overcome these challenges, persistent luminescence (PL) has been attracted significant attention. The PL is continuous luminescence behavior due to the sustain release of the radiant energy stored in nanomaterials for a known period of time. Such materials are commonly known as persistent luminescent nanomaterials (PLN) which emits luminescence even after excitation was stopped. During the excitation, electrons are captured and stored, and then released later for a limited time. Keeping this in view, PL nanomaterials are promising advanced candidates for imaging drug delivery applications<sup>133</sup>. Wang *et al.*, prepared *Lactobacillus reuteri* biofilm coated zinc gallogermanate (ZGGO) mesoporous silica as a bacteria bioinspired nanoparticle system (ZGGO@SiO<sub>2</sub>@LRM). The unique property of this nanosystem is targeted delivery of 5-FU to colorectum. ZGGO supports background-free PL bioimaging and in addition the LRM coating precisely targets the tumor area of the colorectum. In comparison to 5-FU, the ZGGO@SiO<sub>2</sub>@LRM nanosystem reduced the number of tumors per mouse to one-half *in-vivo* chemotherapy. Further, this system has the capability to tolerate the digestion of gastric

acid, the feasibility for intragastric drug delivery, and hence can be used for targeted delivery of oral drugs into colorectum <sup>134</sup>. Jiang *et al.*, designed and formulated persistent luminescent nanomaterials  $\text{ZnGa}_2\text{O}_4:\text{Cr}^{3+}, \text{Sn}^{4+}$  (ZGCS) for image-guided cancer chemotherapy. Mesoporous silica was coated on ZGCS surface for drug loading and delivery. Hyaluronic acid was used as gatekeeper and targeting entity. This nanosystem is able to produce persistent luminescence under red light (550 nm) irradiation. They have delivered paclitaxel (0.187 mg/mg) into MCF cells using nanosystem and simultaneously monitor the distribution and release of drug in the target cell through luminescence imaging. This is a promising nanosystem composed of multiple functionalities such as persistent luminescence, tumor targetability, and control drug delivery. All these features make it a promising candidate for imaging-guided cancer chemotherapy <sup>133</sup>. Chen *et al.*, formulated liposome coated near infrared persistent luminescence nanoparticle (PLNPs:  $\text{Zn}_{1.1} \text{Ga}_{1.8} \text{Ge}_{0.1} \text{O}_4:\text{Cr}^{3+}$ ) (Lipo-PLNPs) to monitor drug (Paclitaxel) delivery in chemotherapy. Lipo-PLNPs showed excellent luminescence, high drug loading capacity, and long-term tracking of drug delivery nanocarrier *in vivo*.  $\text{Zn}_{1.1} \text{Ga}_{1.8} \text{Ge}_{0.1} \text{O}_4:\text{Cr}^{3+}$  PLNP was used as an imaging contrast agent for long persistent luminescence and red LED light renewability <sup>135</sup>. Shi *et al.*, developed magnetic, long persistent luminescent, and mesoporous nanoparticles as a trackable transport carrier for drug delivery. They used core-shell nanostructures  $\text{Gd}_2\text{O}_3@\text{mSiO}_2@\text{CaTiO}_3:\text{Pr}$  which possesses properties such as mesoporous, magnetic, and long persistent luminescence. They showed bright red phosphorescence at 614 nm after UV irradiation. The drug release activity of these nanoparticles can be monitored using luminescence intensity. Further functionalization with PEG, nanoparticles showed good biocompatibility and toxicity. *In vivo* imaging was also observed over 20 minutes using nanoparticles <sup>136</sup>. Z-J. Li *et al.*, reported the  $\text{CaTiO}_3:\text{Pr}^{3+}$  nanoparticles functionalized with mesoporous silica ( $\text{MSNs}@\text{CaTiO}_3:\text{Pr}^{3+}$ ) with

long lasting phosphorescence for drug delivery. They thoroughly investigated the effect of several parameters on size, structure, and properties of nanoparticles. The *in-vivo* studies conformed the early detection (within 12 minutes) via optical imaging of the nanoparticles after being injected into the body. The quercetin loaded MSNs@CaTiO<sub>3</sub>:Pr<sup>3+</sup> nanoparticles showed red phosphorescence of Pr<sup>3+</sup> at 614 nm after UV irradiation<sup>137</sup>. However, further long-lasting persistent luminescence nanomaterials need to be developed for long term imaging-guided drug delivery systems and implants.

## 7. Carbon-based Core-shell Nanostructures (CBCSN)

Nanostructured materials with core-shell assemblies have gained substantial research focuses due to their morphology dependent fascinating properties for their application in environmental remediation<sup>138,139</sup>, catalysis<sup>140</sup>, water splitting and hydrogen generation<sup>141</sup>, supercapacitors,<sup>142</sup> Li-ion batteries<sup>143</sup>, and other electrochemical systems<sup>144,145</sup>. Apart from those applications, biosensing<sup>146</sup>, biomedical<sup>31</sup>, and drug delivery<sup>147</sup> are among the fastest emerging areas for carbon-based core-shell nanostructures. Due to the feasibility to tune the pore sizes, the ability to mimic natural porous systems, high dispersion of active sites, and large accessible surface area for reactions, carbon-based core-shell (CBCS) nanomaterials can deliver fast interfacial transport of reactant and products throughout the chemical reactions at different length scales of pores (macro-, meso- to micro-), and decrease the diffusion effect or bridge diffusion paths which can be proficiently beneficial in drug delivery and biomedical applications. Besides, hierarchical micro and mesopores that are linked to macropores and narrow micropores exposed right at the surface, resulted in large adsorption capacity and ultrafast adsorption/desorption efficiency, which is critical for surface reactions<sup>148</sup>. Porous carbon nanotubes (CNT), carbon nanofibers (CNF), carbon

nanospheres (CNS), and graphene oxides (GO) exhibit better adsorption ability and faster adsorption rate than the traditional carbon materials (for instance, activated carbons), owing to their narrow and uniform pore architecture<sup>149–151</sup>.

Depending on the position of carbon materials, CBCS nanomaterials can be separated into three broad categories i.e. carbon-carbon, carbon-support, and carbon core/carbon shell or hollow carbon<sup>152</sup>. The selection of carbon materials in the CBCSN is mostly reliant on the targeted application. Carbon-based concentric spherical core-shell nanomorphology is the most common, where a spherical carbon particle forms a core, and then completely coated by a carbon shell. Carbon materials can also be used as support materials for other core-shell nanomaterials loaded on its surface. Multiple core-shell morphologies are shaped when a carbon core material is covered with several small particles (or a carbon shell is coated onto several core particles). Above and beyond, it is also imaginable to fabricate a pure hollow carbon particle or a moveable core particle inside a uniform hollow carbon shell after a bilayer coating of the core and then take away the core material by using an appropriate removal technique. Carbon-based core-shell materials can also be formed by metals, metal oxides, semiconductors such as carbon/metal, and carbon/semiconductor or vice versa<sup>153–157</sup>.

Amongst entire multicomponent nanomaterials, CBCS nanomaterials have outstanding properties such as versatility in fabrication, low cost, tunable properties controllability, stability, dispersibility, and finally, improved electrical conductivity by the carbon phase and surfaced nanostructures. The removal or release of the carbon core and shell from core-shell structures can be performed by controlling the temperature, ionic strength, and environmental pH, which is an

imperative requirement in biomedical and drug delivery applications. For instance, Jinmyoung Joo and coworkers<sup>158</sup> demonstrated porous silicon–graphene oxide core-shell nanoparticle-based RNAi delivery platform that shields siRNA payloads counter to nuclease-induced degradation, and efficiently delivers drugs to target cells. Their developed nanocarrier was based on biodegradable mesoporous silicon nanoparticles, where the nanopores of the nanoparticles were loaded with siRNA. The nanoparticles were coated with GO nanosheets and it was reported that the GO coating helps in delaying the release of the oligonucleotide payloads *in-vitro* by a factor of 3.

The CBCS nanomaterials have two key advantages over the bare carbon-based nanomaterials. First, they own not only a high specific surface area and improved electrical conductivity than bare carbon-based materials, but also possess superior structural and mechanical stability owing to their core-shell architecture. Next, they are all great advantageous from short transport paths of ions and electrons, high accessible electroactive surface sites, rich mass-loading, and the attractive synergetic outcome of each constituent.

There are several strategies available for the synthesis of CBCS nanomaterials; particularly, the encapsulation and carbonization method is one of the modest methods to fabricate CBCSN composites. The approach of encapsulating metal nanoparticles into carbon shells is an efficient strategy which can prevent the corrosion of the metal nanoparticles in harsh environment (e. g., acidic media), and more importantly, it increases electrocatalytic reactions on the carbon surface via electron transfer from the encapsulated metal centers<sup>159,160</sup>. For example, a single gold nanoparticle core of diameter ca. 50-100 nm was encapsulated inside a porous carbon/Fe–Zn composite by Lu *et al.*, using metal-organic frameworks as carbon source<sup>161</sup>. The composition of Au core and Zn–Fe–C shell

morphology and the size of the gold nanoparticles were controlled without much difficulty. Cao *et al.*,<sup>162</sup> considered a new form of C/SiO<sub>2</sub> composite with a C–Si–C three-layered core-shell structure in a simplistic process, with mesoporous silica-coated by a carbon shell and core, and used for energy storage. In another approach, Dongshi Zhang and coworkers<sup>163</sup> fabricated carbon-encapsulated metal/metal carbide/metal oxide core-shell nanomorphology by using laser ablation of metals in organic solvents. They have employed 16 bulk metal targets (Cu, Ag, Au, Pd, Pt, Ti, V, Nb, Cr, Mo, W, Ni, Zr, Mn, Fe, and Zn) to demonstrate the realization of the metal carbonization, carbon encapsulation, and metal-catalyzed graphitization phenomena during laser-assisted core-shell material fabrication. It was also reported that owing to the weaker catalytic effect of Zn than Cu, the intermediate state of undeveloped onion-like carbon phase on Zn/ZnO particles was observed, which can be seen in Figure 7(I).

Similar to traditional chemical precipitation, atomic layer deposition (ALD) is a thin-film technique that can deposit materials layer by layer (LbL) pattern at the nanoscale on preferred substrates, and its competences have extended to the new directions together with sustainable energy<sup>164</sup>, catalysis<sup>165</sup>, and biomedical engineering fields in the last few years<sup>166,167</sup>. Recently, Gregorczyk *et al.*, demonstrated the fabrication process for a three-dimensional core-shell multiwalled CNT-RuO<sub>2</sub> morphology through a RuO<sub>2</sub> ALD process, which was used as a Li-ion battery electrode<sup>168</sup>.

Recently, several researchers developed sandwiched core-shell morphologies using carbon nanomaterials as core and covered different nanomaterials as shell or multi shell for advancement in drug delivery. In carbon-based sandwich core-shell type nanocomposites, carbon nanomaterials,

especially graphene, graphene oxide, and reduced graphene oxides sheets, are covered from both sides by different shell materials such as polymers and mesoporous silica. Such shell surfaces are capable to create pores for loading the drug, functionalization for targeting the site of action, targetability, control, and stimuli-responsive delivery. This enables several advantages and overcomes the limitation associated with carbon-based core-shell nano-systems. Wang *et al.*, reported the interesting graphene and silica sandwich nanocomposites. They prepared single layer graphene oxide – periodic mesoporous silica sandwich nanocomposites. They grew periodic mesoporous silica on both sides of GO sheets. Mesoporous channels were vertically aligned to GO surface. This sandwich nanocomposites showed semiconducting behavior with electrical conductivity sensitive to analyte vapor pressure, and hence, suitable for basic and applied research such as electrical stimulated drug delivery <sup>169</sup>. Chen *et al.*, developed NIR responsive drug delivery system utilizing RGO/Carbon/MPS nano cookies. The RGO/C/MPS system successfully delivered the anticancer drug camptothecin loaded (0.88 mmol/g) on NIR exposure. Nano cookies were biocompatible, cellular uptake, and within 14 days eradicated the subcutaneous tumor on a 5 min NIR irradiation. Nano cookies also suitable for diverse application in biomedical engineering and need to be explored <sup>170</sup>. Jiang *et al.*, developed tumor targeted photothermal heating responsive nanoplatform using nanocomposites composed of RGO/MPS/HA. Mesoporous silica was coated on RGO nanosheets, and hyaluronic acid acts as gatekeeper and targeting entity. This nanocomposite showed excellent biocompatibility, targeting efficiency, control delivery of drug (Chlorin e6, loading capacity 0.605 mg/mg), and NIR photothermal responsivity. The delivery of Ce6 enhances single oxygen generation and the destruction of target cancer cells. This nanosystem has great potential for multimodal cancer therapy <sup>171</sup>. Shao *et al.*, developed a nanosystem for targeted chemo-photo thermal therapy for cancer. The nanosystem was prepared through

mesoporous silica coated polydopamine functionalized RGO, which is further modified by hyaluronic acid (pRGO@MS-HA), and doxorubicin was used as a model drug. The nano-system showed good dispersibility, photothermal behavior, specificity, and performance to tumor cells. DOX release was achieved through pH-dependent and NIR laser irradiation. In addition, pRGO@MS(DOX)-HA nanosystem showed superior antitumor efficacy in vivo <sup>172</sup>.

Lately, many types of research on carbon-based core-shell fabrication using chemical vapor deposition (CVD) technology have been reported <sup>173–175</sup>. Other approaches, such as chemical bath deposition/electrodeposition<sup>176</sup>, solvothermal<sup>177</sup>, electrospinning/annealing<sup>178,179</sup>, and hydrothermal treatment<sup>180</sup>, etc. have been frequently employed in combination with the precipitation–deposition technique to fabricate CBCS nanomaterials.

## **8. Applications of Core-Shell Nanostructures**

Compared with single-phase nanoparticles, core-shell nanomaterials have numerous practical applications, particularly in the catalysis, electronics, and biomedical fields. In this section, core-shell nanoparticles applications in drug delivery and biomedical applications such as bioimaging and MRI have been discussed.

### **8.1. Core-Shell Nanostructures in Drug Delivery**

In the last 60 years, due to the development of an advanced healthcare system, life expectancy in several developed countries increased to 80-90 years. Hence, the focus of biomedical science and engineering shifted to nonpathogenic disorders such as cancer and AIDS. Most of the current research is also focusing on cancers. Other inline diseases after cancer are diabetes and

cardiovascular diseases<sup>181</sup>. In recent years, according to the American Cancer Society, the number of deaths associated with cancer found to be decreased in the USA<sup>182</sup>. This might be due to the development of effective techniques for early-stage detection of cancer and effective treatment development. Moreover, the lowered smoking rate is also a factor of consideration. However, cancer death statistics are moving towards worse in developing countries. Surgery, chemotherapy, radiation, and immunotherapy are the conventional treatments that are limited due to the lack of selectivity to access the cancer cells.

The combined treatment of the above-mentioned conventional therapies called multimodal therapy which has shown better chances of survival. Different nanocarrier systems such as dendrimers, micelles, emulsions, nanocrystal of the bare drug, and liposomes have been developed for the targeted delivery of drugs<sup>183</sup>. For a successful delivery system, nanoparticle-based drug delivery system should have unique properties such as suitable combination, particle size, shape, drug-nanoparticles interaction or loading types such as attached, adsorbed or encapsulation, surface chemistry, hydrophilicity, hydrophobicity, functionalization of surface, biodegradability, stimuli, and physical response such as temperature, pH, electric charge, light, sound, and magnetism<sup>184</sup>. The nature of coating is also important and depends on the desired molecule selected to develop a drug delivery system. Various bio-active molecules such as antibodies, peptides, enzymes, toxins, genes, growth factors, radionucleotides, folic acid, and drugs such as doxorubicin, cisplatin, paclitaxel, motoxantrone, tamoxifen, cefradine, ammonium glycyrrhizinate, fludarabine, danorubicin, gemcitabine, pingyangmycin, NSAIDs, amethopterin, mitomycin, diclofenac sodium, and adriamycin have been loaded through physical absorption or chemical functionalization for delivery applications<sup>183–186</sup>. The research and development moved from drug

development and formulation to controlled and targeted drug delivery system development with the high specificity of the site of action<sup>187</sup>. Due to very low therapeutic effectiveness of drugs in the treatment of cancer and static tumors, targeted delivery is one of the possible solutions to improve the effectiveness of drug delivery. The most challenging issue is the delivery of drugs to the active site in order to specifically affect the disease/disorder cells only<sup>188</sup>. Moreover, recent progress and development in science, engineering, and nanotechnology have been more customized for local delivery <sup>189</sup>.

### **8.1.1. Targeting**

Targeted delivery of a therapeutic cargo has two types: 1) active targeting, and 2) passive targeting. In active targeting, nanocarrier surface is decorated with ligands e.g. antibodies, peptides, and vitamins which have the ability to attach to respective receptors on the cell surface through receptor mediated endocytosis process<sup>190</sup>. This process comprises of three steps i.e., (i) binding the ligand with the receptor, (ii) formation of endosomes, and (iii) transfer of endosome at the desired site followed by release the drug under local physiological conditions such as pH or enzyme <sup>191</sup>. In passive targeting, natural conditions facilitate the drug to reach the target tissue or organ direct the drug to the site of action<sup>186</sup>.

Targeted drug delivery has several significant benefits: Firstly, it delivers the drug selectively to the targeted cells and hence minimize the toxicity and side effects. Secondly, it enables the delivery of highly potent drugs which may not be effective in nontargeted delivery form <sup>192</sup>. There are several targeted drug delivery formulations approved by FDA such as T-DM1, an antibody-drug conjugated system composes of trastuzumab emtansine. The maximum tolerated dose in rats and

monkeys are 40 mg/kg and 30 mg/kg respectively, which cannot be achieved through free drug delivery<sup>193</sup>. Third, the dose number and dose frequency will be low for targeted drug delivery formulation. Due to specific binding of ligands with receptor improve the distribution of drug and drug concentration at targeted tissue or cells, and it may allow a sustained release to improve the duration of therapeutic effect<sup>192</sup>. Furthermore, it is more important to select the ligand based on receptor as they are key components in targeted drug delivery. However, targeted drug delivery efficiency further depends on the receptor selection, receptor location, internalization mechanism of the receptor, the topography of receptor, and the competition of receptors. At the same time, ligands properties such as ligand size, ligands acceptability, topography, ligand binding affinity and specificity, strategies and chemistry involved between the ligand with the receptor, stability, ligand immunogenicity, and cost of formulations are also play key roles in the formulation of targeted drug delivery<sup>192</sup>. In some cases, a linker can be used for targeted drug delivery. The receptors such as glucose transporter 1 (Glut1), aminopeptidase N (APN), low density lipoprotein receptor related protein 1 (LRP1), Folate receptor (FR), and targeting ligands such as folic acid, angiopep2 are used in several targeted drug delivery formulations and some of them are under clinical trials<sup>192</sup>.

Considering targeted delivery, reaching nanocarriers to the targeted site is based on the nature of the targeting agent. In some cases, the drug cannot be easily released from the carrier system, or it is not possible to formulate the suitable drug delivery system due to the lack of feasibilities or limitations associated with drug or nanocarriers. In such cases, targeted delivery can be achieved through utilizing external and internal trigger which is called stimulus. The widely used stimuli are light, magnetic, ultrasound, electrical, and chemical<sup>187</sup>. In photo responsive targeted drug

delivery, photocleavable reactions, chemical bonds, photoisomerization, upconversion, photodynamic reaction, and photothermal effects are used. Au/MnO<sub>2</sub> nanoparticles are reactive to GSH (glutathione) or pH of the microenvironment in the tumor. The decomposition of the MnO<sub>2</sub> shell leads to the release of the drug. NIR light with an 808 nm laser is suitable for the degradation of MnO<sub>2</sub> <sup>194</sup>. In magnetic based targeted drug delivery heating, mechanical deformation and magnetic guidance are used. Cavitation, phase transition, and heating are the major techniques used in ultrasound assisted targeted drug delivery. Redox reactions are used in electrical field induced drug delivery, and chemical binding, interaction, and ligation are utilized in chemical changes-based drug delivery <sup>195</sup>. There are also internal stimuli such as reactive oxygen species, local pH, enzymes, and proteins. Kundu *et al.*, attempted chitosan grafted PAMAM-alginate core-shell nanoparticles (98-150 nm) for insulin (27% of insulin loading) delivery in an animal model. Both polymers are biodegradable and biocompatible. Results showed a pH-sensitive release of insulin and good protection from enzymatic deactivation in the GI tract. The in-vivo performance showed 11.78% of relative bioavailability in diabetic mice by oral administration <sup>196</sup>. Tao *et al.*, used angiopep-2-conjugated core-shell hybrid nano vehicle for pH-responsive delivery of Arsenic trioxide into Glioma <sup>197</sup>. Han *et al.*, developed the pH-responsive system for triple-stage targeted delivery of DOX to tumor <sup>198</sup>. In brief, tremendous progress has been made in this class of core-shell nanoparticle-based drug delivery systems. To overcome the issues associated with the path of drug delivery system, multi stimuli responsive drug delivery system can be used. Wang *et al.*, developed a dual responsive drug delivery system using polymeric yolk-shell nano capsules with UCNPs as core and PMAA as the shell <sup>131</sup>. Multi stimuli responsive targeted drug delivery is a more effective and complex system to reach the complex microenvironment such as brain. Several researchers reported the dual and triple responsive targeted drug delivery for cancer. However,

further innovative stimuli responsive delivery system needs to be developed to achieved facile targeting to complex systems such as brain and neural network to treat related diseases.

Core-shell nanoparticles are promising materials as nanocarrier systems for targeted drug delivery applications. The coating of biocompatible materials makes core-shell nanoparticles non-toxic and improves their pharmacokinetics behavior. The drug can be loaded into the shell or on the surface of the core-shell nanoparticle for delivery. Due to the high surface area of core-shell nanoparticles, high drug loading can be achieved. The surface of drug loaded core-shell nanoparticles further functionalized with targeting ligands. The ligands assist the nanosystem to reach the targeted receptor which exists at the site of disease. External stimuli are also used to facilitate the drug delivery system at the injured site. By using the stimuli such as pH, temperature, and light, due to the responsive nature of nanocarriers, the drug can be released from the delivery system at the site of action. Through labeling core-shell nanoparticles with magnetic or optical semiconductor nanoparticles, or fluorescence compounds, the delivery of drug can be monitored externally <sup>13</sup>. The targeted drug delivery system based on core-shell nanoparticle gives many other advantages such as combination of physicochemical properties of the core as well as shell <sup>185</sup>. Recently, Lu *et al.*, reported co-assembly of various proteins with poly(4-vinylpyridine) to prepare core-shell nanoparticles <sup>199,200</sup>. They demonstrated the preparation of core-shell nanostructures by the co-assembly of a pyridine-grafted diblock copolymer poly(caprolactone-graft-pyridine)-block-poly(caprolactone) [P(CL-g-Py)-b-PCL] and transferrin (as shown in Figure 7(II)) for targeted drug delivery of anticancer drug doxorubicin (DOX) <sup>201</sup>. Ying *et al.*, developed a magnetic nanocatalytic system compose of glucose oxidase loaded hollow iron oxide nanoparticles for starvation-chemodynamic-hyperthermia synergistic therapy for tumors. Fe<sup>2+</sup> generates ROS through the

Fenton reaction. The conversion of hydrogen peroxide into oxygen enhances oxygen levels. In-vivo results showed effective inhibition of tumor growth in PC3 tumor bearing mice <sup>202</sup>. Hosseine *et al.*, delivered the DOX using a double-layered core-shell ( $\text{Fe}_3\text{O}_4$  core and Salep as the shell) magnetic nanoparticles <sup>203</sup>. The outcomes of this research showed that the cellular uptake is time-dependent, and internalization is through the endocytosis process. The most interesting core-shell nanoparticles based targeted drug delivery systems also presented in Tables 1 to 5. Several formulations are at the stage of clinical trials. However, many targeted drug delivery systems have excellent performance in lab-scale, but their application is limited due to difficulties at industrial scale, commercialization, unknown long-term side effect, and being very expensive.

### 8.1.2. Drug Loading and Releasing

To achieve the desired therapeutic effectiveness, the drug delivery system should have high drug loading capacity. Drug loading can proceed in two different strategies: 1) incorporating the drug candidate during the formulation of nanoparticles or nanocarrier system, and 2) adsorption or absorption of drug after formulation of nanoparticles or nanocarrier system. Through incubation of nanocarrier in a solution of drug with the desired concentration, drug adsorption/absorption can be achieved. Drug loading mainly depends on drug solubility, nanocarriers composition, the interaction of drugs with nanocarriers, availability of functional group nanocarrier and/or drug which facilitate the interaction<sup>187</sup>.

At the same time, releasing the targeted drug from the drug delivery system is an important step to achieve effective therapy. Drug release can be burst release, sustain release, long term release, and uncontrolled release <sup>204,205</sup>. The drug release kinetics depends on the drug desorption

efficiency, degradation of nanocarriers, interaction strength, physicochemical behavior, the stability of nanocarriers at physiological conditions, and diffusion and/or erosion of nanocarriers. The weak interaction between drug and nanocarrier enables the burst release of the drug. Mostly in the case of bare drug nanoparticles, the drug absorbed on the surface of nanocarriers exhibits a burst release profiles<sup>206,207</sup>. Drug loaded on the pores of the shell of core-shell nanoparticles such as mesoporous silica coated magnetic nanoparticles allows sustained release of the drug, as the drug is trapped in the porous structures<sup>208</sup>. So, the drug initially releases from the pores far from the core material followed by drug from the depth of the pore. To achieve further sustain release or long-term release, drug loaded mesoporous shell surface can be coated with different materials such as polymers or other stimuli responsive materials. Such system hold the drug in a pore and release the drug at the site of action where the physiological conditions remove the coating materials from the pore and allow the drug to release<sup>209</sup>. Liu *et al.*, formulated  $\text{Fe}_3\text{O}_4@\text{mSiO}_2@\text{lipid-PEG-methotrexate}$  nanoparticles chemo photodynamic therapy. Both in vitro and in vivo results showed improved tumor accumulation of Dox, cellular uptake, and anticancer activity<sup>209</sup>. Formulations such as drug encapsulated inside the nanocarriers, the release of drugs mainly depends on the degradation of nanocarrier system<sup>206,210–213</sup>. Different nanocarriers follow different degradation kinetics and drug releases accordingly. Mostly, polymeric nanocarrier undergo degradation, diffusion, and/or erosion. Molecular weight, size, and ration of copolymers affects the release of drug from polymers<sup>214</sup>. Hence, the selection of drug and nanocarrier system is very crucial for successful drug loading and releasing for effective therapy for which polymers and lipids are on high priority.

Core-shell nanoparticles system mostly allows loading on the drug on shell materials. Compare to bare nanoparticles based nanocarriers, core-shell nanoparticles system provides higher drug loading capacity. Several core-shell nanoparticles used in drug delivery are presented in tables 1 to 5 along with drug loading capacity. From tables 1-5, among the several magnetic core-shell nanoparticles, mesoporous silica coated magnetic nanoparticles based nanocarriers showed higher drug loading capacity. The  $\text{ecc-(con-Fe}_3\text{O}_4\text{@mSiO}_2\text{)}\text{@PAA}$  and  $\text{Fe}_3\text{O}_4\text{@SiO}_2$  core-shell nanoparticles achieved 90% and 86.5 % of drug loading, respectively<sup>74,215</sup>. This is due to the large pore area and high thickness of the shell compare to other shell materials. Moreover, mesoporous silica nanoparticles coated with polymer (MSNs-PLH-PEG) and/or lipid (lipid coated  $\text{MSN@p(NIPAM-co-MA)}$ ) showed excellent drug loading efficiencies 22.5 and 56 wt%, respectively<sup>216,217</sup>. The core-shell Au/MnO<sub>2</sub> nanoparticle prepared by Zhang *et al.*, showed excellent biodegradability, and drug DOX loaded through electrostatic interaction, hydrogen bonding, physical absorption, and achieved 99.1 % of drug loading. Kumar *et al.*, utilized the Diels-Alder chemistry (Figure 8I) to load the siRNA on the surface of the Au-Ag-Ag core-shell nanoparticles. siRNA release through photothermal cleave of siRNA from surface<sup>218</sup>. It concludes that releasing of the drug is more critical than loading. The different diseases demand different drug release kinetics. Hence, formulation with controllable and tunable rate of release is on demand.

### 8.1.3. siRNA delivery

SiRNA is an emerging class of bio-active compounds which can act like a drug of selective and high efficacy. Several studies reported the potential of siRNA such as inhibiting the HIV life cycle<sup>219</sup>. Furthermore, siRNA targets a range of proteins, and hence can be utilized for gene to treat

several diseases by silencing related genes. SiRNA targets the gene such as VEGF, RSV, p53, HBV, and RTP801<sup>220,221</sup>. SiRNA is also used for various cancer such as pancreatic, liver, breast, lung, cervical, and ovarian cancer<sup>221</sup>. Interestingly, After the understanding of the mechanism of RNAi, siRNA entered in clinical trials within 10-year.

However, there are several remaining challenges for siRNA such as effecting “off target” gene expression which leads to potential toxicity. Hence, the selection of siRNAs is crucial for therapeutic application, and several parameters are required to be considered such as internal repeated sequences, GC content, preferred base position, and length<sup>222</sup>. This can be overcome by developing the computation process to identify the off targets interaction of siRNA. Moreover, naked siRNA delivery at the site of action is a major hurdle due to rapid degradation by enzymes in plasma, renal elimination, and the limited capacity of uptake by tissue cells.

In the last 15 years, several strategies have been developed for the delivery of siRNA. Different strategies-based delivery systems have been reviewed by several researchers. Here, our major focus is core-shell nanoparticles and we have discussed the core-shell nanoparticles-based delivery of siRNA. The successful siRNA delivery system should be biocompatible, biodegradable, nonimmunogenic, efficiently delivered to the target cell, provide protection, and the capability of endocytosis. The widely used nanocarriers system for delivery of siRNA is lipid based nano-systems such as liposomes, micelles, emulsions, and solid lipid nanoparticles<sup>223</sup>. Cationic lipids are the best choice due to their favorable interaction with siRNA<sup>224</sup>. Another promising nanocarrier is polymer-based nanoparticles such as PEI, PLL, cyclodextrin, chitosan, atelocollagen, and cationic polypeptides<sup>225</sup>. Similar to cationic lipids, cationic polymers are the

best choice for siRNA delivery. SiRNA forms polyplexes with cationic polymers and lipoplexes with cationic lipids. Hence, lipid and polymer coated core-shell nanoparticles are the widely studied and promising candidates as nanocarriers for siRNA delivery<sup>226</sup>. Interestingly, core-shell nanoparticles designed with the positively charged surface are more likely to allow loading of siRNA due to the strong affinity towards the positive charge. Yin *et al.*, utilized multifunctional magnetic core-shell ( $\text{ZnFe}_2\text{O}_4@\text{mSiO}_2$ ) nanoparticles for micro RNA therapeutics with anticancer drugs. The *in vivo* studies on tumor-bearing nude mice (Figure 8(III)) suggested the higher rate of tumor inhibition compared to DOX alone<sup>227</sup>. Interestingly, no change in mice body weight was observed. Gao *et al.*, used core-shell type lipid/rPAA-Chol polymer hybrid nanoparticles for siRNA delivery<sup>228</sup>. Feng *et al.*, reported the co-delivery of VEGF siRNA and paclitaxel by vapreotide modified core-shell nanoparticles for synergistic inhibition of breast cancer<sup>229</sup>. Vapreotide is a targeting agent. Wei *et al.*, delivered siRNA to brain tumors with transferrin receptor mediated core-shell nanoparticles<sup>230</sup>. He *et al.*, utilized aggregation induced emission luminogen (AIE) as shell on Ag nanoparticles core. Core-shell Ag@AIE nanoparticles showed excellent delivery of siRNA, target gene knockdown, and cancer cell inhibition *in vitro*.<sup>231</sup> Wang *et al.*, developed transdermal delivery of siRNA using microneedle patches composed of UCNPs@mSiO<sub>2</sub>. Due to photoluminescence behavior, UCNPs core allows tracking of microneedles skin penetration through imaging<sup>232</sup>. Shi *et al.*, designed core-shell lipid-polymer-lipid hybrid nanoparticles for delivery of siRNA<sup>233</sup>. Kumal *et al.*, studied the NIR photothermal release of siRNA from the surface of Au-Ag-Ag core-shell-shell (CSS) nanoparticles. SiRNA attached to the surface of nanoparticle through Diels-Alder chemistry (Figure 8I). Results revealed that the photothermal cleave of siRNA from CSS nanoparticle is significantly higher than the bare gold nanoparticles<sup>218</sup>. Based on literature reports and best of our knowledge, we observed that, it

is always recommended to formulate the nanocarrier system with positive surface charge for successful siRNA delivery.

#### **8.1.4. Biomedical evaluation (*in-vitro* & *in-vivo*)**

For a couple of decades, tremendous progress has been evolved in the field of core-shell nanoparticles and their application in drug and gene delivery, as reflected from continuously increasing research papers. Besides, the number of patents and formulations entering clinical trials is also increasing over time. However, the studies from bench to market is very limited and very few in comparison with publications. Biomedical evaluation is the major hurdle where most of the formulations have been failed. The main reason for failure is the differences between biological evaluation in the lab and physiological condition in the human body. Hence, very frequently, *in vivo* performance is poor compared with *in vitro*. However, several nanotechnology based formulations have already been approved for treatment such as nanomedicines<sup>234–239</sup>. We have comprehensively summarized the various nanoparticles based drug and formulation approved by FDA and available in the market commercially in our recent review<sup>240</sup>. Compare to nanoparticle-based formulations, core-shell nanoparticles-based formulation for drug delivery or targeted drug delivery are limited. Chatterjee *et al.*, comprehensively reviewed the biomedical application of core-shell nanoparticles. They have summarized the different core-shell nanoparticles, surface modifications, conjugation of ligands on the surface, and their application in biomedical use<sup>31</sup>. They thoroughly discussed the different nanomaterials such as metals, metal alloys, oxides, semiconductor, lanthanides, organic core such as polymer core-based core-shell nanoparticles. The applications of core-shell nanoparticles range from drug delivery, gene silencing, gene transfection, optical imaging, MRI, and biosensors<sup>31</sup>.

Recently, He *et al.*, demonstrated inorganic-organic core-shell nanoparticles (Ag@AIE) for SiRNA delivery with high efficiency, low cytotoxicity, and real-time monitoring feasibility<sup>231</sup>. The *in-vivo* studies (Figure 8II) by intra-tumoral injection to tumor-bearing mice showed that intense fluorescence signal was observed at the tumor site even after 24 h. Further ex-vivo fluorescence imaging of isolated tissues suggested the effective accumulation of core-shell nanocarriers in tumor tissue. Moreover, strong inhibition of tumor growth was observed after 18 days of treatment. Biodistribution studies further supported the excellent *in-vivo* biocompatibility of nanoparticles<sup>231</sup>. Lin *et al.*, developed a cyclodextrin-based supramolecular core-shell nanocapsule for magnetothermal chemotherapy. Cellular uptake studies revealed that compared to DEC, P-DEC showed a larger number of capsules absorbed on the cell, and residing in the cells suggested the P-DEC feasibility to localize effectively with the cancer cell without any targeting entities (Figure 9I). This is due to a change in surface properties, as it is well-known that negative charge particles (P-DEC) diffuse faster and perform better in drug delivery compared to positive or neutral charge particles (DEC)<sup>241</sup>. *In-vivo* biodistribution studies showed results similar to *in vitro* performance. Specifically, both P-DEC and PTX-CD-HA accumulated stronger in tumors even after 48 h of injection (Figure 9II). Compared to PTX-CD-HA, P-DEC showed 20 fold higher accumulation in tumor, determined by the intensity of fluorescence<sup>241</sup>. Qin *et al.*, investigated the double layer core-shell nanoparticles to deliver PTX. Self-assembly of mPEG-g-CS envelope on PLGA nanoparticles system was formulated, and *in vitro* and *in vivo* antitumor activity was evaluated<sup>242</sup>. *In-vitro* studies showed no influence on the cell viability on MCF-7 and HUVEC cells even at a concentration of 1000  $\mu\text{g}/\text{mL}$  for 48 h. Efficient cell internalization was observed in confocal imaging. Core-shell nanoparticles on intravenous injection to nude mice bearing MCF-7 breast tumor showed improved antitumor and antiangiogenic effect, longer retention time,

improved distribution, and reduction of the density of micro vessels in tumor tissue was observed. Figure 10 presents the tissue distribution of CyS labelled NPs in tumor breaking nude mice <sup>242</sup>.

Above paragraphs summarize that compare to several core-shell systems, polymer and lipid based core-shell nanoparticles are in the front line in entering the clinical trial due to biocompatibility, biodegradability, non-toxic nature, and tunable physicochemical properties of polymers. Hence, further careful biomedical evaluation tools need to develop, and studies should be conducted thoroughly to understand the cytotoxicity effect of formulations. Moreover, recently developed 3D biomedical models needed to be in use with the aim to develop next generation nano-therapeutics.

## 8.2. Core-shell Magneto-electronic Nanomaterials for Drug Delivery

Magneto-electric nanoparticles (MENPs) are the core-shell nanoparticles and are known to exhibit tunable magnetic and electric properties<sup>243</sup>. Small size and tunable properties make MENPs suitable for various biomedical applications, mainly site-specific drug delivery <sup>9,10,244–246</sup>. One of such smart functionalized nano-system is MENPs composed of  $\text{CoFe}_2\text{O}_4$  as core and  $\text{BaTiO}_3$  as shell <sup>244</sup>. The ferromagnetic core and piezoelectric shell ( $\text{BaTiO}_3@ \text{CoFe}_2\text{O}_4$ ) make these nano-systems responsive to ac-magnetic stimulation. The ac-magnetic field stimulation causes polarization attributed to MENPs surface charge change and acoustics due to magneto-acoustics. These controlled features may be useful to achieve high cell-uptake, magnetically guided drug delivery, on-demand drug release, image-guided therapy, etc<sup>243</sup>. Keeping these aspects in mind, our group has utilized MENPs-assisted drug delivery systems for central nervous system (CNS) diseases, including management of neuroHIV/AIDS in management manner <sup>9,10,244–246</sup>. The MENPs based pharmacologically relevant therapeutic charge was designed and delivered across

the blood-brain barrier (BBB) with ac-magnetic field stimulation based on-demand release of a targeted drug <sup>247</sup>. The nanoformulation of MENP found to be responsive to ac-magnetic field and releases a targeted drug (AZTTP, Beclin1, CRISPR Cas9/gRNA) on stimulation, which causes rapid polarization variation between the bond formed between drug and MENPs (Figure 11(I)). The MENPs based nanoformulation was more effective than the pure drug due to easy cell uptake caused by the generation of magneto-acoustic by MENP on-magnetic field stimulation at the cell surface. (Figure 11(II)) <sup>248</sup>. These MENPs demonstrated all the desired features if we keep the aspects of a smart drug nano-carriers in view. To develop a nano-therapy, it becomes very crucial to deliver MENPs to the brain of small animals, i.e. mice <sup>249</sup> (Figure 11 III) and non-human primates, i.e. monkey, baboon, etc., <sup>250</sup> using the approach which in drug delivery is magnetically guided. The results of studies confirmed that the MENPs could be delivered to the brain of mice and baboons, and drug nano-carriers were uniformly distributed in the brain. Exploring the biocompatibility of MENPs is also crucial to present them as a potential drug nano-carrier <sup>188</sup> (Figure 11 IV). This group has explored the bio-distribution of MENPs in the brain, histology, blood toxicity profiling, and neurobehavior assessment. The outcomes suggested that MENPs were distributed in all cell types without agglomeration and without affecting tissues health and hepatic and renal function of animals. Keeping advancements in view, bio-compatible, and stimuli-responsive MENPs have the potential to promote advanced biomedical applications due to multi-functionality.

### **8.3. Core-Shell Nanostructures in Magnetic Resonance Imaging (MRI)**

MRI is one of the powerful bioimaging tools commercially available. It produces images of internal organs of the human body with high quality. The main use of this technique is for the

detection of inflammation, infection, degenerative diseases, tumors, and irregularities that exist in tissues or organs. The working principle of MRI is based on nuclear magnetic resonance and radiofrequency pulses<sup>251</sup>. A contrast agent is a major component in MRI imaging. Lanthanide and transition metals are ideal candidates as contrast agents in MRI bioimaging due to their paramagnetic nature<sup>252</sup>. The most common contrast agent is gadolinium (Gd)-based compounds because of large magnetic moments. The Gd-DTPA (diethylenetriamine penta-acetic acid) is a commercially available contrast agent<sup>253</sup>. Based on imaging modality, contrast agents are classified into two categories i.e.  $T_1$  and  $T_2$ .

Core-shell nanoparticles can be used as  $T_1$  and  $T_2$  contrast agents. Gadolinium oxide ( $Gd_2O_3$ ), gadolinium fluoride ( $GdF_3$ ), and sodium gadolinium phosphate ( $NaGdF_4$ ) are used as MRI contrast agents<sup>254–256</sup>. It was reported that surface coating enhances the contrast properties of Gd compounds. Silica coated Gd core-shell nanoparticles showed excellent properties<sup>257</sup>. MnO doped  $Gd_2O_3$  nanoparticles showed enhanced contrast properties in mouse<sup>258</sup>. The major issue with Gd based core-shell nanoparticle is the toxicity of Gd in ionic form, and risk is associated with the replacement of Zn and Cu ions. Moreover, Gd has no biochemical cycle, so that it accumulates inside the body<sup>259</sup>. Recently, several contrast agents have been reported such as Mn, Fe, and Cu chlorides<sup>260–262</sup>. Core-shell nanoparticles of mesoporous silica-coated hollow MnO nanoparticles showed superior performance<sup>263</sup>. Several Iron-based magnetic core-shell nanoparticles also attracted considerable attention. Iron-carbon,  $Fe_3O_4$ -Au, FePt- $Fe_2O_3$  core-shell, and  $Fe_3O_4$ -polymer-Au core-shell-shell nanoparticles are few of magnetic core-shell nanoparticles recently developed as contrast agent in MRI bioimaging<sup>264–266</sup>. Superparamagnetic nanoparticles and core-shell superparamagnetic nanoparticles are promising nanoparticles as  $T_2$  contrast agents in MRI.

Lee *et al.*<sup>267</sup> fabricated biocompatible multifunctional  $\text{Fe}_3\text{O}_4/\text{TiO}_x$  core-shell nanoparticles and injected those particles intravenously to a rat with a tumor for MRI and computed tomography (CT). The observed tumor-associated vessel with core-shell nanoparticles using CT and magnetic resonance imaging disclosed the high and low vascular regions of the tumor, respectively. Figure 12(I) describes the strategy for synthesis and modification of  $\text{Fe}_3\text{O}_4/\text{TaO}_x$  core-shell NPs together with the actual TEM micrographs. Recently, Tiwari *et al.*, developed the method for fabrication of multifunctional core-shell superparamagnetic iron oxide nanoparticles as the core, and carbon as shell, through the hydrothermal method. The authors have demonstrated excellent performance in drug delivery in vitro, in vivo, and MRI imaging<sup>50,57</sup>.

#### 8.4. Core-Shell Nanoparticles for Bioimaging

Bioimaging is facilitating a multi-functional approach to monitor the delivery and performance of a developed drug delivery system specific to a targeted disease. Bioimaging technique is a key technology that is used in diagnosis, treatment, and disease prevention. For bioimaging, several techniques have been developed such as optical imaging, magnetic resonance imaging, ultrasound imaging, positron emission tomography, and other techniques for both in vitro and in vivo bioimaging and drug delivery<sup>268–271</sup>. Optical and MRI imaging are widely used and acceptable. Various types of nanomaterials are used for bioimaging<sup>272</sup>. In compared with bare metallic nanoparticles such as gold, silver, and other metallic and metal oxide nanoparticles, core-shell nanoparticles are more interesting due to the feasibility to tuning the optical properties and flexibility to use optical active materials as core or shell. Yang *et al.*, formulated core-shell chitosan microcapsules compose of PLGA nanoparticles and drug for programmed sequential drug release. Acid responsive drug release behavior from microcapsules was studied using CLSM. Figure 12(II)

shows the CLSM images of different core-shell chitosan microcapsules<sup>108</sup>. Figure 12 (III) shows CLSM microscope images of acid responsive release process from microcapsules. One is microcapsules containing free curcumin and curcumin loaded PLGA nanoparticles. Another one is microcapsules containing free RhB and RhB loaded PLGA nanoparticles<sup>108</sup>. He *et al.*, formulated Ag@AIE core-shell nanoparticles for siRNA delivery and real-time efficiency was monitored using fluorescence microscopy. Figure 12(IV) presents the confocal fluorescence microscopy images of cellular uptake and intracellular distribution and real-time monitoring images of siRNA delivery in HeLa cells. The perfect overlap of FAM and Ag@AIE suggested the tight binding of siRNA with nanoparticles, which helps protecting enzyme from degradation during endocytosis<sup>231</sup>. However, among the various core-shell nanoparticles, magnetic and upconversion core-shell nanoparticles are promising candidates over polymeric and silica-based core-shell nanoparticles. Magnetic nanoparticles and their use in MRI discussed in previous section<sup>273</sup>. Recently, UCNPs have been gained significant interest. UCNPs are composed of host matrix, sensitizer, and activator. UCNPs such as NaYF<sub>4</sub>, NaGdF<sub>4</sub>, NaLuGdF<sub>4</sub>, Y<sub>2</sub>O<sub>3</sub>, Y<sub>2</sub>O<sub>2</sub>S, and GdOCl are the most promising UCNPs with excellent optical behavior such as low phonon energy and good stability. Yb<sup>3+</sup> exhibits two-photon absorption, and Er<sup>3+</sup>, Tm<sup>3+</sup>, Ho<sup>3+</sup>, Tb<sup>3+</sup>, Eu<sup>3+</sup>, Dy<sup>3+</sup>, Sm<sup>3+</sup>, and Gd<sup>3+</sup> have been used as sensitizers and activators. Energy transfers from Yb<sup>3+</sup> to activator upon excitation with suitable laser<sup>274</sup>. The degree of energy transfer can be tuned or enhanced by a proper selection of host matrix, activator, and sensitizers. In the last decades, UCNPs have extensively used as potential bioimaging candidates in imaging techniques such as fluorescence, ultrasound, Raman, and multimodality imaging. UCNPs work based on NIR light, which has several benefits such as less photodamage and deep penetration capability, and low phototoxicity, autofluorescence, and light scattering. The biocompatibility and optical properties

can be tuned through modification of the surface such as coating with inorganic or organic materials e.g. mesoporous silica and polymers. Several UCNPs used for drug delivery and bioimaging applications are presented in Table 4. UCNPs such as NaYF<sub>4</sub>:Yb<sup>3+</sup> used for loading of cisplatin on silica shell to deliver to the tumor through chemo-/radiotherapy <sup>275</sup>. The NaYF<sub>4</sub>:Yb<sup>3+</sup>/Tm<sup>3+</sup>@Fe<sub>3</sub>O<sub>4</sub> core-shell nanoparticles showed potential use in lymphatic imaging <sup>276</sup>. Multifunction UCNPs Fe<sub>3</sub>O<sub>4</sub>@NaLuF<sub>4</sub>:Yb<sup>3+</sup>, and Er<sup>3+</sup>/Tm<sup>3+</sup> are used as multimodal imaging in vitro and in vivo by Zhu et al <sup>277</sup>. There are a large number of reports on UCNPs used in bioimaging. Recently, Rafique *et al.*, comprehensively reviewed the UCNPs for bioimaging applications <sup>274</sup>. However, there are major challenges such as the formulation of aqueous soluble UCNPs, and thus, UCNPs based imaging technique need to be developed for single molecular imaging, and facile synthesis and surface modification strategies.

To overcome the limitations associated with UCNP, advanced functional nanoparticles, known as persistent luminescence nanomaterials, have recently been developed. The PLN showed luminescence for a certain period of time even after excitation was stopped. In this process, PLN gains and stores energy during the excitation, and released later even in the absence of excitation. The time of PL depends on the storage capacity of PLN. Hence, they allow continuous bioimaging to understand the performance of formulation in vivo. The most well-known PLNs are ZGGO@SiO<sub>2</sub>@LRM <sup>134</sup>, ZnGa<sub>2</sub>O<sub>4</sub>:Cr<sup>3+</sup>,Sn<sup>4+</sup> <sup>133</sup>, Zn<sub>1.1</sub> Ga<sub>1.8</sub> Ge<sub>0.1</sub> O<sub>4</sub>:Cr<sup>3+</sup> <sup>135</sup>, Gd<sub>2</sub>O<sub>3</sub>@mSiO<sub>2</sub>@CaTiO<sub>3</sub>:Pr <sup>136</sup>, and MSNs@CaTiO<sub>3</sub>:Pr<sup>3+</sup> <sup>137</sup>. Li *et al.*, achieve 12 minutes of continuous optical imaging after injection using PLN MSNs@CaTiO<sub>3</sub>:Pr<sup>3+</sup> by exciting 614 nm UV irradiation <sup>137</sup>. The Gd<sub>2</sub>O<sub>3</sub>@mSiO<sub>2</sub>@CaTiO<sub>3</sub>:Pr nanoparticles functionalized with PEG, showed an improved *in-vivo* imaging capacity up to 20 minutes <sup>136</sup>. Further functionalization

reduced toxicity and enhanced biocompatibility. PLN of core-shell nanoparticles is more interesting; however, further studies may enhance the continuous bioimaging capabilities.

## 9. Summary

This review highlights various core-shell nano morphologies towards effective drug delivery and biomedical applications with the help of approximately two hundred appropriate and representative researches (Figure 13). It was evident that core-shell nanoparticles of dissimilar core and shell materials are interesting nanocarriers due to the desired and tunable physicochemical properties of both core and shell counterparts. Among several types of core-shell nanoparticles, magnetic core-shell nanoparticles are a promising applicant for controlled, sustained, and targeted drug delivery systems to investigate nano-therapeutics. Mesoporous silica is another desired material of choice for investigating shell required to formulate advanced core-shell nanoparticles. In terms of easy fabrication, coating of a core using silica as a shell is simple, facile to control the thickness and potential of scaling up ability. It is also very expedient to control porous nanostructures with tunable pore size to extract further advantages out of the silica coatings, owing to the availability of hydroxy groups that make them precedence as the shell. Recently, carbon-based core-shell nanoparticles have been attracted huge attention in the drug delivery and bioimaging field. Porous CNT, carbon nanofibers, carbon nanospheres, and graphene oxides show improved adsorption ability and faster adsorption rate than the traditional materials, owing to their narrow and uniform pore architecture and accordingly applications.

This review also concludes that polymeric core-shell nanoparticles are also a good choice. However, the use of renewable biopolymer needs further investigation. Furthermore, upconversion

nanoparticles are also gaining more interest lately due to their advantages over optical properties but limited to lanthanide metals only. The core-shell metallic nanoparticles are not well-established in the biomedical areas due to the limitation of physicochemical properties, which make them more challenging. Moreover, the toxicity of metal-metal core-shell nanoparticles is a major concern that needs to be considered, and thorough investigation and analysis are needed before implementing in vivo and clinical studies.

Due to tunable properties, stimuli responsiveness targeted delivery even to the brain, and its biocompatibility, we believe that these core-shell nano-systems are the potential candidates to develop next-generation theranostics in a personalized manner. Though, focused and dedicated efforts are required to achieve objectives as claimed. This review is an attempt to present the potentials of core-shell nano-systems to develop next-generation multi-functional combination therapies, that mainly include image-guided therapy, stimuli-responsive multi-tasking therapeutics cargos, controlled drug release, real-time diseases monitoring, etc. Overall, core-shell assisted therapies can be manageable to design and develop treatment in a personalized manner. Though, significant future researches need to be planned and requested through this report.

## 10. Future Outlook

The impact of core-shell nanoparticles is of high significant drug delivery, biomedical, and tissue engineering <sup>278,279</sup>. The safe and effective chemotherapy delivery methods of core-shell nanoparticles can be modified to have diverse biological features and can be used in a variety of settings <sup>280</sup>. Approximately 12,000 reports were published in the past decade on the topic of nanomaterials as carriers of drugs over cancer treatment <sup>281</sup>. During the last 50 years, numerous nanodrugs have been created (Figure 14). Despite such developments, there remains a gap between

advances in technology and clinical applications. For instance, we know that certain nanoparticles deliver siRNA, mRNA, or CRISPR drugs to a mouse cell that is regulated by certain genes<sup>282,283</sup>. Is the delivery of the drugs in a mouse is viable or predicts the same for humans? Can the same nano-drug (animal-tested nano-drug) predict the efficacy and safety in human beings? Based on the size of the nanoparticles used as nano-drug delivery may cause severe or mild side effects e.g. inflammation, rashes, reverse immune responses, or toxicity reduction while maintaining therapeutic effects, safety, biocompatibility, etc., respectively<sup>284</sup>. Can the size of the nanoparticles used in drug delivery be compromised? However, the research has so far missed the scientific paradigm of potential (adverse) nanopartic reactivity and we have no understanding of the basics of the relationship between nanoparticles and living cells, organs, and species. The form of hazards that are added by nanoparticles in medicine is beyond that presented by traditional hazards caused by chemicals. In terms of the biological interactions with nanoparticles, the key emerging issue is those particles of little or no solubility or are not degradable at the place of aggregation. Nanoparticles and biological systems are still communicating in many unclear aspects.

### Tables

Table 1. Recent advancements in magnetic core-shell nanoparticles system in drug delivery.

S. No.	Core-Shell nanoparticle system	Description	Particle size	Drug loading	Comments	References
1	Fe <sub>2</sub> O <sub>3</sub> @PNIPAM	Fe <sub>2</sub> O <sub>3</sub> @PNIPAM nanoparticles used for doxorubicin delivery	43 nm	2.5 % of the total weight of drug nanoparticles	Thermo responsive drug delivery system	<sup>285</sup>
2	Fe <sub>3</sub> O <sub>4</sub> -SCH <sub>2</sub> CH <sub>2</sub> CONHN=C-DOX+ smart polymer	Fe <sub>3</sub> O <sub>4</sub> nanoparticles functionalized with 3-mercaptopropionic acid hydrazide (HSCH <sub>2</sub> CH <sub>2</sub> CONHNH <sub>2</sub> ) then Dox was attached and encapsulated into smart polymer dextran-g-poly(NIPAAm-co-DMAAm)	5-8 nm	~9 % weight of drug in carrier	Temperature (LCST 38 C) and pH responsive drug delivered of DOX	<sup>286</sup>
3	M-MSN(Dox/Ce6)PEM/-gp	Magnetic mesoporous silica nanoparticles (M-MSNs) then photosensitize Ce6 and antitumor drug Dox absorbed. Then alginate/chitosan polyelectrolyte multilayer (PEM) assembled	280 nm		pH responsive drug delivered, good biocompatible and low toxicity	<sup>66</sup>
4	F127-MNPs nanospheres	Magnetic iron oxide nanoparticle embedded in thermo sensitive Pluronic F127	10-20 nm	DOX	High frequency magnetic field responsive delivery	<sup>70</sup>
5	Fe <sub>3</sub> O <sub>4</sub> @PMAA@PNIPAM	Superparamagnetic Fe <sub>3</sub> O <sub>4</sub> nanoparticles coated with stimuli responsive polymers PMAA and PNIPAM	~100 nm	29.8 % Dox loading	Multi stimuli (Reduction/pH/temperature) responsive nanoparticles for targeted and control antitumor drug delivery	<sup>72</sup>

6	Ecc-(con- Fe <sub>3</sub> O <sub>4</sub> @fmSiO <sub>2</sub> )@PA A NCs	Multifunction fluorescent magnetic pH responsive eccentric(concentric- Fe <sub>3</sub> O <sub>4</sub> @SiO <sub>2</sub> ) polyacrylic acid core - double shell nanocomposite	127 nm	90% in 10 mg/mL	pH responsive drug delivery	74
7	Fe <sub>3</sub> O <sub>4</sub> @SBA-15	Magnetic iron oxide nanoparticle loaded in mesoporous silica nanoparticles for aspirin delivery	500 nm	13 wt%	Biocompatible with L929 fibroblast cells, sustain release of aspirin in vitro	79
8	Fe <sub>3</sub> O <sub>4</sub> @SiO <sub>2</sub>	Doxorubicin grafted SiO <sub>2</sub> coated Fe <sub>3</sub> O <sub>4</sub> nanoparticles	~50 nm	86.5 % (144.2 ug per milligram Fe <sub>3</sub> O <sub>4</sub> @Si O <sub>2</sub> nps	Magnetic targeted drug delivery	215
9	Fe <sub>3</sub> O <sub>4</sub> @nSiO <sub>2</sub> @mSi O <sub>2</sub>	Fe <sub>3</sub> O <sub>4</sub> microspheres encapsulated in nonporous silica and further coated with mesoporous silica. Surface further functionalized with YVO <sub>4</sub> :Eu <sup>3+</sup> phosphors	350 nm	125 mg/g	Magnetic, luminescent and mesoporous core-shell trackable and monitorable nanocarriers for drug delivery of ibuprofen	287
10	Fe <sub>3</sub> O <sub>4</sub> @MSNs- PNIPAAm	Thermo responsive polymer PNIPAAm coated magnetic mesoporous silica nanoparticles	190 nm	220 nm	Magnetic, reductive and thermo responsive that is triple responsive drug delivery system for DOX	288
11	Fe <sub>3</sub> O <sub>4</sub> @nSiO <sub>2</sub> @mSi O <sub>2</sub> -APTES	Nonmesoporous silica coated Fe <sub>3</sub> O <sub>4</sub> nanoparticles as core and mesoporous silica as shell nanoparticle system functionalized with APTES for delivery of VP16 natural medicine etoposide as a model anticancer drug	167 nm core	10 mg (0.017 mmol)	Investigate the interaction force between drug and nanocarriers on drug loading and release process	97
12	Fe <sub>3</sub> O <sub>4</sub> @mSiO <sub>2</sub> @Au	Mesoporous silica coated magnetic iron oxide Fe <sub>3</sub> O <sub>4</sub> nanoparticles, doxorubicin hydrochloride was	50 nm	--	Multifunctional core-shell nanoparticles for pH responsive drug delivery of doxorubicin hydrochloride	96

		adopted and connected gold nanoparticle to block mesopores.				
--	--	---	--	--	--	--

**Table 2. Recent advancements in silica-based core-shell nanoparticles system in drug delivery.**

S. No.	Core-Shell nanoparticle system	Description	Particle size	Drug loading	Comments	References
1	MSN@PDA	Polydopamine coated mesoporous silica core-shell nanoparticles	145 nm	13.6 wt%	pH and ultrasound dual responsive controlled Dox drug delivery	<sup>289</sup>
2	MSN@PDA-AuNPs	Mesoporous silica nanoparticles core polydopamine-gold nanoparticles shell was formulated	~70 nm	~14 wt %	Chemo and photothermal Dox delivery	<sup>290</sup>
3	MSN@PDA-PEG-Apt,	Mesoporous silica nanoparticles surface coated with hydrochloride dopamine or PEG and epithelial cell adhesion molecule aptamer	203 nm	-- 94 % EE	Targeted delivery of DM1 for treatment of colorectal cancer	<sup>291</sup>
4	PM@HMSN	Polydopamine coated MoSe <sub>2</sub> wrapped hollow mesoporous silica nanoparticles	294 nm	-- 93.5% EE	Dual chemo photo thermal Dox delivery for breast cancer therapy	<sup>292</sup>
5	MSN@PDA-TPGA	TPGS functionalized polydopamine modified mesoporous silica	221 nm	10 wt%	pH responsive delivery of Dox for lung cancer chemotherapy against multidrug resistance	<sup>293</sup>
6	MSNs-PLH-PEG	Poly(L-histidine) and poly(ethylene glycol) coated mesoporous silica nanoparticles	160 nm	22.5 wt%	PLH gated reversibly switchable mesoporous silica nanoparticles for control delivery of Sorafenib (SF)	<sup>216</sup>
7	DMSN@PEI-PEG	Dendritic mesoporous silica nanoparticles coated with block copolymer PEI-PEG	205 nm	--	pH responsive delivery of TNF-Alpha (Tumor necrosis factor-alpha)	<sup>294</sup>

8	Lipid coated MSN@p(NIPAM-co-MA)	mesoporous silica nanoparticles are coated with block copolymer NIPAM-co-MA and surface coated with lipid	160 nm	56 % EVO 84% BBR	Thermo and pH responsive dual delivery of hydrophobic drug (Evodiamine: EVO; Berberine: BBR) to enhance antitumor effect	217
9	MSN-SA	Mesoporous silica nanoparticles coated with sodium alginate by disulfide bonds	110 nm	--	Redox ad pH dual responsive delivery of Dox for cancer	295
10	MSN@PEG-Lipid	Mesoporous silica nanoparticles coated with PEGylated lipid bilayer compose of soybean phospholipid, cholesterol and PEG-200.	125 nm	77 %EE TAX 30 %EE CUR	PEGylated lipid bilayer coated MSN for Co-delivery of paclitaxel and curcumin	296

**Table 3. Recent advancements in polymeric core-shell nanoparticles system in drug delivery.**

S. No.	Core-Shell nanoparticle system	Description		Drug loading	Comments	References
1	PEO/TCS-PLA	Thiolates chitosan core/shell nanofibers	~100 nm	14.20%	Promising candidate for topical delivery of HIV/AIDS microbicides such as tenofovir.	107
2	Core-Shel chitosan microcapsuls	Cross linked chitosan hydrogel shell and an oily core containing both free drug and drug loaded PLGA nanoparticles	551.6 nm	12.87 %	Microcapsules with programmed sequential drug delivery	108
3	PLGA/FPL	PLGA/folate coated PEGlated polymeric liposome core-shell nanoparticles Core-shell cationic folic acid coated polymeric liposome -PLGA nanoparticles	435 nm	--	Dox encapsulated in PLGA core and surface was bonded with model DNA pEGFP	297

4	LMWSC-MPEG-Chol	Core shell nanoparticles prepared using Low molecular weight water soluble chitosan modified with methoxy PEG and conjugated with Cholesterol	150nm	--	Anticancer drug paclitaxel delivery	298
5	PLGA-Lipid-PEG	PLGA core conjugated with PEG shell was prepared by using lipid lecithin monolayer at the interface	100 nm	3 wt %	Anticancer drug docetaxel delivery	299
6	Core-shell amphiphilic polymeric nanoparticles	Core-shell nanoparticles are prepared through self-assembly of polymeric amphiphiles made of 3-pentadecylphenol copolymerized with oligoethylene glycol acrylate through RAFT methodology.	230 nm	3.78 wt%	Enzyme and thermal dual responsive amphiphilic polymeric core-shell nanoparticles for Dox delivery to cancer cells	300
7	Core-shell polymeric micelles	Core-shell Curcumin loaded mPEG-b-PLG micelles formulated by dialysis process	136 nm	13.55	Oxidation responsive and aggregation induced emission polymeric micelles for cancer therapy and bioimaging	301
8	Core-shell polymer lipid nanoparticle	PLGA core nanoparticle wrapped by lipid monolayer as shell compose of three components DLPC (1,2-dilauroylphosphatidylcholine), DSPE-PEG2k (1,2-diestearoyl-sn-glycero-3-phosphoethanolamine-N-[methoxy(polyethylene glycol)-200]), and 1,2-distearoyl-sn-glycero-3-phosphoethanolamine-N[folate(polyethylene glycol)-5000]. Further core-shell nanoparticles conjugated with folic acid as targeting agent	200 nm	--	Folic acid conjugated mixed lipid monolayer shell and biodegradable PLGA polymer core nanoparticles for targeted delivery of docetaxel	302

9	Coordination polymer based core-shell nanoparticles	Cisplatin loaded coordination polymer (NCP) core-shell nanoparticles conjugated with photosensitizer pyrolipid	108 nm	25 wt%	Combined chemotherapy and photodynamic therapy for head and neck cancer	303
10						

**Table 4. Recent advancements in Upconversion nanoparticles-based core-shell nanoparticles system in drug delivery.**

S. No.	Core-Shell nanoparticle system	Description	Particle size d/nm	Drug loading	Comments	References
1	UCNP@mSiO <sub>2</sub>	Amine functionalized mesoporous silica coated NaYF <sub>4</sub> :Yb/Er	124 nm	17.4 wt%	Efficient delivery of doxorubicin and curcumin	123
2	UCNC@SiO <sub>2</sub>	NaYF <sub>4</sub> :Yb/Er core encapsulated in Silica shell	25 nm		NIR light enabled optical imaging of cancer cells	126
3	PNIPAM-UCNPs@SiO <sub>2</sub>	PNIPAM coated on UCNPs(OA-NaYF <sub>4</sub> : Yb/Tm@NaYF <sub>4</sub> ) @SiO <sub>2</sub>	35 nm	41 wt%	Thermal and Photo dual responsive delivery of anticancer drug doxorubicin hydrochloride	130
4	UCNPs@PAzo/MAA	UCNPs (OA-NaYF <sub>4</sub> : Yb/Tm@Na) PMAA (polymethacrylic acid) yolk-shell nano capsules	32 nm	17 wt %	pH and NIR light dual responsive delivery of doxorubicin	131
5	LaDe:Yb <sup>3+</sup> , Er <sup>3+</sup> @nSiO <sub>2</sub> @mSiO <sub>2</sub>	LaF <sub>3</sub> :Yb <sup>3+</sup> , Er <sup>3+</sup> nanoparticles encapsulated in mesoporous silica core-shell nanoparticles	130 nm	12 wt%	Green Upconversion photoluminescence core-shell nanoparticles for Drug delivery for ibuprofen	132
6	UCNP-PEG	Polyethylene glycol grafted amphiphilic polymer coated NaYF <sub>4</sub> : Yb <sup>3+</sup> , Er <sup>3+</sup> (UCNP)	~40 nm	8 wt%	pH responsive drug delivery of doxorubicin	304
7	TPGS-UCNPs	NaYF <sub>4</sub> :Er nanoparticles surface modified with TPGS	20 nm	0.113 mmol/g	Dual-modal fluorescent/CT imaging and anticancer	305

					drug delivery to overcome multi-drug resistance	
8	mNaYbF <sub>4</sub> :Er@NaGdF <sub>4</sub> core-shell mUCNPs	Mesoporous core-shell upconversion nanoparticles compose of NaYbF <sub>4</sub> :2%Er core and a mesoporous NaGdF <sub>4</sub> shell. further conjugated with PEI and Folic acid (FA)	70 nm	16.8 wt%	Targeted delivery of doxorubicin and multimodal imaging	<sup>306</sup>
9	NaYF <sub>4</sub> :Yb,Er/NaYF <sub>4</sub>	Tween coated NaYF <sub>4</sub> :Yb, Er core NaYF <sub>4</sub> shell Upconversion nanoparticles	25 nm	7.4 wt%	Drug delivery of Dox and bioimaging. Multifunctional platform for diagnosis and therapeutics	<sup>307</sup>
10	UCNP@SiO <sub>2</sub> (MB)@mSiO <sub>2</sub>	NaYF <sub>4</sub> :Yb, Er coated with silica and loaded photosensitizer MB, Further coated with mesoporous silica.	75 nm	4.52 wt%	NIR light assisted drug delivery, photodynamic therapy and cell imaging	<sup>308</sup>
11	b-NaYF <sub>4</sub> :Yb <sup>3+</sup> , Er <sup>3+</sup> @mSiO <sub>2</sub>	Beta-NaYF <sub>4</sub> :Yb <sup>3+</sup> , Er <sup>3+</sup> upconversion nanoparticles encapsulated in mesoporous silica shell and further modified with PEG and folic acid as cancer targeting ligand	80 nm	12 wt%	Targeted drug delivery of anticancer drug doxorubicin hydrochloride and cell imaging	<sup>309</sup>

Table 5. Recent advancements in carbon nanomaterial-based core-shell nanoparticles system in drug delivery.

S. No.	Core-Shell nanoparticle system	Description	Particle size d/nm	Drug loading	Comments	References
1	Fe <sub>3</sub> O <sub>4</sub> @OCMC@IRMOF-3/FA	Carbon dot embedded nanoscale metal organic frameworks (NMOFs) have been demonstrated as a promising carrier for drug delivery		1.63 g DOX g <sup>-1</sup> magnetic NMOFs	pH Sensitive Targeted Anticancer Drug Delivery	<sup>310</sup>
2	mCNC@mSiO <sub>2</sub>	Mesoporous Carbon Nanocube@Mesoporous		0.78 mg at DOX concentration of	After modification of nanoparticles by	<sup>311</sup>

		Silica@Poly(acrylic acid) composite as potential drug carriers		0.5 mg/mL for 24 h loading.	poly(acrylic acid) (PAA), the mCNC@mSiO <sub>2</sub> @PAA drug capacity had changed from 0.78 to 1.009 mg at the same concentration as a cancer drug carrier due to electrostatic interaction between carboxyl and 5-fluorouracil (5-Fu).	
3	BPQDs@ss-Fe <sub>3</sub> O <sub>4</sub> @C	Black phosphorus quantum dots gated, carbon-coated Fe <sub>3</sub> O <sub>4</sub> nanocapsules with low premature release towards imaging-guided cancer combination therapy		546 mg g <sup>-1</sup> , 54.6% of DOX	Nanoparticles exhibit pH-, NIR- and redox-responsive behavior, and facilitates triple-stimuli contributed to drug continuous release	312
4	Graphitic carbon@silica nanospheres	Core-Shell graphitic carbon@silica nanospheres with dual-ordered mesopores towards cancer-targeted photothermochemotherapy		1.97 ± 0.28 mg/mg, with an entrapment efficiency of ~79% for aromatic DOX molecules	System exhibited efficient drug loading capacity, high targeting ability, sensitive NIR/pH-responsive DOX release, sustained release, and excellent combined antitumor activity.	313
5	GO-Au@PANI nanocomposites	Graphene and AuNP core and polyaniline shell nanocomposites as multifunctional theranostic		DOX-loading efficiency of 189.2%	Sensitive NIR/pH-responsive DOX release	314

		platforms for SERS real-time monitoring and chemophotothermal therapy				
6	Fe <sub>3</sub> O <sub>4</sub> @mTiO <sub>2</sub> -GO nanocarriers	Sono-chemically synthesized magnetic core-shell Fe <sub>3</sub> O <sub>4</sub> @mTiO <sub>2</sub> -GO (where m was shorted mesoporous) hybrids nano-structure for controlled dual targeted colon drug delivery		Drug loading capacity and encapsulation efficiency were 17.85 and 72.45%, respectively.	MTT results demonstrated no significant cytotoxicity of the nanomaterials on human foreskin fibroblast normal cell line (HFF-2 and carriers has retained its anti-cancer properties	315
7	CuS-DOX/GO nanocomposite	Core-shell nanostructure of hollow copper sulfide nanosphere-doxorubicin (DOX)/graphene oxide (GO) (CuS-DOX/GO), was constructed for the controlled drug delivery and improved photothermo-chemotherapeutic effect		DOX loading capacity exhibited a concentration-dependent mode, and a loading factor of up to 1.75 (1.75 g DOX/1.0 g CuS) was encountered at a DOX concentration of 600 µg mL <sup>-1</sup> .	DOX can be efficiently loaded onto the hollow CuS nanoparticles, and its subsequent release from CuS-DOX/GO nanocomposite is prompted in a pH- and near-infrared light-dependent manner.	316
8	NGOHA-AuNRs	Hyaluronic acid (HA)-conjugated NGO-enwrapped AuNR nanocomposites were fabricated for targeted chemophotothermal Therapy of Hepatoma		The loading factor achieved 45% at pH 7.4 with a DOX feeding concentration of 0.5 mg/mL but	Nanocomposite exhibits pH-responsive and near-infrared light-triggered drug-release properties.	317

				decreased to 24% at pH 5.3		
9	ZIF-8/GQD multifunctional nanoparticles	Metal-organic framework/graphene quantum dot nanoparticles explored for synergistic chemo- and photothermal therapy		90% of DOX loading efficiency was achieved, and the DOX loading capacity in the ZIF-8/GQD nanoparticles was estimated to be 47 µg/mg.	After endocytosis by cancer cells, the nanoparticles could not only realize intracellular drug release because of the acidic environment in cancer cells but also induce photothermal therapy by NIR irradiation because of the photothermal effect of graphene quantum dots.	318
10	FGQCs nanocomposites	Super paramagnetic fluorescent Fe <sub>3</sub> O <sub>4</sub> /SiO <sub>2</sub> /graphene-CdTe QDs/CS nanocomposites were fabricated for their biocompatibility and targeted drug delivery application		Nanocomposites were incubated in 2.7 wt% 5-fluorouracil (5-FU) solution and PBS to achieve the loading content and entrapment efficiency of 70 and 50 wt%, respectively.	Nanocomposites exhibited enhanced drug loading capacity and fluorescent properties	319

**Author Contributions:** RK and KM, YKM discussed, designed, and formulated manuscript; AK explored biotechnology-related aspects of nanomaterials; PKP designed the outlook illustration; YKM supervised manuscript and explore aspects of functional materials in drug delivery; RK, KM, Reza A, RA, HGR, AK, PKP, YKM wrote the paper.

**Funding:** This review was funded PBC (Planning and Budget Committee) Postdoctoral Fellowship to Raj Kumar by the Planning and Budget Committee of the Council of Higher Education, Israel.

**Acknowledgments:** Dr. Raj Kumar gratefully acknowledges the Bar-Ilan Institute for Nanotechnology and Advanced Materials (BINA) and Bar-Ilan University. Dr. Raj Kumar is thankful to the Planning and Budgeting Committee (PBC) of the Council of Higher Education, Israel, for awarding the PBC-postdoctoral fellowship. Dr. Kunal Mondal gratefully acknowledges the Energy & Environment S & T at the Idaho National Laboratory, the USA for their support. Prof. Rajeev Ahuja acknowledges the support from the Swedish Research Council (VR grant no. 2016-06014).

## Authors' biography



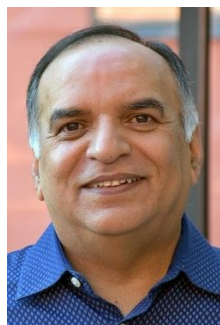
**Raj Kumar** is a Postdoctoral Research Fellow at the University of Michigan USA. He was a PBC Postdoctoral Research Fellow at Bar Ilan University (2017-19), Israel. He did Ph.D. in Chemistry (2017) from the Indian Institute of Technology (IIT) Mandi, India. He is exploring nanotechnology for pharmaceutical sciences, drug/gene delivery, and neural tissue engineering for health wellness. Dr. Kumar is open to collaborative research. His research interest includes nanomaterials, nanocarriers for stimuli responsive drug/gene delivery, nanomaterials for neural tissue engineering, and pharmaceutical nanotechnology. He awarded UGC-JRF (2010, 11), SERB-NPDF (2017), PBC Outstanding Postdoctoral Fellowship (2017-19), and Israel Government Scholarship (2017).



**Kunal Mondal** is a staff scientist at Idaho National Laboratory, USA. His research interests include additive manufacturing, micro/nano fabrication of functional materials, soft and stretchable electronics, microfluidics, liquid metal, colloids and interfaces of soft nanostructures, self and directed assembly, photovoltaics, polymer thin-films, carbon nanomaterials, energy and environmental and health sensors, nuclear sensors, soft electronic skin, and flexible transistors. He earned his Ph. D. from the Indian Institute of Technology, Kanpur, India. Prior to joining Idaho National Laboratory in 2019, he was a postdoctoral fellow at Florida Atlantic University, USA, and a postdoctoral research associate at North Carolina State University, USA.



**Ajeet Kaushik**, Fellow-ICS, is working as Assistant Professor of chemistry at Florida Polytechnic University and is exploring nano-bio-technology for health wellness. Dr. Kaushik is an accomplished scientist (supported by publication, journal editor, edited, books, patents, international collaborations) and recipient of several international awards in support of credentials in the field of nano-biotechnology for health care. Dr. Kaushik is open for collaborative research as his research interest include nano-bio-technology, analytical systems, design & develop nanostructures, nanocarriers for drug delivery, nano-therapeutics for CNS diseases, on-demand site-specific release of therapeutic agents, exploring personalized nano-medicines, biosensors, point-of-care sensing devices, and related areas of health care monitoring.



**Rajeev Ahuja** is professor of Materials Theory in the Department of Physics and Astronomy at Uppsala University and one of the most highly cited researchers in Sweden under 55. He has published 910 scientific papers in peer reviewed journals (H-Index 82 (Google Scholar), i-10-index 535 & citations more than 31200). Ahuja has recently elected (Sept.2019) APS-Fellow by American Physical Society (APS), USA, appointed in the advisory board of Journal of Materials Chemistry A from Royal Society of Chemistry (England) & awarded Beller Lectureship for the APS March Meeting 2017, in New Orleans, USA. He has been awarded the Wallmark prize for 2011 from KVA (Royal Swedish Academy of Sciences), and has previously received the Eder Lilly, Sven Thureus prize and the Benzelius prize from Royal Society of Sciences (KVS). Ahuja is an elected member of the Swedish Royal Society of Sciences and served on the board of the European High-Pressure Research Group as well as of the executive board of the International Association for the Advancement of High-Pressure Science and Technology. Ahuja has supervised 30 PhD students and more than 35 postdocs.



**Horst-Günter Rubahn** is professor and director of the Mads Clausen Institute at the University of Southern Denmark. He also leads the nanotechnology center NanoSYD. Besides a doctoral title and a habilitation from University of Göttingen he owns an honorary doctoral title from Kaunas University of Technology. He is appointed Danish national expert nanotechnology in the Horizon 2020 Programme Committee NMBP and chair of the international PhD school PCAM. Horst-Günter Rubahn's recent research focuses on the development of generic routes towards novel thin film smart materials and nanomaterials. This includes the complete range from fundamental via applied research to device integration.



**Yogendra Kumar Mishra** is Professor MSO at Mads Clausen Institute, NanoSYD, University of Southern Denmark (SDU). Prior to SDU, he was leading a group at Functional Nanomaterials Chair, Kiel University, Germany where he finished Habilitation in Materials Science too in 2015. After Ph. D. (Physics) from JNU New Delhi, India, he migrated to Kiel and continued as Humboldt fellow and subsequently continued there for habilitation degree. He developed a new flame-based process for tetrapod nanostructuring and their 3D networks as cellular solids. These tetrapods showed many applications in engineering and biomedical fields and additionally, they are being used as templates to create tetrapodal networks from almost any desired material. At NanoSYD, the main research focus of his group is in the direction of 'Smart Materials'.

## References

- 1 K. Lingeshwar Reddy, R. Balaji, A. Kumar and V. Krishnan, *Small*, 2018, **14**, 1801304.
- 2 O. C. Farokhzad and R. Langer, *ACS Nano*, 2009, **3**, 16–20.
- 3 T. Dvir, B. P. Timko, D. S. Kohane and R. Langer, *Nat. Nanotechnol.*, 2011, **6**, 13–22.
- 4 Y. K. Mishra and R. Adelung, *Mater. Today*, 2018, **21**, 631–651.
- 5 A. Ahmadivand, B. Gerislioglu, R. Ahuja and Y. K. Mishra, *Mater. Today*, 2020, **32**, 108–130.
- 6 L. Mazzola, *Nat. Biotechnol.*, 2003, **21**, 1137–1143.
- 7 T. Vats, S. Dutt, R. Kumar and P. F. Siril, *Sci. Rep.*, 2016, **6**, 33053.
- 8 N. Sanvicens and M. P. Marco, *Trends Biotechnol.*, 2008, **26**, 425–433.
- 9 M. Nair, R. D. Jayant, A. Kaushik and V. Sagar, *Adv. Drug Deliv. Rev.*, 2016, **103**, 202–217.
- 10 A. Kaushik, R. D. Jayant and M. Nair, *Int. J. Nanomedicine*, 2016, **11**, 4317.
- 11 M. Li, W. Song, Z. Tang, S. Lv, L. Lin, H. Sun, Q. Li, Y. Yang, H. Hong and X. Chen, *ACS Appl. Mater. Interfaces*, 2013, **5**, 1781–1792.
- 12 K. Kim, J. H. Kim, H. Park, Y.-S. Kim, K. Park, H. Nam, S. Lee, J. H. Park, R.-W. Park, I.-S. Kim, K. Choi, S. Y. Kim, K. Park and I. C. Kwon, *J. Control. Release*, 2010, **146**, 219–227.
- 13 J. Tang, B. Kong, H. Wu, M. Xu, Y. Wang, Y. Wang, D. Zhao and G. Zheng, *Adv. Mater.*, 2013, **25**, 6569–6574.

- 14 M. Chawla, R. Kumar and P. F. Siril, *J. Mol. Catal. A Chem.*, 2016, **423**, 126–134.
- 15 A. D. Bangham, M. M. Standish and J. C. Watkins, *J. Mol. Biol.*, 1965, **13**, 238-252.
- 16 N. D. James, R. J. Coker, D. Tomlinson, J. R. W. Harris, M. Gompels, A. J. Pinching and J. S. W. Stewart, *Clin. Oncol.*, 1994, **6**, 294-296.
- 17 M. R. Green, G. M. Manikhas, S. Orlov, B. Afanasyev, A. M. Makhson, P. Bhar and M. J. Hawkins, *Ann. Oncol.*, 2006, **17**, 1263-1268.
- 18 N. Kamaly, Z. Xiao, P. M. Valencia, A. F. Radovic-Moreno and O. C. Farokhzad, *Chem. Soc. Rev.*, 2012, **41**, 2971-3010.
- 19 M. De, P. S. Ghosh and V. M. Rotello, *Adv. Mater.*, 2008, **20**, 4225–4241.
- 20 H. Otsuka, Y. Nagasaki and K. Kataoka, *Adv. Drug Deliv. Rev.*, 2012, **64**, 246–255.
- 21 G. Han, P. Ghosh and V. M. Rotello, *Nanobiotechnol.*, 2007, **3**, 40-45.
- 22 L. Zhang, F. X. Gu, J. M. Chan, A. Z. Wang, R. S. Langer and O. C. Farokhzad, *Clin. Pharmacol. Ther.*, 2008, **83**, 761–769.
- 23 E. C. Dreaden, S. C. Mwakwari, Q. H. Sodji, A. K. Oyelere and M. A. El-Sayed, *Bioconjug. Chem.*, 2009, **20**, 2247–2253.
- 24 V. B. Kumar, M. Marcus, Z. Porat, L. Shani, Y. Yeshurun, I. Felner, O. Shefi and A. Gedanken, *ACS Omega*, 2018, **3**, 1897–1903.
- 25 M. Marcus, A. Smith, A. Maswadeh, Z. Shemesh, I. Zak, M. Motiei, H. Schori, S. Margel, A. Sharoni and O. Shefi, *Nanomaterials*, 2018, **8**, 707.
- 26 M. Marcus, M. Karni, K. Baranes, I. Levy, N. Alon, S. Margel and O. Shefi, *J.*

- Nanobiotechnology*, 2016, **14**, 37.
- 27 M. Marcus, H. Skaat, N. Alon, S. Margel and O. Shefi, *Nanoscale*, 2015, **7**, 1058–1066.
- 28 N. Zilony, M. Rosenberg, L. Holtzman, H. Schori, O. Shefi and E. Segal, *J. Control. Release*, 2017, **257**, 51–59.
- 29 R. Ghosh Chaudhuri and S. Paria, *Chem. Rev.*, 2012, **112**, 2373–2433.
- 30 S. Dutt, R. Kumar and P. F. Siril, *RSC Adv.*, 2015, **5**, 33786–33791.
- 31 K. Chatterjee, S. Sarkar, K. Jagajjanani Rao and S. Paria, *Adv. Colloid Interface Sci.*, 2014, **209**, 8–39.
- 32 A. D. Newman, D. R. Brown, P. Siril, A. F. Lee and K. Wilson, *Phys. Chem. Chem. Phys.*, 2006, **8**, 2893–2902.
- 33 G. Singh and S. P. Felix, *Combust. Flame*, 2003, **132**, 422–432.
- 34 S. Deshpande, S. Sharma, V. Koul and N. Singh, *ACS Omega*, 2017, **2**, 6455–6463.
- 35 F. H. Xavier-Jr, C. Gueutin, H. Chacun, C. Vauthier and E. S. T. Egito, *J. Drug Deliv. Sci. Technol.*, 2019, **53**, 101194.
- 36 C. Von Baeckmann, R. Guillet-Nicolas, D. Renfer, H. Kählig and F. Kleitz, *ACS Omega*, 2018, **3**, 17496–17510.
- 37 Q. Zhang, M. He, B. Chen and B. Hu, *ACS Omega*, 2018, **3**, 3752–3759.
- 38 S. Iraj, F. Ganji and L. Rashidi, *J. Drug Deliv. Sci. Technol.*, 2018, **47**, 468–476.
- 39 N. H. Cho, T. C. Cheong, J. H. Min, J. H. Wu, S. J. Lee, D. Kim, J. S. Yang, S. Kim, Y. K. Kim and S. Y. Seong, *Nat. Nanotechnol.*, 2011, **6**, 675–682.

- 40 L. Xiong, T. Yang, Y. Yang, C. Xu and F. Li, *Biomaterials*, 2010, **31**, 7078–7085.
- 41 V. B. Kumar, R. Kumar, O. Friedman, Y. Golan, A. Gedanken and O. Shefi, *ChemistrySelect*, 2019, **4**, 4222–4232.
- 42 I. Fratoddi, *Nanomaterials*, 2017, **8**, 11.
- 43 R. Kumar, K. R. Aadil, S. Ranjan and V. B. Kumar, *J. Drug Deliv. Sci. Technol.*, 2020, **57**, 101617.
- 44 V. B. Kumar, R. Kumar, A. Gedanken and O. Shefi, *Ultrason. Sonochem.*, 2019, **52**, 205–213.
- 45 F. Winau, O. Westphal and R. Winau, *Microbes Infect.*, 2004, **6**, 786–789.
- 46 M. Arruebo, R. Fernández-Pacheco, M. R. Ibarra and J. Santamaría, *Nano Today*, 2007, **2**, 22–32.
- 47 V. V. Mody, A. Cox, S. Shah, A. Singh, W. Bevins and H. Parihar, *Appl. Nanosci.*, 2014, **4**, 385–392.
- 48 A. A. Abd Elrahman and F. R. Mansour, *J. Drug Deliv. Sci. Technol.*, 2019, **52**, 702–712.
- 49 U. O. Häfeli, J. S. Riffle, L. Harris-Shekhawat, A. Carmichael-Baranauskas, F. Mark, J. P. Dailey and D. Bardenstein, in *Molecular Pharmaceutics*, American Chemical Society, 2009, **6**, 1417–1428.
- 50 A. Tiwari, N. C. Verma, A. Singh, C. K. Nandi and J. K. Randhawa, *Nanoscale*, 2018, **10**, 10389–10394.
- 51 M. Samiei Foroushani, R. Karimi Shervedani, A. Kefayat, M. Torabi, F. Ghahremani and

- F. Yaghoobi, *J. Drug Deliv. Sci. Technol.*, 2019, **54**, 101223.
- 52 L. Balcells, C. Fornaguera, P. Brugada-Vilà, M. Guerra-Rebollo, Ó. Meca-Cortés, G. Martínez, N. Rubio, J. Blanco, J. Santamaría, A. Cascante and S. Borrós, *ACS Omega*, 2019, **4**, 2728–2740.
- 53 H. M. Pezzi, D. J. Niles, J. L. Schehr, D. J. Beebe and J. M. Lang, *ACS Omega*, 2018, **3**, 3908–3917.
- 54 R. Sameer Kumar, G. Shakambari, B. Ashokkumar, D. J. Nelson, S. A. John and P. Varalakshmi, *ACS Omega*, 2018, **3**, 11982–11992.
- 55 M. A. Rahman, Y. Matsumura, S. Yano and B. Ochiai, *ACS Omega*, 2018, **3**, 961–972.
- 56 N. Jain, R. K. Singh, B. P. Singh, A. Srivastava, R. A. Singh and J. Singh, *ACS Omega*, 2019, **4**, 7482–7491.
- 57 A. Tiwari, A. Singh, A. Debnath, A. Kaul, N. Garg, R. Mathur, A. Singh and J. K. Randhawa, *ACS Appl. Nano Mater.*, 2019, **2**, 3060–3072.
- 58 H. Itoh and T. Sugimoto, *J. Colloid Interface Sci.*, 2003, **265**, 283–295.
- 59 G. Molineux, *Cancer Treat. Rev.*, 2002, **28**, 13–16.
- 60 M. M. Yallapu, S. P. Foy, T. K. Jain and V. Labhasetwar, *Pharm. Res.*, 2010, **27**, 2283–2295.
- 61 S. Balakrishnan, M. J. Bonder and G. C. Hadjipanayis, *J. Magn. Magn. Mater.*, 2009, **321**, 117–122.
- 62 G. Reshmi, P. Mohan Kumar and M. Malathi, *Int. J. Pharm.*, 2009, **365**, 131–135.

- 63 A. Ditsch, P. E. Laibinis, D. I. C. Wang and T. A. Hatton, *Langmuir*, 2005, **21**, 6006–6018.
- 64 R. Kumar, P. Soni and P. F. Siril, *ACS Omega*, 2019, **4**, 5424–5433.
- 65 A. Kumar, P. K. Jena, S. Behera, R. F. Lockey, S. Mohapatra and S. Mohapatra, *Nanomedicine Nanotechnology, Biol. Med.*, 2010, **6**, 64–69.
- 66 H. Yang, Y. Chen, Z. Chen, Y. Geng, X. Xie, X. Shen, T. Li, S. Li, C. Wu and Y. Liu, *Biomater. Sci.*, 2017, **5**, 1001–1013.
- 67 S. Giri, B. G. Trewyn, M. P. Stellmaker and V. S.-Y. Lin, *Angew. Chemie - Int. Ed.*, 2005, **44**, 5038–5044.
- 68 Q. Yuan, R. Venkatasubramanian, S. Hein and R. D. K. Misra, *Acta Biomater.*, 2008, **4**, 1024–1037.
- 69 S. Purushotham, P. E. J. Chang, H. Rumpel, I. H. C. Kee, R. T. H. Ng, P. K. H. Chow, C. K. Tan and R. V Ramanujan, *Nanotechnology*, 2009, **20**, 305101.
- 70 T. Y. Liu, S. H. Hu, K. H. Liu, R. S. Shaiu, D. M. Liu and S. Y. Chen, *Langmuir*, 2008, **24**, 13306–13311.
- 71 S. Kurzhals, M. Schroffenegger, N. Gal, R. Zirbs and E. Reimhult, *Biomacromolecules*, 2018, **19**, 1435–1444.
- 72 J. Zeng, P. Du, L. Liu, J. Li, K. Tian, X. Jia, X. Zhao and P. Liu, *Mol. Pharm.*, 2015, **12**, 4188–4199.
- 73 F. Lin, J. Chen, M. Lee, B. Lin and J. Wang, *ACS Appl. Nano Mater.*, 2020, **3**, 1147–1152.

- 74 L. Li, C. Liu, L. Zhang, T. Wang, H. Yu, C. Wang and Z. Su, *Nanoscale*, 2013, **5**, 2249–2253.
- 75 M. Pishnamazi, J. Iqbal, S. Shirazian, G. M. Walker and M. N. Collins, *Int. J. Biol. Macromol.*, 2019, **124**, 354–359.
- 76 Ł. Klapiszewski, J. Zdarta, K. Antecka, K. Synoradzki, K. Siwińska-Stefańska, D. Moszyński and T. Jesionowski, *Appl. Surf. Sci.*, 2017, **422**, 94–103.
- 77 J. Nogués, V. Skumryev, J. Sort, S. Stoyanov and D. Givord, *Phys. Rev. Lett.*, 2006, **97**, 157203.
- 78 Y. H. Deng, C. C. Wang, J. H. Hu, W. L. Yang and S. K. Fu, *Colloids Surfaces A Physicochem. Eng. Asp.*, 2005, **262**, 87–93.
- 79 S. Huang, C. Li, Z. Cheng, Y. Fan, P. Yang, C. Zhang, K. Yang and J. Lin, *J. Colloid Interface Sci.*, 2012, **376**, 312–321.
- 80 Y. Deng, D. Qi, C. Deng, X. Zhang and D. Zhao, *J. Am. Chem. Soc.*, 2008, **130**, 28–29.
- 81 A. Guerrero-Martínez, J. Pérez-Juste and L. M. Liz-Marzán, *Adv. Mater.*, 2010, **22**, 1182–1195.
- 82 H. Cao, J. He, L. Deng and X. Gao, *Appl. Surf. Sci.*, 2009, **255**, 7974–7980.
- 83 J. Huang, Q. Shu, L. Wang, H. Wu, A. Y. Wang and H. Mao, *Biomaterials*, 2015, **39**, 105–113.
- 84 M. Donolato, P. Vavassori, M. Gobbi, M. Deryabina, M. F. Hansen, V. Metlushko, B. Ilic, M. Cantoni, D. Petti, S. Brivio and R. Bertacco, *Adv. Mater.*, 2010, **22**, 2706–2710.

- 85 H. Skaat, G. Shafir and S. Margel, *J. Nanoparticle Res.*, 2011, **13**, 3521–3534.
- 86 J. J. Lin, J. S. Chen, S. J. Huang, J. H. Ko, Y. M. Wang, T. L. Chen and L. F. Wang, *Biomaterials*, 2009, **30**, 5114–5124.
- 87 R. Zhang, C. Wu, X. Wang, Q. Sun, B. Chen, X. Li, S. Gutmann and G. Lv, *Mater. Sci. Eng. C*, 2009, **29**, 1697–1701.
- 88 J. K. Lim, S. A. Majetich and R. D. Tilton, *Langmuir*, 2009, **25**, 13384–13393.
- 89 D. Tarn, C. E. Ashley, M. Xue, E. C. Carnes, J. I. Zink and C. J. Brinker, *Acc. Chem. Res.*, 2013, **46**, 792–801.
- 90 J. E. Lee, N. Lee, T. Kim, J. Kim and T. Hyeon, *Acc. Chem. Res.*, 2011, **44**, 893–902.
- 91 F. Tang, L. Li and D. Chen, *Adv. Mater.*, 2012, **24**, 1504–1534.
- 92 E. Ahmadi, N. Dehghannejad, S. Hashemikia, M. Ghasemnejad and H. Tabebordbar, *Drug Deliv.*, 2014, **21**, 164–172.
- 93 Z. Li, J. C. Barnes, A. Bosoy, J. F. Stoddart and J. I. Zink, *Chem. Soc. Rev.*, 2012, **41**, 2590–2605.
- 94 C. Argyo, V. Weiss, C. Bräuchle and T. Bein, *Chem. Mater.*, 2014, **26**, 435–451.
- 95 Q. Zhang, F. Liu, K. T. Nguyen, X. Ma, X. Wang, B. Xing and Y. Zhao, *Adv. Funct. Mater.*, 2012, **22**, 5144–5156.
- 96 L. Cui, H. Lin, C. Yang, X. Han, T. Zhang and F. Qu, *Eur. J. Inorg. Chem.*, 2014, **2014**, 6156–6164.
- 97 W. Zhao, B. Cui, H. Peng, H. Qiu and Y. Wang, *J. Phys. Chem. C*, 2015, **119**, 4379–4386.

- 98 R. Kumar, in *Nanocarriers for Drug Delivery*, Elsevier, 2019, pp. 249–284.
- 99 A. Tiwari, R. Kumar, O. Shefi and J. K. Randhawa, *ACS Appl. Bio Mater.*, 2020, **3**, 4665–4673.
- 100 R. Kumar, S. V. Dalvi and P. F. Siril, *ACS Appl. Nano Mater.*, 2020, **3**, 4944–4961.
- 101 J. M. Chan, L. Zhang, K. P. Yuet, G. Liao, J. W. Rhee, R. Langer and O. C. Farokhzad, *Biomaterials*, 2009, **30**, 1627–1634.
- 102 H. Otsuka, Y. Nagasaki and K. Kataoka, *Curr. Opin. Colloid Interface Sci.*, 2001, **6**, 3–10.
- 103 A. Mattes and O. Seitz, *Angew. Chemie - Int. Ed.*, 2001, **40**, 3178–3181.
- 104 H. Cabral, Y. Matsumoto, K. Mizuno, Q. Chen, M. Murakami, M. Kimura, Y. Terada, M. R. Kano, K. Miyazono, M. Uesaka, N. Nishiyama and K. Kataoka, *Nat. Nanotechnol.*, 2011, **6**, 815–823.
- 105 Q. Huo, J. Liu, L. Q. Wang, Y. Jiang, T. N. Lambert and E. Fang, *J. Am. Chem. Soc.*, 2006, **128**, 6447–6453.
- 106 K. Kataoka, A. Harada and Y. Nagasaki, *Adv. Drug Deliv. Rev.*, 2012, **64**, 37–48.
- 107 J. Meng, V. Agrahari, M. J. Ezoulin, C. Zhang, S. S. Purohit, A. Molteni, D. Dim, N. A. Oyler and B. B. C. Youan, *Mol. Pharm.*, 2016, **13**, 4129–4140.
- 108 X. L. Yang, X. J. Ju, X. T. Mu, W. Wang, R. Xie, Z. Liu and L. Y. Chu, *ACS Appl. Mater. Interfaces*, 2016, **8**, 10524–10534.
- 109 Z. Qin, H. Sun, Z. Jiang, X. Jiao and D. Chen, *CrystEngComm*, 2013, **15**, 897–902.
- 110 Y. Kang and T. A. Taton, *Macromolecules*, 2005, **38**, 6115–6121.

- 111 L. M. Bronstein, S. N. Sidorov, P. M. Valetsky, J. Hartmann, H. Golfen and M. Antonietti, *Langmuir*, 1999, **15**, 6256–6262.
- 112 D. Zopes, B. Stein, S. Mathur and C. Graf, *Langmuir*, 2013, **29**, 11217–11226.
- 113 Y. Nagasaki, *Sci. Technol. Adv. Mater.*, 2010, **11**, 054505.
- 114 J. B. Kim, M. L. Bruening and G. L. Baker, *J. Am. Chem. Soc.*, 2000, **122**, 7616–7617.
- 115 S. Maji, B. Cesur, Z. Zhang, B. G. De Geest and R. Hoogenboom, *Polym. Chem.*, 2016, **7**, 1705–1710.
- 116 D. Li, Q. He, Y. Cui and J. Li, *Chem. Mater.*, 2007, **19**, 412–417.
- 117 K. M. Ho, W. Y. Li, C. H. Wong and P. Li, *Colloid Polym. Sci.*, 2010, **288**, 1503–1523.
- 118 Y. Lu, Y. Mei, M. Drechsler and M. Ballauff, *Angew. Chemie - Int. Ed.*, 2006, **45**, 813–816.
- 119 D. V. Talapin, I. Mekis, S. Götzinger, A. Kornowski, O. Benson and H. Weller, *J. Phys. Chem. B*, 2004, **108**, 18826–18831.
- 120 R. Xie, U. Kolb, J. Li, T. Basché and A. Mews, *J. Am. Chem. Soc.*, 2005, **127**, 7480–7488.
- 121 K. L. Reddy, M. Venkateswarulu, K. R. Shankar, S. Ghosh and V. Krishnan, *ChemistrySelect*, 2018, **3**, 1793–1800.
- 122 R. Kumar, V. B. Kumar and A. Gedanken, *Ultrason. Sonochem.*, 2020, **64**, 105009.
- 123 K. L. Reddy, P. K. Sharma, A. Singh, A. Kumar, K. R. Shankar, Y. Singh, N. Garg and V. Krishnan, *Mater. Sci. Eng. C*, 2019, **96**, 86–95.
- 124 K. L. Reddy, N. Prabhakar, R. Arppe, J. M. Rosenholm and V. Krishnan, *J. Mater. Sci.*,

- 2017, **52**, 5738–5750.
- 125 K. L. Reddy, M. Rai, N. Prabhakar, R. Arppe, S. B. Rai, S. K. Singh, J. M. Rosenholm and V. Krishnan, *RSC Adv.*, 2016, **6**, 53698–53704.
- 126 K. L. Reddy, N. Prabhakar, J. M. Rosenholm and V. Krishnan, *Micromachines*, 2018, **9**, 400.
- 127 K. Lingeshwar Reddy, V. Srinivas, K. R. Shankar, S. Kumar, V. Sharma, A. Kumar, A. Bahuguna, K. Bhattacharyya and V. Krishnan, *J. Phys. Chem. C*, 2017, **121**, 11783–11793.
- 128 R. Balaji, S. Kumar, K. L. Reddy, V. Sharma, K. Bhattacharyya and V. Krishnan, *J. Alloys Compd.*, 2017, **724**, 481–491.
- 129 A. Kumar, K. L. Reddy, S. Kumar, A. Kumar, V. Sharma and V. Krishnan, *ACS Appl. Mater. Interfaces*, 2018, **10**, 15565–15581.
- 130 X. Wang, C. Liu, Z. Li, C. Y. Tang, W. C. Law, X. Gong, Z. Liu, Y. Liao, G. Zhang, S. Long and L. Chen, *J. Phys. Chem. C*, 2019, **123**, 10658–10665.
- 131 X. Wang, X. Liu, L. Wang, C. Y. Tang, W. C. Law, G. Zhang, Y. Liao, C. Liu and Z. Liu, *Macromolecules*, 2018, **51**, 10074–10082.
- 132 Y. Yang, Y. Qu, J. Zhao, Q. Zeng, Y. Ran, Q. Zhang, X. Kong and H. Zhang, *Eur. J. Inorg. Chem.*, 2010, **2010**, 5195–5199.
- 133 W. Jiang, L. Huang, F. Mo, Y. Zhong, L. Xu and F. Fu, *J. Mater. Chem. B*, 2019, **7**, 3019–3026.
- 134 Z. H. Wang, J. M. Liu, C. Y. Li, D. Wang, H. Lv, S. W. Lv, N. Zhao, H. Ma and S. Wang,

- ACS Appl. Mater. Interfaces*, 2019, **11**, 36409–36419.
- 135 L. J. Chen, C. X. Yang and X. P. Yan, *Anal. Chem.*, 2017, **89**, 6936–6939.
- 136 J. Shi, H. Fu, X. Sun, J. Shen and H. Zhang, *J. Mater. Chem. B*, 2015, **3**, 635–641.
- 137 Z. J. Li, Y. J. Zhang, H. W. Zhang and H. X. Fu, *Microporous Mesoporous Mater.*, 2013, **176**, 48–54.
- 138 K. Mondal and P. Moitra, in *Metal Semiconductor Core-shell Nanostructures for Energy and Environmental Applications*, Elsevier, 2017, ISBN 9780323449229, pp. 133–157.
- 139 K. Mondal and A. Sharma, *RSC Adv.*, 2016, **6**, 83589–83612.
- 140 Q. Zhang, I. Lee, J. B. Joo, F. Zaera and Y. Yin, *Acc. Chem. Res.*, 2013, **46**, 1816–1824.
- 141 B. Alotaibi, H. P. T. Nguyen, S. Zhao, M. G. Kibria, S. Fan and Z. Mi, *Nano Lett.*, 2013, **13**, 4356–4361.
- 142 S. V. Prabhakar Vattikuti, A. K. R. Police, J. Shim and C. Byon, *Sci. Rep.*, 2018, **8**, 4194.
- 143 L. Su, Y. Jing and Z. Zhou, *Nanoscale*, 2011, **3**, 3967–3983.
- 144 K. C. Ho and L. Y. Lin, *J. Mater. Chem. A*, 2019, **7**, 3516–3530.
- 145 L. Xu, M. L. Yin and S. Liu, *Sci. Rep.*, 2014, **4**, 6745.
- 146 H. Dzudzevic Cancar, S. Soylemez, Y. Akpinar, M. Kesik, S. Göker, G. Gunbas, M. Volkan and L. Toppare, *ACS Appl. Mater. Interfaces*, 2016, **8**, 8058–8067.
- 147 Y. Cao, B. Wang, Y. Wang and D. Lou, *RSC Adv.*, 2014, **4**, 30430–30439.
- 148 S. Katiyar, K. Mondal and A. Sharma, *RSC Adv.*, 2016, **6**, 12298–12310.

- 149 M. M. Titirici, R. J. White, N. Brun, V. L. Budarin, D. S. Su, F. Del Monte, J. H. Clark and M. J. MacLachlan, *Chem. Soc. Rev.*, 2015, **44**, 250–290.
- 150 K. Mondal, G. Pawar, M. D. McMurtrey and A. Sharma, *Mater. Today Chem.*, 2020, **16**, 100269.
- 151 K. Mondal, M. A. Ali, C. Singh, G. Sumana, B. D. Malhotra and A. Sharma, *Sensors Actuators, B Chem.*, 2017, **246**, 202–214.
- 152 H. P. Feng, L. Tang, G. M. Zeng, J. Tang, Y. C. Deng, M. Yan, Y. N. Liu, Y. Y. Zhou, X. Y. Ren and S. Chen, *J. Mater. Chem. A*, 2018, **6**, 7310–7337.
- 153 M. Taale, F. Schütt, T. Carey, J. Marx, Y. K. Mishra, N. Stock, B. Fiedler, F. Torrisi, R. Adelung and C. Selhuber-Unkel, *ACS Appl. Mater. Interfaces*, 2019, **11**, 5325–5335.
- 154 M. Taale, D. Krüger, E. Ossei-Wusu, F. Schütt, M. A. U. Rehman, Y. K. Mishra, J. Marx, N. Stock, B. Fiedler, A. R. Boccaccini, R. Willumeit-Römer, R. Adelung and C. Selhuber-Unkel, *ACS Biomater. Sci. Eng.*, 2019, **5**, 4393–4404.
- 155 F. Rasch, F. Schütt, L. M. Saure, S. Kaps, J. Strobel, O. Polonskyi, A. S. Nia, M. R. Lohe, Y. K. Mishra, F. Faupel, L. Kienle, X. Feng and R. Adelung, *ACS Appl. Mater. Interfaces*, 2019, **11**, 44652–44663.
- 156 A. Muhulet, F. Miculescu, S. I. Voicu, F. Schütt, V. K. Thakur and Y. K. Mishra, *Mater. Today Energy*, 2018, **9**, 154–186.
- 157 F. Schütt, S. Signetti, H. Krüger, S. Röder, D. Smazna, S. Kaps, S. N. Gorb, Y. K. Mishra, N. M. Pugno and R. Adelung, *Nat. Commun.*, 2017, **8**, 1215.
- 158 J. Joo, E. J. Kwon, J. Kang, M. Skalak, E. J. Anglin, A. P. Mann, E. Ruoslahti, S. N.

- Bhatia and M. J. Sailor, *Nanoscale Horizons*, 2016, **1**, 407–414.
- 159 X. Sun and Y. Li, *Angew. Chemie - Int. Ed.*, 2004, **43**, 597–601.
- 160 Y. Peng and S. Chen, *Green Energy Environ.*, 2018, **3**, 335–351.
- 161 J. Lu, W. Zhou, L. Wang, J. Jia, Y. Ke, L. Yang, K. Zhou, X. Liu, Z. Tang, L. Li and S. Chen, *ACS Catal.*, 2016, **6**, 1045–1053.
- 162 X. Cao, X. Chuan, R. C. Massé, D. Huang, S. Li and G. Cao, *J. Mater. Chem. A*, 2015, **3**, 22739–22749.
- 163 D. Zhang, C. Zhang, J. Liu, Q. Chen, X. Zhu and C. Liang, *ACS Appl. Nano Mater.*, 2019, **2**, 28–39.
- 164 X. Meng, X. Q. Yang and X. Sun, *Adv. Mater.*, 2012, **24**, 3589–3615.
- 165 C. Detavernier, J. Dendooven, S. Pulinthanathu Sree, K. F. Ludwig and J. A. Martens, *Chem. Soc. Rev.*, 2011, **40**, 5242–5253.
- 166 H. Im, N. J. Wittenberg, N. C. Lindquist and S. H. Oh, *J. Mater. Res.*, 2012, **27**, 663–671.
- 167 S. A. Skoog, J. W. Elam and R. J. Narayan, *Int. Mater. Rev.*, 2013, **58**, 113–129.
- 168 K. E. Gregorczyk, A. C. Kozen, X. Chen, M. A. Schroeder, M. Noked, A. Cao, L. Hu and G. W. Rubloff, *ACS Nano*, 2015, **9**, 464–473.
- 169 Z. M. Wang, W. Wang, N. Coombs, N. Soheilnia and G. A. Ozin, *ACS Nano*, 2010, **4**, 7437–7450.
- 170 Y.-W. Chen, P.-J. Chen, S.-H. Hu, I.-W. Chen and S.-Y. Chen, *Adv. Funct. Mater.*, 2014, **24**, 451–459.

- 171 W. Jiang, F. Mo, X. Jin, L. Chen, L. J. Xu, L. Guo and F. Fu, *Adv. Mater. Interfaces*, 2017, **4**, 1700425.
- 172 L. Shao, R. Zhang, J. Lu, C. Zhao, X. Deng and Y. Wu, *ACS Appl. Mater. Interfaces*, 2017, **9**, 1226–1236.
- 173 C. Nan, Z. Lin, H. Liao, M. K. Song, Y. Li and E. J. Cairns, *J. Am. Chem. Soc.*, 2014, **136**, 4659–4663.
- 174 W. Wang, Y. Wang, L. Gu, R. Lu, H. Qian, X. Peng and J. Sha, *J. Power Sources*, 2015, **293**, 492–497.
- 175 S. Mrozowski and M. L. Studebaker, 1967, 11101.
- 176 F. Cao, G. X. Pan, J. Chen, Y. J. Zhang and X. H. Xia, *J. Power Sources*, 2016, **303**, 35–40.
- 177 G. Wang, Z. Ma, G. Shao, L. Kong and W. Gao, *J. Power Sources*, 2015, **291**, 209–214.
- 178 J. Burtscher, S. F. Koch, J. Bauer, H. Wagner and J. Fleischer, in *Procedia CIRP*, Elsevier, 2015, **31**, 70–75.
- 179 S. H. Park and W. J. Lee, *Sci. Rep.*, 2015, **5**, 9754.
- 180 Y. Luo, X. Zhou, Y. Zhong, M. Yang, J. Wei and Z. Zhou, *Electrochim. Acta*, 2015, **154**, 136–141.
- 181 H. Eyre, R. Kahn, R. M. Robertson, N. G. Clark, C. Doyle, Y. Hong, T. Gansler, T. Glynn, R. A. Smith, K. Taubert and M. J. Thun, *Circulation*, 2004, **109**, 3244–3255.
- 182 A. Jemal, R. Siegel, J. Xu and E. Ward, *CA. Cancer J. Clin.*, 2010, **60**, 277–300.

- 183 H. Hillaireau and P. Couvreur, *Cell. Mol. Life Sci.*, 2009, **66**, 2873–2896.
- 184 J. W. Yoo, D. J. Irvine, D. E. Discher and S. Mitragotri, *Nat. Rev. Drug Discov.*, 2011, **10**, 521–535.
- 185 A. Z. Wang, R. Langer and O. C. Farokhzad, *Annu. Rev. Med.*, 2012, **63**, 185–198.
- 186 N. Bertrand, J. Wu, X. Xu, N. Kamaly and O. C. Farokhzad, *Adv. Drug Deliv. Rev.*, 2014, **66**, 2–25.
- 187 A. Kaushik, B. Kateb and M. Nair, in *Advances in Personalized Nanotherapeutics*, Springer International Publishing, Cham, 2017, pp. 231–234.
- 188 A. Kaushik, *Front. Nanotechnol.*, 2019, **1**, 1.
- 189 C. Deng, Y. Jiang, R. Cheng, F. Meng and Z. Zhong, *Nano Today*, 2012, **7**, 467–480.
- 190 K. E. Albinali, M. M. Zagho, Y. Deng and A. A. Elzatahry, *Int. J. Nanomedicine*, 2019, **14**, 1707–1723.
- 191 Y. H. Bae and K. Park, *J. Control. Release*, 2011, **153**, 198–205.
- 192 M. Srinivasarao and P. S. Low, *Chem. Rev.*, 2017, **117**, 12133–12164.
- 193 J. M. Lambert and R. V. J. Chari, *J. Med. Chem.*, 2014, **57**, 6949–6964.
- 194 Z. Zhang and Y. Ji, *Ind. Eng. Chem. Res.*, 2019, **58**, 2991–2999.
- 195 Y. Wang and D. S. Kohane, *Nat. Rev. Mater.*, 2017, **2**, 1–14.
- 196 P. Mukhopadhyay and P. P. Kundu, *RSC Adv.*, 2015, **5**, 93995–94007.
- 197 J. Tao, W. Fei, H. Tang, C. Li, C. Mu, H. Zheng, F. Li and Z. Zhu, *Mol. Pharm.*, 2019, **16**,

- 786–797.
- 198 L. Han, C. Tang and C. Yin, *ACS Appl. Mater. Interfaces*, 2016, **8**, 23498–23508.
- 199 T. Li, Z. Niu, T. Emrick, T. P. Russell and Q. Wang, *Small*, 2008, **4**, 1624–1629.
- 200 N. Suthiwangcharoen, T. Li, L. Wu, H. B. Reno, P. Thompson and Q. Wang, *Biomacromolecules*, 2014, **15**, 948–956.
- 201 L. Lu, L. Yuan, J. Yan, C. Tang and Q. Wang, *Biomacromolecules*, 2016, **17**, 2321–2328.
- 202 W. Ying, Y. Zhang, W. Gao, X. Cai, G. Wang, X. Wu, L. Chen, Z. Meng, Y. Zheng, B. Hu and X. Lin, , DOI:10.1021/acsnano.0c00910.
- 203 S. H. Hosseini, S. Alipour and N. Zohreh, *Langmuir*, 2018, **34**, 13735–13744.
- 204 R. Kumar, *J. Drug Deliv. Sci. Technol.*, 2019, **53**, 101221.
- 205 R. Kumar, *ChemistrySelect*, 2020, **5**, 1478–1490.
- 206 R. Kumar, A. Singh, N. Garg and P. F. Siril, *Ultrason. Sonochem.*, 2018, **40**, 686–696.
- 207 R. Kumar and P. F. Siril, *J. Nanoparticle Res.*, 2015, **17**, 256.
- 208 W. Zhao, H. Chen, Y. Li, A. Li, M. Lang and J. Shi, *Adv. Funct. Mater.*, 2008, **18**, 2780–2788.
- 209 G. Liu, J. Ma, Y. Li, Q. Li, C. Tan, H. Song, S. Cai, D. Chen, Z. Hou, Q. Chen and X. Zhu, *Int. J. Pharm.*, 2017, **521**, 19–32.
- 210 R. Kumar, A. Singh and N. Garg, *J. Drug Deliv. Sci. Technol.*, 2019, **54**, 101277.
- 211 R. Kumar, A. Singh and N. Garg, *ACS Omega*, 2019, **4**, 13360–13370.

- 212 R. Kumar, A. Singh, K. Sharma, D. Dhasmana, N. Garg and P. F. Siril, *Mater. Sci. Eng. C*, 2019, **106**, 110184.
- 213 B. Surnar, K. Sharma and M. Jayakannan, *Nanoscale*, 2015, **7**, 17964–17979.
- 214 T. Patel, J. Zhou, J. M. Piepmeier and W. M. Saltzman, *Adv. Drug Deliv. Rev.*, 2012, **64**, 701–705.
- 215 F. H. Chen, Q. Gao and J. Z. Ni, *Nanotechnology*, 2008, **19**, 165103.
- 216 S. Mu, Y. Liu, T. Wang, J. Zhang, D. Jiang, X. Yu and N. Zhang, *Acta Biomater.*, 2017, **63**, 150–162.
- 217 Y. Feng, N. X. Li, H. L. Yin, T. Y. Chen, Q. Yang and M. Wu, *Mol. Pharm.*, 2019, **16**, 422–436.
- 218 R. R. Kumal, M. Abu-Laban, P. Hamal, B. Kruger, H. T. Smith, D. J. Hayes and L. H. Haber, *J. Phys. Chem. C*, 2018, **122**, 19699–19704.
- 219 P. Kumar, H. S. Ban, S. S. Kim, H. Wu, T. Pearson, D. L. Greiner, A. Laouar, J. Yao, V. Haridas, K. Habiro, Y. G. Yang, J. H. Jeong, K. Y. Lee, Y. H. Kim, S. W. Kim, M. Peipp, G. H. Fey, N. Manjunath, L. D. Shultz, S. K. Lee and P. Shankar, *Cell*, 2008, **134**, 577–586.
- 220 Y. Dong, D. J. Siegwart and D. G. Anderson, *Adv. Drug Deliv. Rev.*, 2019, **144**, 133–147.
- 221 Y. K. Oh and T. G. Park, *Adv. Drug Deliv. Rev.*, 2009, **61**, 850–862.
- 222 M. Rodriguez, J. Lapierre, C. R. Ojha, A. Kaushik, E. Batrakova, F. Kashanchi, S. M. Dever, M. Nair and N. El-Hage, *Sci. Rep.*, 2017, **7**, 1862.

- 223 M. Zheng, W. Tao, Y. Zou, O. C. Farokhzad and B. Shi, *Trends Biotechnol.*, 2018, **36**, 562–575.
- 224 A. Schroeder, C. G. Levins, C. Cortez, R. Langer and D. G. Anderson, in *J. Intern. Med.*, 2010, **267**, 9–21.
- 225 Y. Patil and J. Panyam, *Int. J. Pharm.*, 2009, **367**, 195–203.
- 226 S. Zhang, B. Zhao, H. Jiang, B. Wang and B. Ma, *J. Controlled. Release*, 2007, **123**, 1–10.
- 227 P. T. Yin, T. Pongkulapa, H. Y. Cho, J. Han, N. J. Pasquale, H. Rabie, J. H. Kim, J. W. Choi and K. B. Lee, *ACS Appl. Mater. Interfaces*, 2018, **10**, 26954–26963.
- 228 L. Y. Gao, X. Y. Liu, C. J. Chen, J. C. Wang, Q. Feng, M. Z. Yu, X. F. Ma, X. W. Pei, Y. J. Niu, C. Qiu, W. H. Pang and Q. Zhang, *Biomaterials*, 2014, **35**, 2066–2078.
- 229 Q. Feng, M. Z. Yu, J. C. Wang, W. J. Hou, L. Y. Gao, X. F. Ma, X. W. Pei, Y. J. Niu, X. Y. Liu, C. Qiu, W. H. Pang, L. L. Du and Q. Zhang, *Biomaterials*, 2014, **35**, 5028–5038.
- 230 L. Wei, X. Y. Guo, T. Yang, M. Z. Yu, D. W. Chen and J. C. Wang, *Int. J. Pharm.*, 2016, **510**, 394–405.
- 231 X. He, F. Yin, D. Wang, L. H. Xiong, R. T. K. Kwok, P. F. Gao, Z. Zhao, J. W. Y. Lam, K. T. Yong, Z. Li and B. Z. Tang, *Nano Lett.*, 2019, **19**, 2272–2279.
- 232 M. Wang, Y. Han, X. Yu, L. Liang, H. Chang, D. C. Yeo, C. Wiraja, M. L. Wee, L. Liu, X. Liu and C. Xu, *Adv. Healthc. Mater.*, 2020, **9**, 1900635.
- 233 J. Shi, Z. Xiao, A. R. Votruba, C. Vilos and O. C. Farokhzad, *Angew. Chemie - Int. Ed.*, 2011, **50**, 7027–7031.

- 234 W. Fan, B. Yung, P. Huang and X. Chen, *Chem. Rev.*, 2017, **117**, 13566–13638.
- 235 Y. Min, J. M. Caster, M. J. Eblan and A. Z. Wang, *Chem. Rev.*, 2015, **115**, 11147–11190.
- 236 C. M. Hartshorn, M. S. Bradbury, G. M. Lanza, A. E. Nel, J. Rao, A. Z. Wang, U. B. Wiesner, L. Yang and P. Grodzinski, *ACS Nano*, 2018, **12**, 24–43.
- 237 N. Panwar, A. M. Soehartono, K. K. Chan, S. Zeng, G. Xu, J. Qu, P. Coquet, K. T. Yong and X. Chen, *Chem. Rev.*, 2019, **119**, 9559–9656.
- 238 S. K. Verma, E. Jha, P. K. Panda, A. Thirumurugan, S. Patro, S. K. S. Parashar and M. Suar, *Mater. Sci. Eng. C*, 2018, **92**, 807–818.
- 239 B. Sarkar, S. K. Verma, J. Akhtar, S. P. Netam, S. K. Gupta, P. K. Panda and K. Mukherjee, *Chemosphere*, 2018, **206**, 560–567.
- 240 R. Kumar, S. V. Dalvi and P. Felix Siril, *ACS Appl. Nano Mater.*, 2020, **3**, 4944–4961.
- 241 I.-C. Lin, J.-H. Fang, C.-T. Lin, S.-Y. Sung, Y.-L. Su and S.-H. Hu, *Macromol. Biosci.*, 2016, **16**, 1273–1286.
- 242 J. Qin, X. Wei, H. Chen, F. Lv, W. Nan, Y. Wang, Q. Zhang and H. Chen, *ACS Biomater. Sci. Eng.*, 2018, **4**, 1651–1660.
- 243 P. Pandey, G. Ghimire, J. Garcia, A. Rubfiaro, X. Wang, A. Tomitaka, M. Nair, A. Kaushik and J. He, *ACS Sensors*, , DOI:10.1021/acssensors.0c00664.
- 244 A. Kaushik, R. D. Jayant, V. Sagar and M. Nair, *Expert Opin. Drug Deliv.*, 2014, **11**, 1635–1646.
- 245 A. Kaushik, R. D. Jayant, V. Bhardwaj and M. Nair, *Drug Discov. Today*, 2018, **23**,

- 1007–1015.
- 246 A. Tomitaka, A. Kaushik, B. D. Kevadiya, I. Mukadam, H. E. Gendelman, K. Khalili, G. Liu and M. Nair, *Drug Discov. Today*, 2019, **24**, 873–882.
- 247 A. Kaushik, A. Yndart, V. Atluri, S. Tiwari, A. Tomitaka, P. Gupta, R. D. Jayant, D. Alvarez-Carbonell, K. Khalili and M. Nair, *Sci. Rep.*, 2019, **9**, 1–11.
- 248 A. Kaushik, R. Nikkhah-Moshaie, R. Sinha, V. Bhardwaj, V. Atluri, R. D. Jayant, A. Yndart, B. Kateb, N. Pala and M. Nair, *Sci. Rep.*, 2017, **7**, 45663.
- 249 A. Kaushik, R. D. Jayant, R. Nikkhah-Moshaie, V. Bhardwaj, U. Roy, Z. Huang, A. Ruiz, A. Yndart, V. Atluri and N. El-Hage, *Sci. Rep.*, 2016, **6**, 25309.
- 250 A. Kaushik, J. Rodriguez, D. Rothen, V. Bhardwaj, R. D. Jayant, P. Pattany, B. Fuentes, H. Chand, N. Kolishetti and N. El-Hage, *ACS Appl. Bio Mater.*, 2019, **2**, 4826–4836.
- 251 H. Bin Na, I. C. Song and T. Hyeon, *Adv. Mater.*, 2009, **21**, 2133–2148.
- 252 J. Paris, C. Gameiro, V. Humblet, P. K. Mohapatra, V. Jacques and J. F. Desreux, *Inorg. Chem.*, 2006, **45**, 5092–5102.
- 253 P. S. Tofts, *J. Magn. Reson. Imaging*, 1997, **7**, 91–101.
- 254 M. Ahrén, L. Selegård, A. Klasson, F. Söderlind, N. Abrikossova, C. Skoglund, T. Bengtsson, M. Engström, P.-O. Käll and K. Uvdal, *Langmuir*, 2010, **26**, 5753–5762.
- 255 T. Passuello, M. Pedroni, F. Piccinelli, S. Polizzi, P. Marzola, S. Tambalo, G. Conti, D. Benati, F. Vetrone, M. Bettinelli and A. Speghini, *Nanoscale*, 2012, **4**, 7682–7689.
- 256 N. J. J. Johnson, W. Oakden, G. J. Stanisz, R. Scott Prosser and F. C. J. M. Van Veggel,

- Chem. Mater.*, 2011, **23**, 3714–3722.
- 257 Y. Kobayashi, J. Imai, D. Nagao, M. Takeda, N. Ohuchi, A. Kasuya and M. Konno, *Colloids Surfaces A Physicochem. Eng. Asp.*, 2007, **308**, 14–19.
- 258 E. S. Choi, J. Y. Park, M. J. Baek, W. Xu, K. Kattel, J. H. Kim, J. J. Lee, Y. Chang, T. J. Kim, J. E. Bae, K. S. Chae, K. J. Suh and G. H. Lee, *Eur. J. Inorg. Chem.*, 2010, **2010**, 4555–4560.
- 259 N. R. Puttagunta, W. A. Gibby and G. T. Smith, *Invest. Radiol.*, 1996, **31**, 739–742.
- 260 I. Aoki, Y. Takahashi, K. H. Chuang, A. C. Silva, T. Igarashi, C. Tanaka, R. W. Childs and A. P. Koretsky, *NMR Biomed.*, 2006, **19**, 50–59.
- 261 Z. Zhao, Z. Zhou, J. Bao, Z. Wang, J. Hu, X. Chi, K. Ni, R. Wang, X. Chen, Z. Chen and J. Gao, *Nat. Commun.*, 2013, **4**, 2266.
- 262 D. Patel, A. Kell, B. Simard, B. Xiang, H. Y. Lin and G. Tian, *Biomaterials*, 2011, **32**, 1167–1176.
- 263 T. Kim, E. Momin, J. Choi, K. Yuan, H. Zaidi, J. Kim, M. Park, N. Lee, M. T. McMahon, A. Quinones-Hinojosa, J. W. M. Bulte, T. Hyeon and A. A. Gilad, *J. Am. Chem. Soc.*, 2011, **133**, 2955–2961.
- 264 I. Hilger and W. A. Kaiser, *Nanomedicine*, 2012, **7**, 1443–1459.
- 265 C. Blanco-Andujar, A. Walter, G. Cotin, C. Bordeianu, D. Mertz, D. Felder-Flesch and S. Begin-Colin, *Nanomedicine*, 2016, **11**, 1889–1910.
- 266 B. Chertok, B. A. Moffat, A. E. David, F. Yu, C. Bergemann, B. D. Ross and V. C. Yang, *Biomaterials*, 2008, **29**, 487–496.

- 267 N. Lee, H. R. Cho, M. H. Oh, S. H. Lee, K. Kim, B. H. Kim, K. Shin, T. Y. Ahn, J. W. Choi, Y. W. Kim, S. H. Choi and T. Hyeon, *J. Am. Chem. Soc.*, 2012, **134**, 10309–10312.
- 268 Q. Shao, Z. Yang, G. Zhang, Y. Hu, Y. Dong and J. Jiang, *ACS Omega*, 2018, **3**, 188–197.
- 269 Z. Xing, J. Wang, H. Ke, B. Zhao, X. Yue, Z. Dai and J. Liu, *Nanotechnology*, 2010, **21**, 145607.
- 270 T. Zhou, B. Wu and D. Xing, *J. Mater. Chem.*, 2012, **22**, 470–477.
- 271 M. S. Judenhofer, H. F. Wehrl, D. F. Newport, C. Catana, S. B. Siegel, M. Becker, A. Thielscher, M. Kneilling, M. P. Lichy, M. Eichner, K. Klingel, G. Reischl, S. Widmaier, M. Röcken, R. E. Nutt, H. J. Machulla, K. Uludag, S. R. Cherry, C. D. Claussen and B. J. Pichler, *Nat. Med.*, 2008, **14**, 459–465.
- 272 R. Liang, M. Wei, D. G. Evans and X. Duan, *Chem. Commun.*, 2014, **50**, 14071–14081.
- 273 C. Sun, J. S. H. Lee and M. Zhang, *Adv. Drug Deliv. Rev.*, 2008, **60**, 1252–1265.
- 274 R. Rafique, S. K. Kailasa and T. J. Park, *TrAC - Trends Anal. Chem.*, 2019, **120**, 115646.
- 275 W. Fan, B. Shen, W. Bu, F. Chen, K. Zhao, S. Zhang, L. Zhou, W. Peng, Q. Xiao, H. Xing, J. Liu, D. Ni, Q. He and J. Shi, *J. Am. Chem. Soc.*, 2013, **135**, 6494–6503.
- 276 L. Cheng, K. Yang, Y. Li, J. Chen, C. Wang, M. Shao, S. T. Lee and Z. Liu, *Angew. Chemie - Int. Ed.*, 2011, **50**, 7385–7390.
- 277 X. Zhu, J. Zhou, M. Chen, M. Shi, W. Feng and F. Li, *Biomaterials*, 2012, **33**, 4618–4627.
- 278 J. Shi, A. R. Votruba, O. C. Farokhzad and R. Langer, *Nano Lett.*, 2010, **10**, 3223–3230.
- 279 A. P. Ramos, M. A. E. Cruz, C. B. Tovani and P. Ciancaglini, *Biophys. Rev.*, 2017, **9**, 79–

- 89.
- 280 D. A. LaVan, T. McGuire and R. Langer, *Nat. Biotechnol.*, 2003, **21**, 1184-1191.
- 281 Z. Li, S. Tan, S. Li, Q. Shen and K. Wang, *Oncol. Rep.*, 2017, **38**, 611-624.
- 282 C. D. Sago, M. P. Lokugamage, F. Z. Islam, B. R. Krupczak, M. Sato and J. E. Dahlman, *J. Am. Chem. Soc.*, 2018, **140**, 17095-17105.
- 283 C. D. Sago, M. P. Lokugamage, K. Paunovska, D. A. Vanover, C. M. Monaco, N. N. Shah, M. G. Castro, S. E. Anderson, T. G. Rudoltz, G. N. Lando, P. M. Tiwari, J. L. Kirschman, N. Willett, Y. C. Jang, P. J. Santangelo, A. V. Bryksin and J. E. Dahlman, *Proc. Natl. Acad. Sci. U. S. A.*, 2018, **16**, E9944-E9952.
- 284 W. H. De Jong and P. J. A. Borm, *Int. J. Nanomedicine*, 2008, **3**, 133-149.
- 285 S. Purushotham, P. E. J. Chang, H. Rumpel, I. H. C. Kee, R. T. H. Ng, Chow P. K. H., C. K. Tan and R. V. Ramanujan, *Nanotechnology*, 2009, **20**, 305101.
- 286 J. Zhang and R. D. K. Misra, *Acta Biomater.*, 2007, **3**, 838-850.
- 287 P. Yang, Z. Quan, Z. Hou, C. Li, X. Kang, Z. Cheng and J. Lin, *Biomaterials*, 2009, **30**, 4786-4795.
- 288 M. Hegazy, P. Zhou, G. Wu, L. Wang, N. Rahoui, N. Taloub, X. Huang and Y. Huang, *Polym. Chem.*, 2017, **8**, 5852-5864.
- 289 X. Li, C. Xie, H. Xia and Z. Wang, *Langmuir*, 2018, **34**, 9974-9981.
- 290 N. Rahoui, B. Jiang, M. Hegazy, N. Taloub, Y. Wang, M. Yu and Y. D. Huang, *Colloids Surf. B*, 2018, **171**, 176-185.

- 291 Y. Li, Y. Duo, S. Bao, L. He, K. Ling, J. Luo, Y. Zhang, H. Huang, H. Zhang and X. Yu, *Int. J. Nanomedicine*, 2017, **12**, 6239–6257.
- 292 S. Chai, S. Kan, R. Sun, R. Zhou, Y. Sun, W. Chen and B. Yu, *Int. J. Nanomedicine*, 2018, **13**, 7607–7621.
- 293 W. Cheng, C. Liang, L. Xu, G. Liu, N. Gao, W. Tao, L. Luo, Y. Zuo, X. Wang, X. Zhang, X. Zeng and L. Mei, *Small*, **2017**, 1700623.
- 294 A. Kienzle, S. Kurch, J. Schlöder, C. Berges, R. Ose, J. Schupp, A. Tuettenberg, H. Weiss, J. Schultze, S. Winzen, M. Schinnerer, K. Koynov, M. Mezger, N. K. Haass, W. Tremel and H. Jonuleit, *Adv. Healthc. Mater.*, 2017, **6**, 1700012.
- 295 N. ning Yuan, S. ji Li and G. qiang Li, *J. Drug Deliv. Sci. Technol.*, 2018, **46**, 348–353.
- 296 J. Lin, Q. Cai, Y. Tang, Y. Xu, Q. Wang, T. Li, H. Xu, S. Wang, K. Fan, Z. Liu, Y. Jin and D. Lin, *Int. J. Pharm.*, 2018, **536**, 272–282.
- 297 H. Wang, P. Zhao, W. Su, S. Wang, Z. Liao, R. Niu and J. Chang, *Biomaterials*, 2010, **31**, 8741–8748.
- 298 M. K. Jang, Y. Il Jeong and J. W. Nah, *Colloids Surf. B*, 2010, **81**, 530–536.
- 299 L. Zhang, J. M. Chan, F. X. Gu, J. W. Rhee, A. Z. Wang, A. F. Radovic-Moreno, F. Alexis, R. Langer and O. C. Farokhzad, *ACS Nano*, 2008, **2**, 1696–1702.
- 300 S. Kashyap, N. Singh, B. Surnar and M. Jayakannan, *Biomacromolecules*, 2016, **17**, 384–398.
- 301 H. He, W. Zhuang, B. Ma, X. Su, T. Yu, J. Hu, L. Chen, R. Peng, G. Li and Y. Wang, *ACS Biomater. Sci. Eng.*, 2019, **5**, 2577–2586.

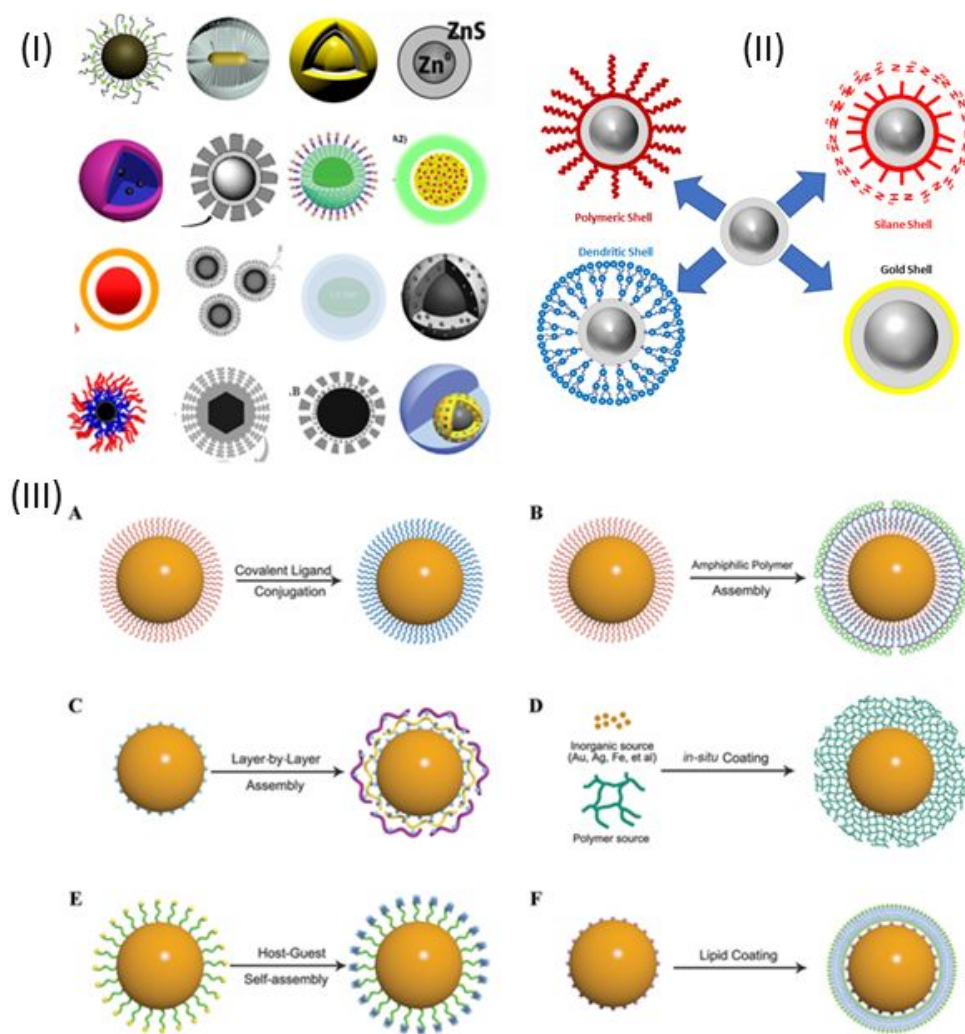
- 302 Y. Liu, K. Li, J. Pan, B. Liu and S. S. Feng, *Biomaterials*, 2010, **31**, 330–338.
- 303 C. He, D. Liu and W. Lin, *ACS Nano*, 2015, **9**, 991–1003.
- 304 C. Wang, L. Cheng and Z. Liu, *Biomaterials*, 2011, **32**, 1110–1120.
- 305 G. Tian, X. Zheng, X. Zhang, W. Yin, J. Yu, D. Wang, Z. Zhang, X. Yang, Z. Gu and Y. Zhao, *Biomaterials*, 2015, **40**, 107–116.
- 306 L. Zhou, X. Zheng, Z. Gu, W. Yin, X. Zhang, L. Ruan, Y. Yang, Z. Hu and Y. Zhao, *Biomaterials*, 2014, **35**, 7666–7678.
- 307 W. Ren, G. Tian, S. Jian, Z. Gu, L. Zhou, L. Yan, S. Jin, W. Yin and Y. Zhao, *RSC Adv.*, 2012, **2**, 7037–7041.
- 308 H. Wang, R. L. Han, L. M. Yang, J. H. Shi, Z. J. Liu, Y. Hu, Y. Wang, S. J. Liu and Y. Gan, *ACS Appl. Mater. Interfaces*, 2016, **8**, 4416–4423.
- 309 C. Li, Z. Hou, Y. Dai, D. Yang, Z. Cheng, P. Ma and J. Lin, *Biomater. Sci.*, 2013, **1**, 213–223.
- 310 A. R. Chowdhuri, T. Singh, S. K. Ghosh and S. K. Sahu, *ACS Appl. Mater. Interfaces*, 2016, **8**, 16573–16583.
- 311 Xiao Song, L. Hu, X. Pang and S. Li, *Russ. J. Phys. Chem. A*, 2019, **93**, 1349–1356.
- 312 M. Zhang, W. Wang, F. Wu, K. Graveran, J. Zhang and C. Wu, *Chem. - A Eur. J.*, 2018, **24**, 12890–12901.
- 313 Y. Wang, K. Wang, R. Zhang, X. Liu, X. Yan, J. Wang, E. Wagner and R. Huang, *ACS Nano*, 2014, **8**, 7870–7879.

- 314 H. Chen, Z. Liu, S. Li, C. Su, X. Qiu, H. Zhong and Z. Guo, *Theranostics*, 2016, **6**, 1096–1104.
- 315 M. Rostami, M. Aghajanzadeh, M. Zamani, H. K. Manjili and H. Danafar, *Res. Chem. Intermed.*, 2018, **44**, 1889–1904.
- 316 L. Han, Y. N. Hao, X. Wei, X. W. Chen, Y. Shu and J. H. Wang, *ACS Biomater. Sci. Eng.*, 2017, **3**, 3230–3235.
- 317 C. Xu, D. Yang, L. Mei, Q. Li, H. Zhu and T. Wang, *ACS Appl. Mater. Interfaces*, 2013, **5**, 12911–12920.
- 318 Z. Tian, X. Yao, K. Ma, X. Niu, J. Grothe, Q. Xu, L. Liu, S. Kaskel and Y. Zhu, *ACS Omega*, 2017, **2**, 1249–1258.
- 319 J. Ou, F. Wang, Y. Huang, D. Li, Y. Jiang, Q. H. Qin, Z. H. Stachurski, A. Tricoli and T. Zhang, *Colloids Surf. B*, 2014, **117**, 466–472.
- 320 J. Shen, W. Zhang, R. Qi, Z. W. Mao and H. Shen, *Chem. Soc. Rev.*, 2018, **47**, 1969–1995.
- 321 J. Liu, W. Bu, S. Zhang, F. Chen, H. Xing, L. Pan, L. Zhou, W. Peng and J. Shi, *Chem. - A Eur. J.*, 2012, **18**, 2335–2341.
- 322 J. Xu, S. S. Y. Lee, H. Seo, L. Pang, Y. Jun, R. Y. Zhang, Z. Y. Zhang, P. Kim, W. Lee, S. J. Kron and Y. Yeo, *Small*, 2018, **14**, 180360.
- 323 Alexander Myskiw DataArt, *Eur. Pharm. Manuf. (EPM Mag. www.epmmagazine.com)*, 2017.



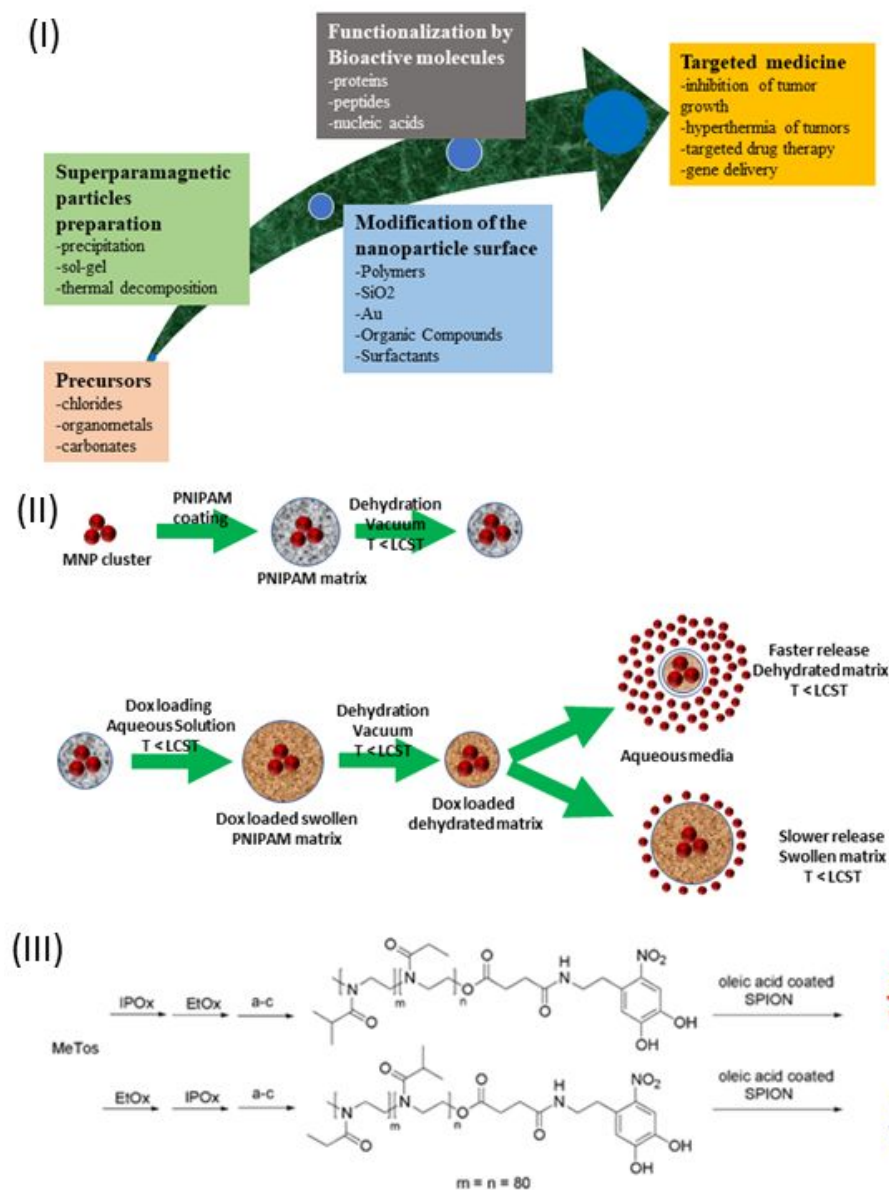
## Figures and Captions

### Figure 1



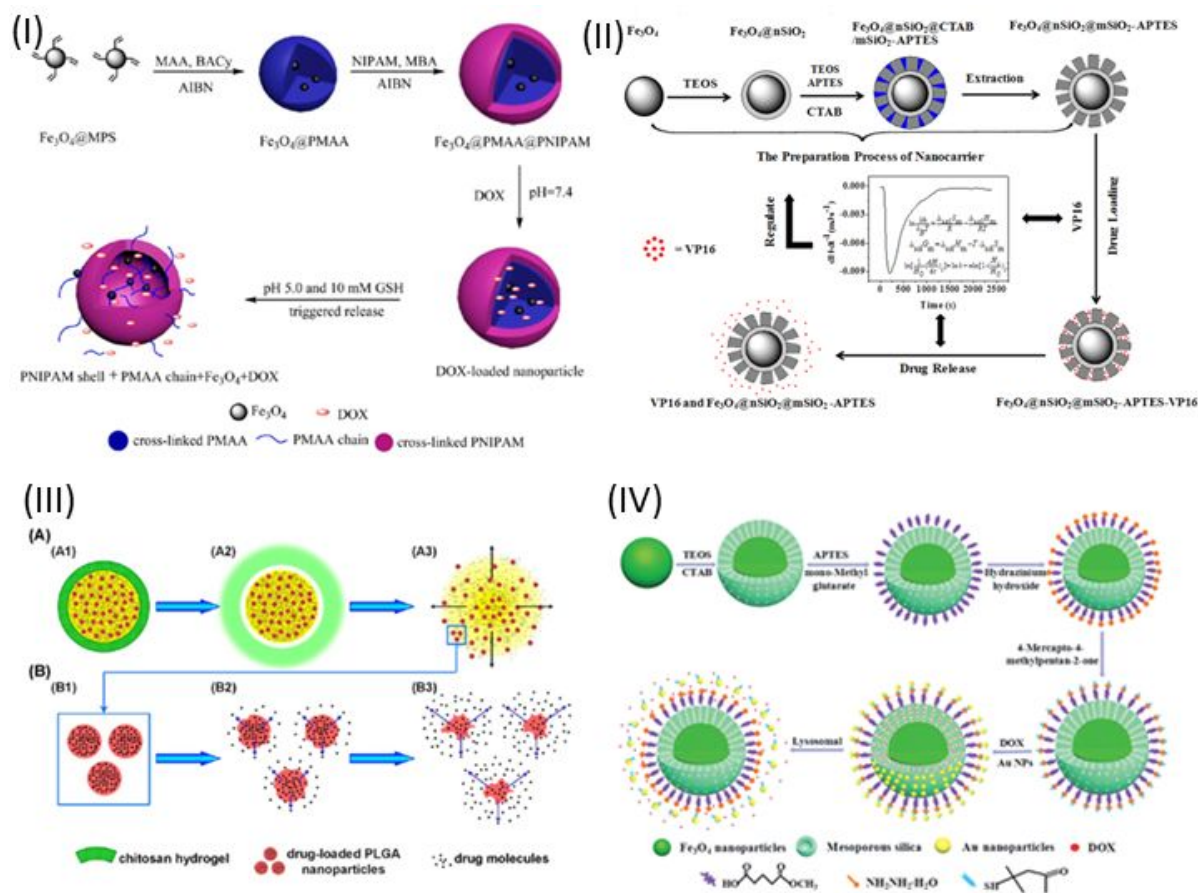
**Figure 1.** (I) various types of core-shell nanoparticles used for drug delivery applications. (II) Core-shell nanoparticles with different functional materials. (III) The strategies of surface engineering of inorganic nanoparticles. (A) covalent ligand conjugation, (B) amphiphilic polymer assembly, (C) electrostatic layer-by-layer assembly, (D) in situ ligand coating during synthesis, (E) Host-guest supramolecular ligand self-assembly, (F) lipid shell coating. Reproduced with permission from ref.<sup>320</sup>. Copyright 2018 American Chemical Society.

Figure 2



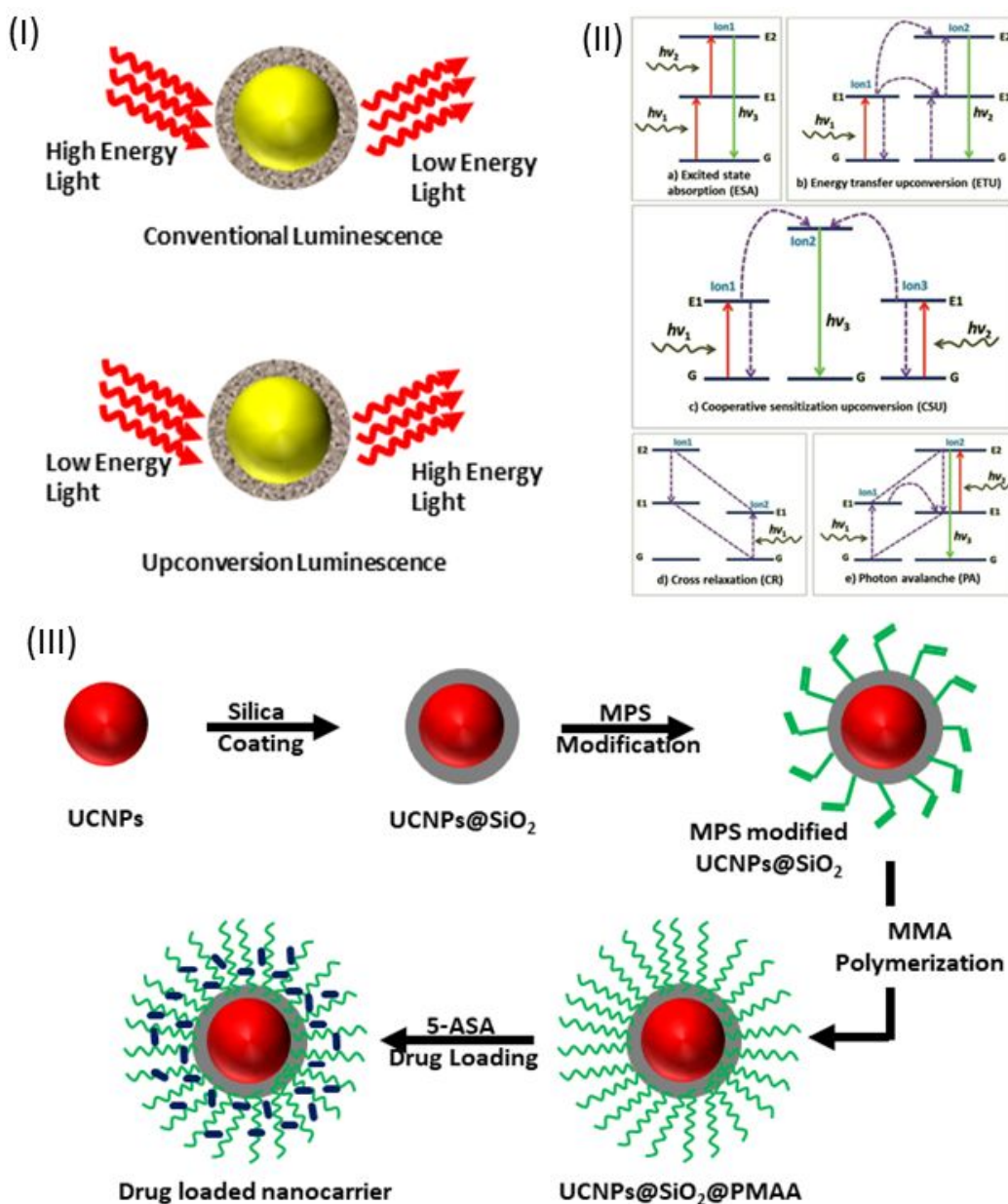
**Figure 2.** (I) Various steps involved in the process of magnetic nanoparticles preparation for drug delivery application. (II) Schematic overview of the preparation of magnetic nanoparticles, drug loading, and drug release processes. (III) Synthetic process of block copolymer modified SPIONs, MeTos: methyl tosylate, IPOx: 2-isopropylloxazoline, EtOx: 2-ethylloxazoline. (a-c) End group transformation: (a) quench with water, (b) reaction with succinic anhydride, (c) reaction with 6-nitrodopamine, ligand exchange reaction of NDA-modified block copolymers on oleic acid-coated SPION. Reproduced with permission from ref. <sup>71</sup>. Copyright 2017 American Chemical Society.

Figure 3



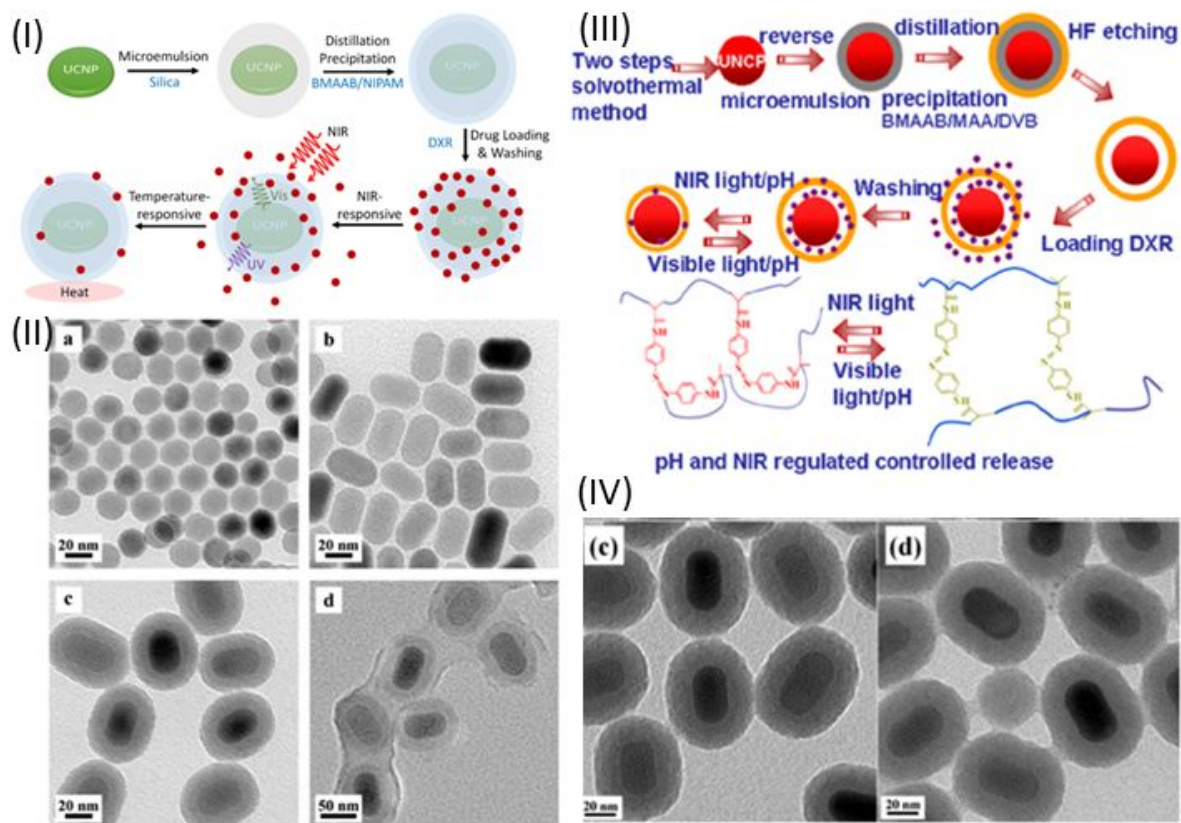
**Figure 3.** (I) Schematic presentation of the synthesis, biodegradation, and multistimuli responsive drug release of the Fe<sub>3</sub>O<sub>4</sub>@PMAA@PNIPAM core-shell nanoparticles. (II) Schematic illustration of the core-shell magnetic nanoparticles synthesis and control release of drug. TEM images of (a) Fe<sub>3</sub>O<sub>4</sub> (b) Fe<sub>3</sub>O<sub>4</sub>@mSiO<sub>2</sub>, HRTEM images of (c) Fe<sub>3</sub>O<sub>4</sub>@mSiO<sub>2</sub>, and (d) Dox Fe<sub>3</sub>O<sub>4</sub>@mSiO<sub>2</sub>@Au nanoparticles. (III) step by step preparation process of Fe<sub>3</sub>O<sub>4</sub>@nSiO<sub>2</sub>@mSiO<sub>2</sub>-APTES microsphere and their study of drug loading and release mechanism using the microcalorimetric technique. (IV) Schematic illustration of the programmed sequential core-shell chitosan microcapsule preparation and drug release. (A) First, burst release of free drug and decomposition of chitosan shell in acidic solution following the release of drug loaded PLGA nanoparticles and (B) sustained release of drug from the PLGA nanoparticles through diffusion by the degradation of PLGA. Reproduced with permission from ref. <sup>72,96,97,108</sup>. Copyrights 2015, 2015, 2016, 2014 American Chemical Society, American Chemical Society, American Chemical Society, and Wiley VCH, respectively.

Figure 4



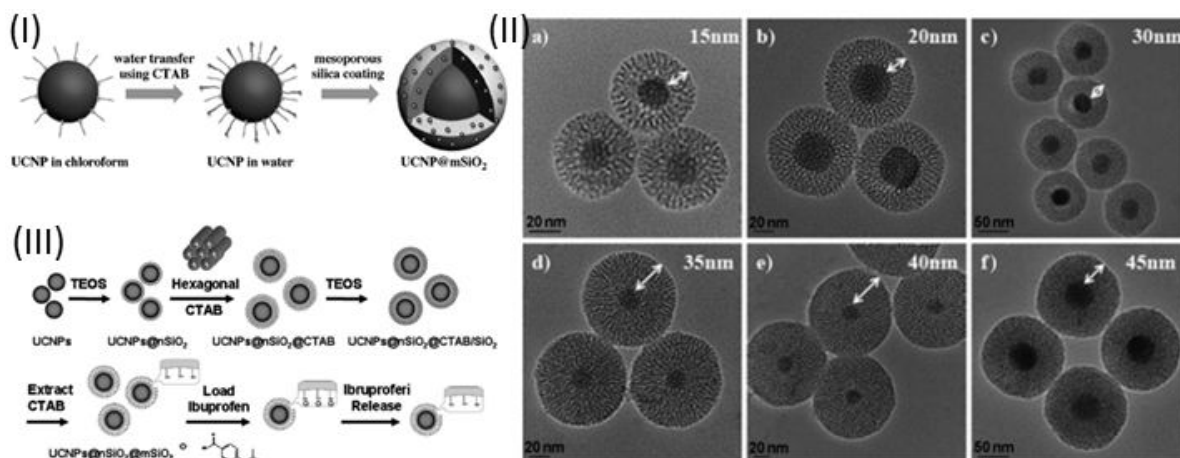
**Figure 4.** (I) Illustration of conventional and upconversion luminescence. (II) Upconversion process principle in Ln-doped UCNPs, a) excited state absorption (ESA), b) energy transfer Upconversion (ETU), c) cooperative sensitization Upconversion (CSU), d) cross relaxation (CR), and e) photon avalanche (PA). (III) Schematic view of the preparation process of silica coated upconversion core-shell nanoparticles functionalized with polymer for drug delivery applications. Reproduced with permission from ref.<sup>1</sup>. Copyright 2018 Wiley VCH.

Figure 5



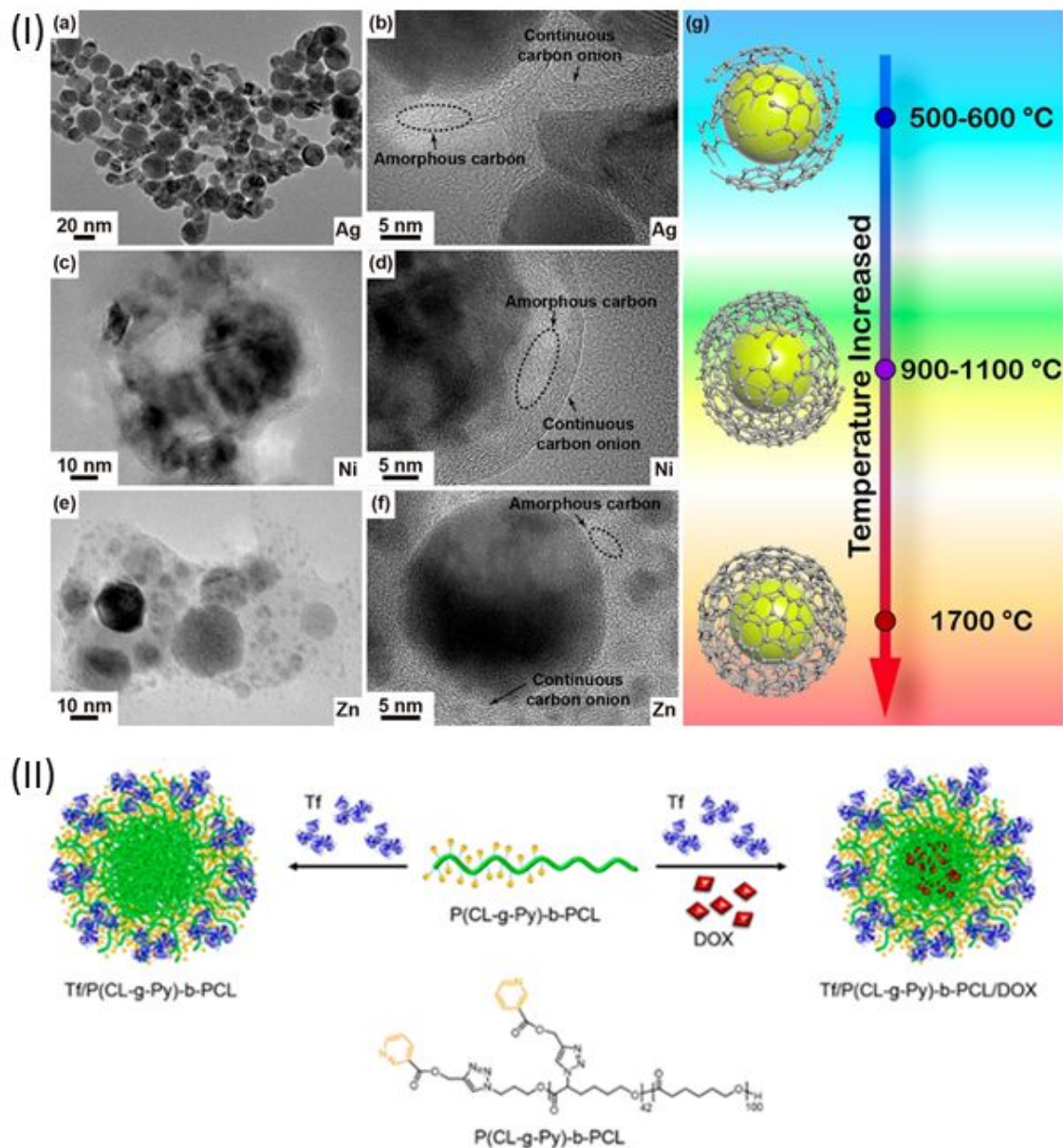
**Figure 5.** (I) Synthetic route of dual responsive nanocarrier and the loading and release of DXR. TEM images of (a) NaYF<sub>4</sub>: Yb<sup>3+</sup>/Tm<sup>3+</sup>, (b) UCNPs, (c) UCNPs@SiO<sub>2</sub>, and (d) DR-NCs. (II) Route of UCNPs@PAzo/MAA NCs and loading and release of DXR. TEM images of (a) NaYF<sub>4</sub>: Yb<sup>3+</sup>/Tm<sup>3+</sup> and (b) NaYF<sub>4</sub>:Yb<sup>3+</sup>/Tm<sup>3+</sup>@NaYF<sub>4</sub>. TEM micrographs of core/shell/shell structure of NaYF<sub>4</sub>:Yb<sup>3+</sup>/Tm<sup>3+</sup>@NaYF<sub>4</sub>@SiO<sub>2</sub> particles prepared under initial amount of NaYF<sub>4</sub>:Yb<sup>3+</sup>/Tm<sup>3+</sup>@NaYF<sub>4</sub>: (a) 1.0, b) 1.4, c) 0.7, d) 0.5 mL. Reproduced with permission from refs. <sup>130,131</sup>. Copyright 2019, 2018 American Chemical Society and American Chemical Society, respectively.

Figure 6



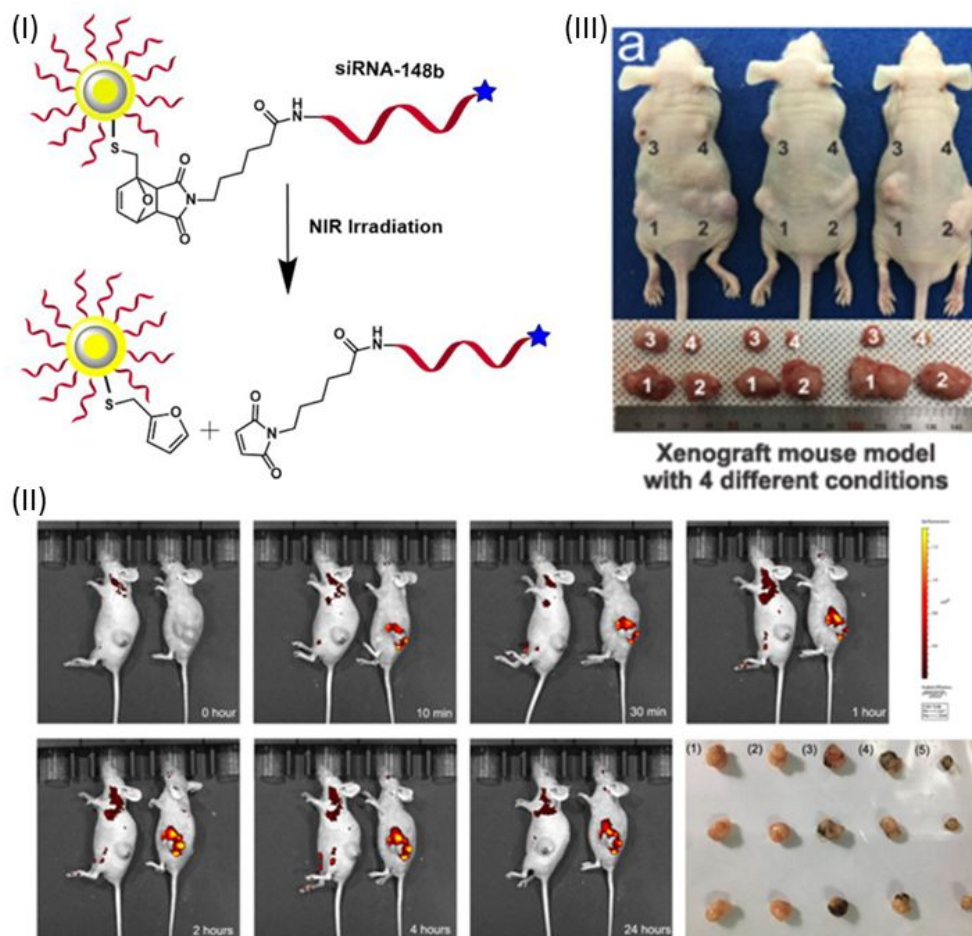
**Figure 6.** (I) Synthesis procedure of UCNPs/mSiO<sub>2</sub> core-shell nanocomposite. TEM images of uniform NaYF<sub>4</sub>:Tm/Yb@mSiO<sub>2</sub> nanocomposite with different mesoporous shell thickness: a) 15, b) 20, c) 30, d) 35, e) 40, f) 45. (II) Schematic view of synthesis of LaF<sub>3</sub>:Yb<sup>3+</sup>,Er<sup>3+</sup>@nSiO<sub>2</sub>@mSiO<sub>2</sub> microspheres, and the subsequent loading and release of the ibuprofen drug. Reproduced with permission from refs. <sup>132,321</sup>. Copyright 2012, 2010 Wiley-VCH, Wiley VCH, respectively.

Figure 7



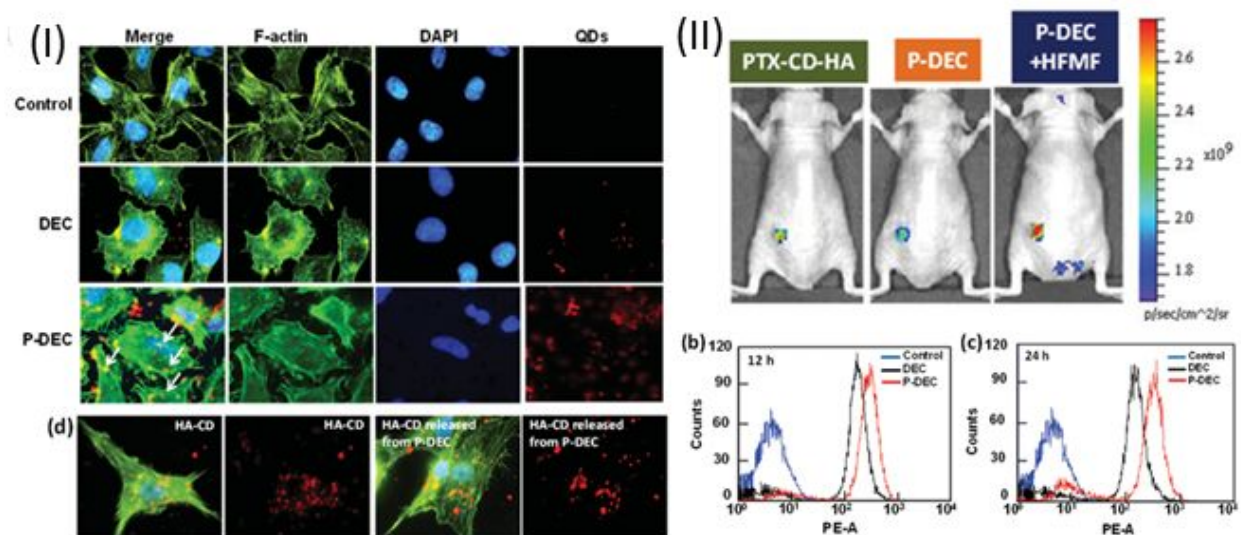
**Figure 7.** (I) TEM and HRTEM images of the laser ablation assisted carbon-encapsulated Ag (a, b), Ni/Ni<sub>3</sub>C (c, d), and Zn/ZnO (e, f) nanoparticles. (g) Graphic illustrations of the transformation of carbon onion structure with the increase in temperature. Continuous outer carbon onion shell and inner amorphous carbon show the laser-induced graphitization. Reprinted from reference <sup>163</sup> with the permission of American Chemical Society, Copyright 2018. (II) Preparation of Tf/P(CL-g-Py)-b-PCL core-shell nanoparticles and DOX-Loaded Tf/P(CL-g-Py)-b-PCL core-shell nanoparticles. Reprinted from reference <sup>201</sup> with the permission of American Chemical Society, Copyright 2016.

Figure 8



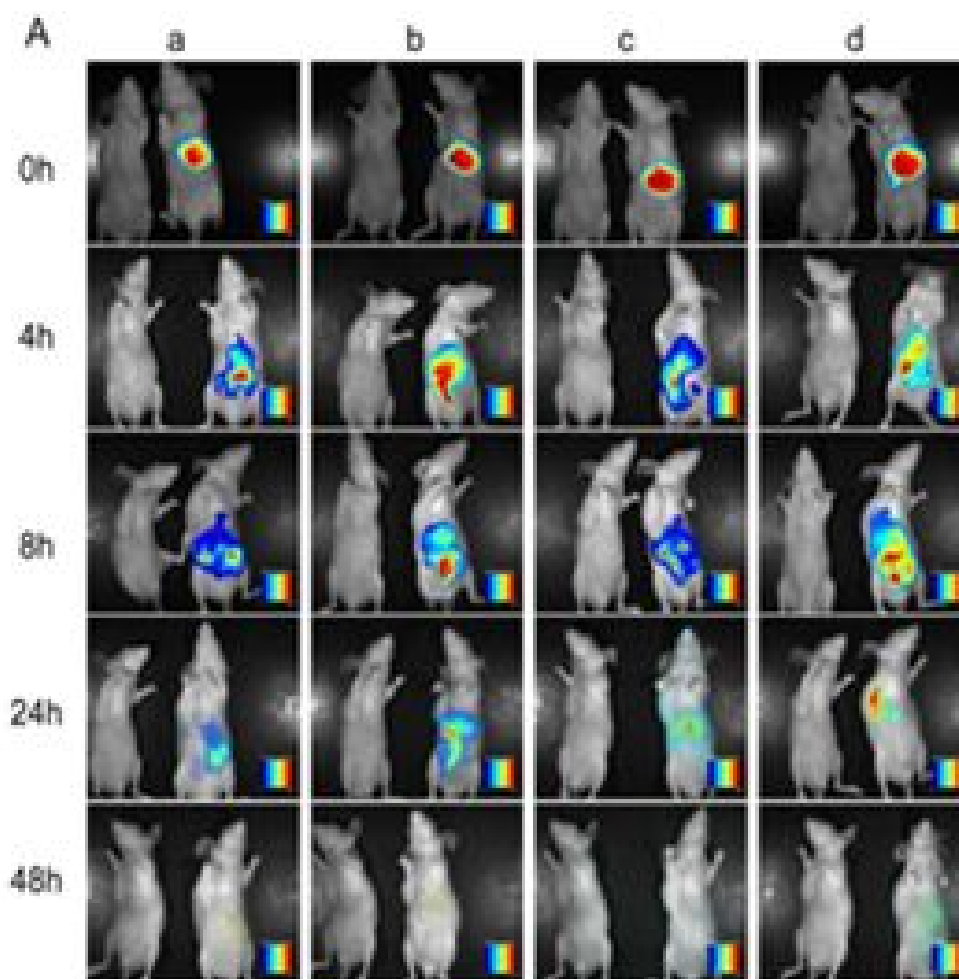
**Figure 8.** (I) Using Diels-Alder chemistry SiRNA attachment on the surface of Au-Ag-Au core-shell-shell nanoparticles and release mechanism presence of NIR light. (II) in vivo fluorescence imaging and RNA interference therapy, (A) fluorescence imaging of tumor tissues in HeLa tumor-bearing mice at different time intervals after intratumoral injection of PBS or Ag@AIR/PAH/survivin siRNA, and the representative images of tumor tissues treated with (1) PBS blank, (2) free surviving siRNA (3) nude Ag@AIR nanocarrier, (4) Ag@AIR/PAH/scramble siRNA and (5) Ag@AIE/PAH/surviving siRNA. (III) in vivo anticancer efficacy of multifunctional MCNPs-based combined miRNA and DOX therapy. (a) images of tumor-bearing nude mice and dissected tumors from xenograft treated with four different conditions: (1) PBS as control; (2) DOX-loaded MCNP, (3) let-7a-complexed MCNP, and (4) DOX-loaded and let-7a-complexed MCNP. The four different treatment conditions were directly injected into the MDA-MB-231 tumors of mice every 3 days for 5 weeks. Each mouse received a particle dose of 5 mg/kg for each injection. Reproduced with permission from ref. <sup>218,227,231</sup>. Copyright 2018, 2018, 2019 American Chemical Society, American Chemical Society, American Chemical Society, respectively.

Figure 9



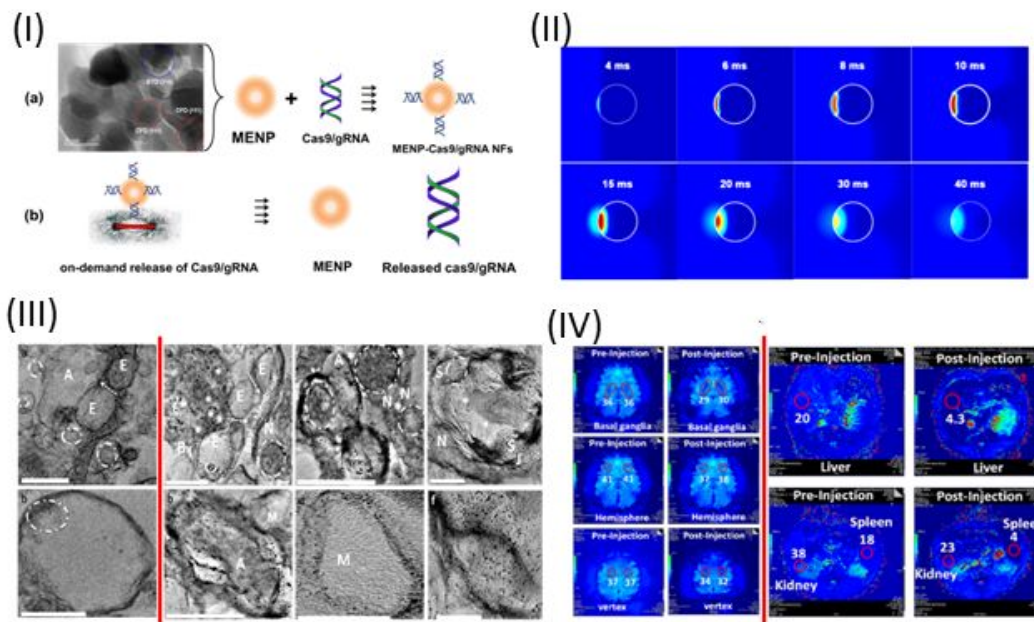
**Figure 9.** (I) Cellular uptake of DEC and P-DEC in HeLa cells after 24 h of incubation. Particles stained and QDs exhibit a red color, the cytoplasm presents a green color, and the nuclei appear in blue. Flowcytometry histograms of HeLa cells after b)12 h and c) 24 h of incubation with DEC and P-DEC, d)cellular uptake of HA-CDs and HA-CD from P-DEC triggered release by 10 min of HFMF. (II) (a) fluorescence images of nude mice xenograft models that used the RG2 cancer cell line treated by PTX-CD-HA, P-DEC, and P-DEC with 10 min of HFMF through intravenous injection via the tail vein for 2 days. Reproduced with permission from ref. <sup>241</sup>. Copyright 2016 Wiley VCH.

Figure 10



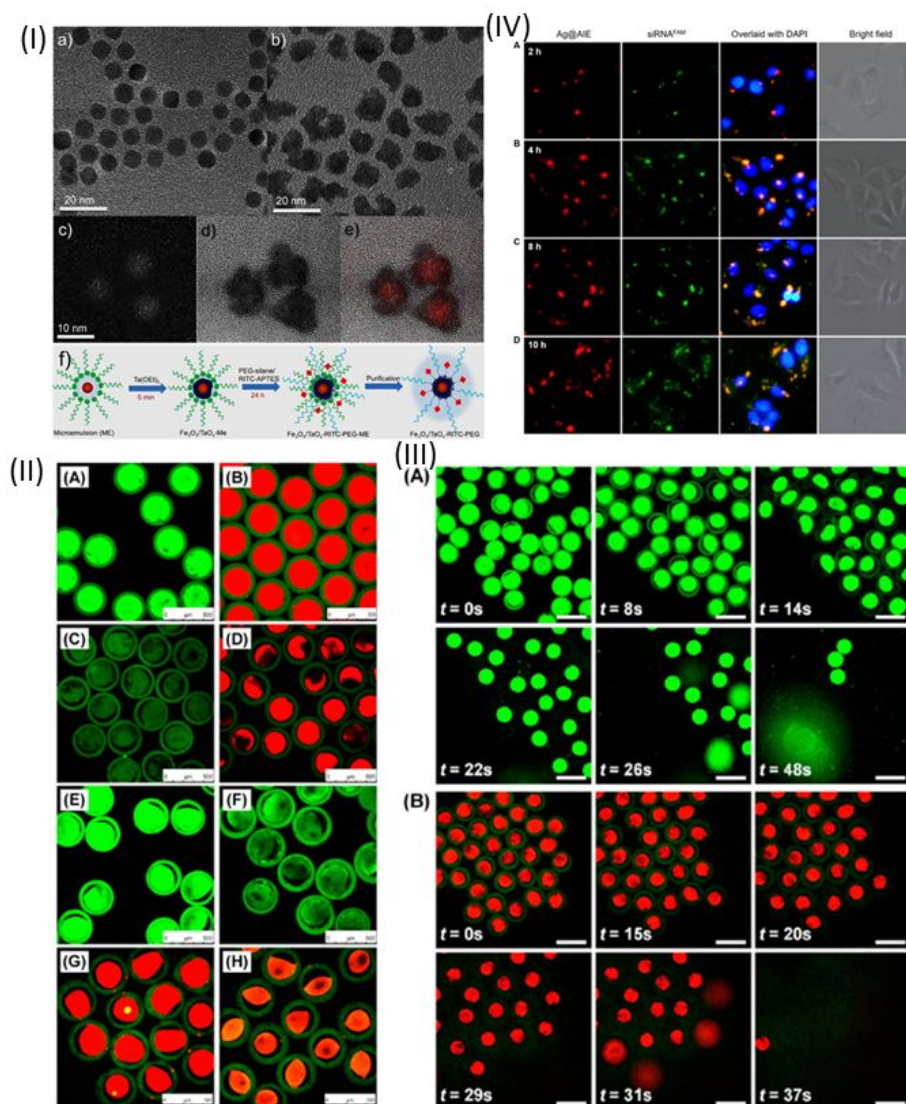
**Figure 10.** Tissue distribution of CyS.S-labeled NPs in tumor bearing nude mice. (A) fluorescence images of tumor bearing mice treated with (a) free CyS.S, (b) CyS.S-labeled PLGA nanoparticles, (c) CyS.S-labeled mPEG-g-CS nanoparticles, and (d) CyS.S-labeled core-shell nanoparticles at time points 0, 4, 8, 24, 48 h after administration. Reproduced with permission from ref. <sup>242</sup>. Copyright 2018 American Chemical Society.

Figure 11



**Figure 11.** (I) schematics illustration of CRISPR Cas9/gRNA binding with MENPs and its release on applying an ac-magnetic field. Reprinted from reference <sup>247</sup> with the permission of Nature Publishing Group, Copyright 2019. (II) Magneto nano-electroporation caused by magneto-elastic phenomena produced by MENPs at the interface with cells on applying an ac-magnetic field stimulation. Reprinted from reference with <sup>248</sup> the permission of Nature Publishing Group, Copyright 2017. (III) Magnetically guided delivery of MENPs to the CNS. Under the influence of the static magnetic field, MENPs cross the BBB without affecting BBB-associated cell junction and uniformly distributed in call types (right side), as illustrated in comparison of control mice (left side). Reprinted from reference <sup>249</sup> with the permission of Nature Publishing Group, Copyright 2016. (IV) MRI-assisted MENPs delivery to the brain of non-human primate (baboon). The MRI image analysis confirmed the presence of MENPs in the periphery (left side) and brain (right side). Reprinted from reference <sup>250</sup> with the permission of American Chemical Society, Copyright 2019.

Figure 12



**Figure 12.** (I) (a, b) TEM images of (a) Fe<sub>3</sub>O<sub>4</sub> NPs fabricated through the thermal decomposition of Fe–oleate complexes and (b) Fe<sub>3</sub>O<sub>4</sub>/TaO<sub>x</sub> core/shell NPs formed by Fe<sub>3</sub>O<sub>4</sub> NPs. (c) Elemental mapping image for Fe. (d) Bright-field TEM image of Fe<sub>3</sub>O<sub>4</sub>/TaO<sub>x</sub> core/shell NPs. (e) Overlay micrograph of (c) and (d). (f) Pictorial Illustration of synthesis and modification of Fe<sub>3</sub>O<sub>4</sub>/TaO<sub>x</sub> Core/Shell NPs. Reprinted from reference<sup>267</sup> with the permission of American Chemical Society, Copyright 2016. (II) CLSM images of different core-shell chitosan microcapsules. microcapsules containing (a) free curcumin only, (B) free RhB only (C) Cur-PLGA NPs (D) RhB-PLGA NPs, (E) both free curcumin and cur-PLGA NPs (F) free curcumin and RhB-PLGA NPs (G) free RhB and RhB-PLGA NPs and (H) Free RhB and Cur-PLGA NPs. A, C, E are on a green fluorescent channel, B, D, F-H are overlaps of images on green and red channels. (III) CLSM microscope images of the acid-triggered burst release process of microcapsules containing both free CUR and CUR-PLGA NPs, A-green fluorescent channel; and microcapsules containing both free RhB and

RhB-PLGA NPs (B, Overlap of images on green and red fluorescent channels. HCl solution with pH 1.5 is used at time 0 s. (IV) Real-time monitoring of siRNA delivery in HeLa cells at (A) 2h (B) 4h (c) 8 h and (D) 10 h. the signals from FAM, Ag@AIE, and DAPI (for nuclei staining) were green, red, and blue, respectively. Reproduced with permission with ref. <sup>108,231</sup>. Copyrights 2016 and 2019 American Chemical Society, American Chemical Society, respectively.

Figure 13

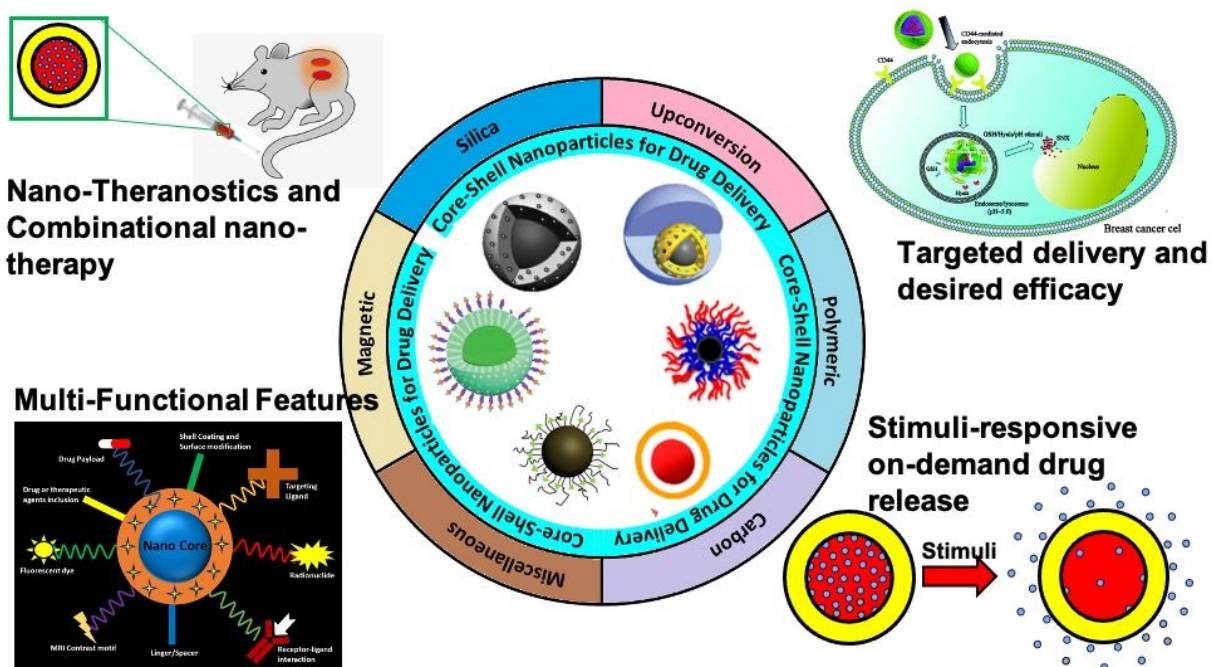
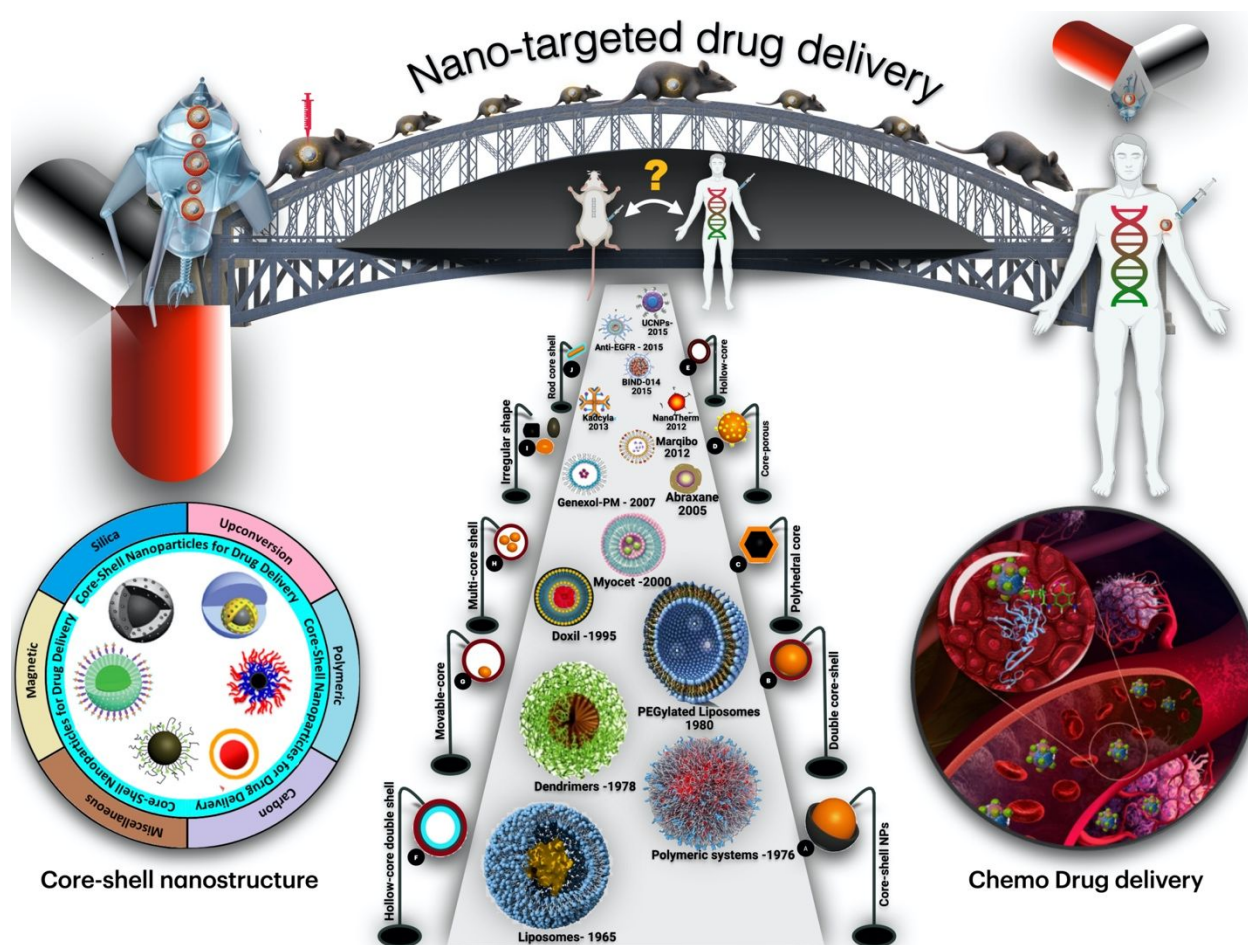


Figure 13: Schematic illustration of Core-shell nanoparticles and drug delivery approaches



**Figure 14: Schematic illustration and outlook of the Nano-targeted drug delivery with the nanomedicine development timeline.** Reproduced with permission from ref.<sup>281</sup>. Copyright 2017 Oncology Reports. The Chemo drug delivery illustration has been adapted from ref. <sup>322,323</sup>. Copyright 2018, Wiley, and EPM Magazine.